AMERICAN UNIVERSITY OF BEIRUT

Controlled Particle Size Synthesis of ZIF-L-(Zn, Co), ZIF-(8, 67) And their Mixed Metal Derivatives Using A Multi-Inlet Vortex Mixer (MIVM)

by

MOHAMMAD AHMAD FAHDA

A thesis
submitted in partial fulfillment of the requirements
for the degree of Master of Science
to the Department of Chemistry
of the Faculty of Arts and Sciences
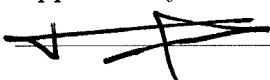at the American University of Beirut

Beirut, Lebanon
January 2020

AMERICAN UNIVERSITY OF BEIRUT

Controlled Particle Size Synthesis of ZIF-L-(Zn, Co), ZIF-(8, 67) And their Mixed Metal Derivatives Using A Multi-Inlet Vortex Mixer (MIVM)

by

MOHAMMAD AHMAD FAHDA

Approved by:

_____ T𝑎𝑟𝑒𝑓 G-𝑙𝑎𝑑𝑑𝑎𝑛 _____

Dr. Mazen Al-Ghoul, Professor   Advisor

Chemistry

_____ /𝑜ℎ𝑚𝑚𝑎𝑙 𝐻𝑚𝑎𝑑𝑒ℎ _____

Dr. Mohamad Hmadeh, Assistant Professor   Member of Committee

Chemistry

_____ 𝑊𝑎𝑙𝑖𝑑 𝑆𝑎𝑎𝑑 _____

Dr. Walid Saad, Associate Professor   Member of Committee

Chemical and Petroleum Engineering

Date of thesis defense: January 29, 2020

AMERICAN UNIVERSITY OF BEIRUT

THESIS, DISSERTATION, PROJECT
RELEASE FORM

Student Name: __Fahda_____ __Mohammad__ __Ahmad__
              Last   First   Middle

☑ Master's Thesis   ○ Master's Project   ○ Doctoral Dissertation

☐   I authorize the American University of Beirut to: (a) reproduce hard or electronic copies of my thesis, dissertation, or project; (b) include such copies in the archives and digital repositories of the University; and (c) make freely available such copies to third parties for research or educational purposes.

☑   I authorize the American University of Beirut, to: (a) reproduce hard or electronic copies of it; (b) include such copies in the archives and digital repositories of the University; and (c) make freely available such copies to third parties for research or educational purposes after:

        One _ _ _ _ year from the date of submission of my thesis , dissertation or project.
        Two _✓_years from the date of submission of my thesis , dissertation or project.
        Three _ _ _ _ years from the date of submission of my thesis , dissertation or project.

_____   17-09-2020
    Signature   Date

Acknowledgements

An Abstract of the Thesis of

Mohammad Ahmad Fahda   for   Master of Science
Major: Chemistry

Title: Controlled Particle Size Synthesis Of ZIF-L-(Zn, Co), ZIF-(8, 67) And Their Mixed Metal Derivatives Using A Multi-Inlet Vortex Mixer (MIVM).

Zeolitic Imidazolate Frameworks (ZIFs) have attracted extensive attention due to their high porosity, exceptional surface area and remarkable thermal and chemical stability leading to a distinguished performance in various fields like catalysis, gas separation, carbon dioxide storage, and drug delivery. Some major challenges in the ZIF research are concerned with the synthesis of high-quality ZIF-(8, 67) crystals in an aqueous medium with reduced organic ligand consumption and controlled particle size. Herein, we report the controlled transition from ZIF-L-(Zn, Co) to ZIF-(8,67) and the controlled particle size synthesis of ZIF-(8, 67) and their mixed metal derivatives in a multi-inlet vortex mixer (MIVM). The method consists of using the precursor solutions (metal ion solutions, organic ligand solution) in four pump-controlled syringes that feed them into the MIVM at various flow rates. The collected ZIF particles are then fully characterized and their composition is determined. We show that this technique provides superior control over the transition from ZIF-L to ZIF-(8,67) via the flow rates of the initial ZIF precursors and their molar ratio. Moreover, using the MIVM we are able to synthesize ZIF-8 nanoparticles with a minimum mean particle size of 76 nm $\pm$ 2 nm compared to a mean particle size of 97 nm $\pm$ 20 nm using the traditional batch technique. The controlled doping of ZIF-8 by cobalt is also implemented.

Contents

List of Figures

List of Tables

Chapter 1

Introduction

1.1 Mixing and Chemical Reactions

1.1.1 Definition of Mixing

Mixing is the process of homogenizing separated fluid elements in a given volume that differ at least in one property such as temperature, concentration, viscosity, color etc. through accelerating mass and heat transfer[8].

1.1.2 Fluid Flow Regimes

It is necessary to understand that there exist three flow regimes for fluids which are Laminar, Turbulent and a transition regime between both. The fluid flow regime can be specified using the dimensionless Reynolds number (Re) that is the ratio of inertial forces to viscous forces,

$$Re = \frac{\rho u L}{\mu} \tag{1.1}$$

where ρ is the density of the fluid, u is the inlet flow velocity, L is the mixing chamber diameter and μ is the dynamic viscosity of the fluid. The Laminar flow regime occurs at $Re < 2100$ where viscous forces dominate resulting in a smooth flow of fluid particles along highly regular paths with little or no mixing. The most common illustration for the Laminar regime is the flow of a viscous liquid through a pipe, where the fluid particles flow along parallel planes with a velocity profile that increases form zero to maximum starting from the pipe walls to the cross sectional center of the vessel. As for the Turbulent regime, it results from the domination of inertial forces over viscous forces that occurs at $Re > 4000$ where the fluid's motion is characterized by chaotic changes in pressure and flow velocity

(see Fig. 1.1). Accordingly, the transition regime possess the characteristics of both laminar and turbulent flow and is dominant for $2000 < Re < 4000$.

Laminar Flow
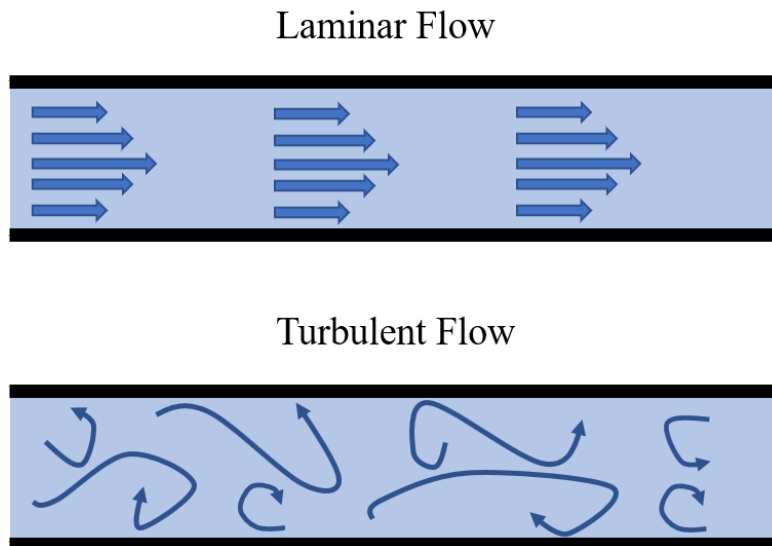
Turbulent Flow

Figure 1.1: Schematic representation of laminar and turbulent flow.

1.1.3 Definition of Micromixers

Micromixers are three-dimensional reactors characterized by mixing chamber dimensions in the range of 10 μm up till few 100 μm[9, 10]. The main advantage of micromixers over traditional batch reactors is the high surface-area-to-volume ratio that increases the interfacial surface contact area between the reactants. Consequently the timescale of molecular diffusion across the mixing chamber is significantly reduced, thereby mixing time in microreactors typically falls within the range of several milliseconds[11]. Moreover, the miniaturized reactor volume and short mixing time enhances the heat exchange efficiency among the reactants through minimizing the chances of local heat accumulation resulting from strongly exothermic reactions such as polymerization, thus ensuring higher safety measures than typical batch reactors[12].

1.1.4 Types of Micromixers

The micro scale design of micromixers usually results in low Re where the laminar flow regime dominates during the process of a chemical reaction. Accordingly, the mixing of two reactants in a micromixer leads to the formation of two parallel streamlines known as stratified flow between both reactants where the main mixing process is via molecular diffusion. However, diffusion is a slow process especially in case of viscous reactants where complete mixing needs several minutes

to be achieved. Consequently, scientists managed to modify the micromixers design to enhance the mixing process either by using external energy sources (ultrasound, acoustic, periodic variation of flow rate, etc.) thus forming Active micromixers, or by modifying the internal geometrical structure to induce chaotic advection and these mixers are known as Passive micromixers (no external energy sources utilized other than that of the pumps)[13, 14, 15, 16].

1.1.5   Measures of Mixedness

Mixedness is the measure of homogeneity achieved by mixing in a certain reactor. The two main parameters for evaluating the mixedness of any mixing reactor are the i) scale of segregation, and ii) intensity of segregation. The scale of segregation is a measure of the large scale breakup of the solution without the action of diffusion, as represented in Fig. 1.2-a, it is the size of the white fluid packets that can be distinguished form the surrounding black fluid packets. As for the intensity of segregation, it is the measure of the concentration difference between pure fluid A and pure fluid B along the reactor resulting from the action of molecular diffusion as observed in Fig. 1.2-b. Although molecular diffusion takes place in presence or absence of mixing, however, the highly reduced scale of segregation that results from an ideal mixing scenario increases the interfacial area between fluids A and B, thereby reducing the intensity of segregation leading to a more homogeneous solution (Fig. 1.2-c)[1].

1.1.6   The Damkoehler Number

The decision on whether to conduct a chemical reaction using a traditional batch reactor or a micromixer depends on the reaction's timescale compared to the reactor's mixing time. For instance, if the timescale needed to reach the half-life of a chemical reaction is in the order of minutes that is much longer than the mixing times of micormixers (milliseconds), a batch reactor should be used. However, in the case of ultra-fast reactions such as an acid-base neutralization with a half-life of 0.001 seconds, the use of a micromixer becomes critical. Where in such a case, the mixing time is slower than the reaction time, thus the rate of the chemical reaction would be the rate of mixing and not the rate of molecular diffusion between reactants. Accordingly, to facilitate the process of choosing a reactor for conducting chemical reactions, the scientific community defined a dimensionless number called the Damkoehler number (Da_M) which is the ratio of the characteristic mixing time of the reactor (τ_M) to the reaction time (τ_R).

$$Da_M = \frac{\tau_M}{\tau_R} \tag{1.2}$$

Large Da_M numbers imply that mixing is important and the use of a micromixer is favorable, while small Da_M numbers indicate that mixing is not a concern and
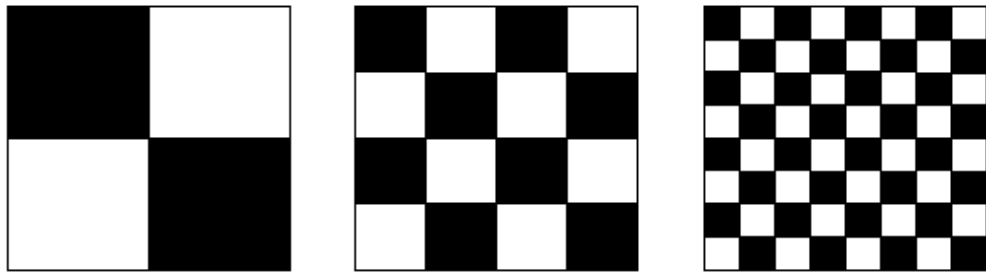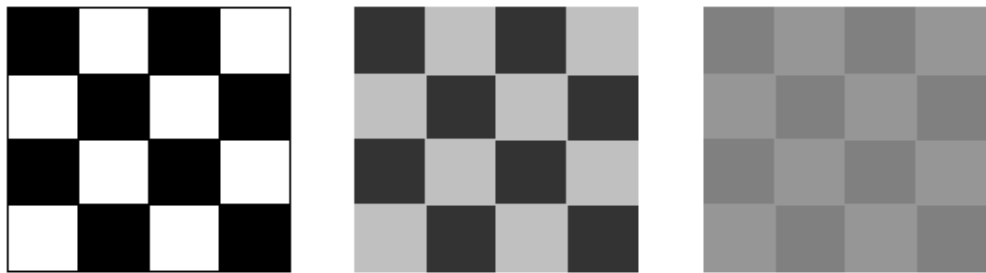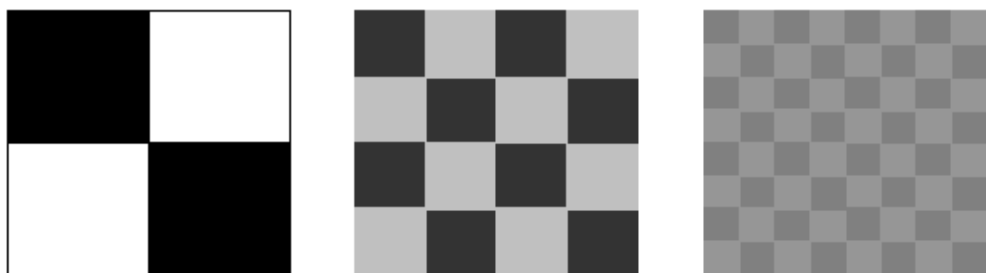
Figure 1.2: Intensity and scale of segregation: (a) reduction in scale of segregation; (b) reduction in intensity of segregation; (c) simultaneous reduction of intensity and scale of segregation. Adapted from [1].

using a traditional batch reactor would suffice

1.1.7   Applications of Micromixers

The miniaturized mixing volume, the instantaneous mixing times, and the ease of control over the fluid regimes inside the micromixers qualified them for diverse synthetic applications.

Nanoparticle synthesis

The use of micromixers for nanoparticle synthesis in fields such as pharmaceutical development and catalyst design is considered one of the most efficient alternatives for the traditional synthetic methods like stirring tanks. The synthesis of nanoparticles is a two step process that consists of nucleation followed by particle growth. Since the rate of nucleation is dictated by the levels of supersaturation achieved through the mixing process, thus the nucleation kinetics are strongly influenced by the quality of mixing. Accordingly, the synthesis kinetics are poorly understood in conventional synthetic methods due to the macromixing scale property of such techniques. However, the use of micromixers for nanoparticle synthesis ensures full control over the mixing process through calculating Re (eq. 1.1) that allows a clear understanding of the crystallization process[17]. For instance, Schwarzer et al.[18, 19] investigated the synthesis of barium sulfate nanoparticles using a T-shaped micromixer at different Re numbers (Re= 200—15000). They reported that the computational simulations for the crystallization process were in good agreement with the mean size of the synthesized particles which confirms the superior performance of micromixers for the controlled particle size synthesis.

Polymer synthesis

One of the main challenges for polymerization applications is the controlled molecular weight synthesis of polymers. The two main parameters that influence the molecular weight dispersity of polymerization products are the homogeneity and thermal control of the reaction mixture. Polymerization products obtained from traditional batch techniques possess high degrees of molecular weight poly dispersity due to the long mixing time scale that results in low profiles of homogeneity and improper heat transfer among the reactants. Meanwhile, the miniaturized mixing scale of micromixers offers high surface to volume ratio that ensures instantaneous mixing time along with rapid heat transfer between reactants, thus highly mono disperse polymers would be obtained[20, 21, 22]. For example, Nagaki et al.[23] studied the effect of a micromixer on the controlled/living polymerization of vinyl ethers. In their study, they reported that polymers obtained from a conventional batch reactor showed a broad molecular weight distribution (M_w/M_n= 2.25), however, highly mono disperse molecular

weight distribution was obtained upon using the micromixer (M_w/M_n= 1.14).

Organic synthesis

The interest in micromixers for organic synthesis has widely increased as a result of the continuous search for cost-effective synthetic techniques to act as an alternative to traditional batch methods. In general, organic synthesis at the industrial scale is achieved through conventional stirring tanks that have high energy consumption. Moreover, the poor mixing at the macroscale of stirring tanks may result in long reaction times, reduced yield and selectivity in case of competitive reactions. Accordingly the use of micromixers for organic synthesis have been reported for several types of reactions such as Knovenagel condensation, Diels-Alder addition, drug synthesis, etc.[24]. For instance, Reddy and his co-workers[25] investigated the synthesis of benzimidazole drugs (Lansoprazole, Pantaprazole, and Rabeprazole) using a setup of two micromixers connected in series. They reported that the reaction time was reduced from 3 hours in batch reactor to 1 second using the mixer with high percent yields and purity.

1.1.8 Multi-Inlet Vortex Mixer (MIVM)

The concept and design of the multi-inlet vortex mixer (MIVM) was developed by Liu and his co-workers[26] to overcome the limitations imposed by confined impinged micromixers (CIJ) for flash nano-precipitation applications. Flash nano-precipitation (FNP) is an advanced process for the controlled synthesis of nanoparticles through the fast mixing of a stream containing a dissolved solute and stabilizing amphiphilic polymer with an opposing miscible stream that acts as an anti-solvent for the solute and the amphiphilic polymer. The rapid mixing of the streams in a confined volume at the turbulent regime creates a high level of supersaturation condition required for the simultaneous precipitation of the solute and the amphiphilic polymer. The growth of the solute nanoparticles is inhibited by the adsorption of the amphiphilic polymer on its surface providing a steric stabilization that uniformly stops the growth to produce narrow particle size distribution[27].

The CIJ mixer design consists of two inlet streams opposite to each other that meet in the mixing chamber, and an outlet through which the products exit the mixer. Although the mixing times achieved using CIJ mixers is at the range of few milliseconds, the geometric design of the mixer demands that both inlet streams (solvent and anti-solvent) operate at the same flow rate. This would decrease the level of supersaturation created by the anti-solvent, where the final concentration of the effluent is the average of the two stream concentrations, therefore the solute nanoparticles stability by the polymer is compromised[28, 29]. On the other hand, the geometric design of the MIVM featuring four inlets allows for operating each stream at different flow rate from the other, since the main concept of the MIVM

is that each stream contributes independently to the mixing process. This allows for increasing the volumetric flow rate of the anti-solvent solution such that the final fluid phase of the effluent is predominantly anti-solvent, thereby increasing the stability of the nanoparticles[26].
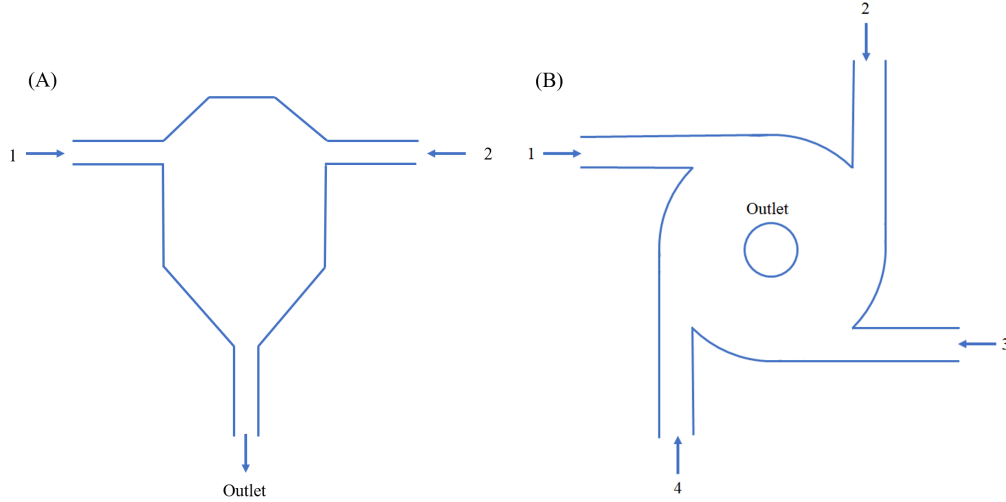
Figure 1.3: Schematic representation showing the geometric design of (A) a confined impinging jet (CIJ) micromixer, and (B) a multi-inlet vortex mixer (MIVM).

1.2 Zeolites and Zeolitic Imidazolate Frameworks (ZIFs)

1.2.1 Zeolites

Zeolites are natural crystalline aluminosilicate materials formed up by the corner sharing of the tetrahedrally coordinated silicon-aluminum-oxygen atoms TO_4 (T= Si and Al) (Fig. 1.4). The 2D and 3D zeolitic framework can be interpreted as a network of secondary building units (SBUs) as introduced by Meier[30] and smith[31], where the possible numbers of SBUs formed by the TO_4 units is 18 shown in figure 1.5. The zeolite framework topology is dictated by the connectivity between the cages formed that are constructed by the combination of one or more SBUs. To illustrate, let us consider the zeolitic topologies Sodalite (SOD) and Tschernichite (LTA). Both SOD and LTA frameworks are constructed from 3D sodalite cages (also known as β-cages) that are formed by six 4-rings and eight 6-rings, however, in the case of SOD topology, the β-cages are linked by sharing 4-rings while for the LTA topology occurs when the β-cages are linked through double 4-rings (Fig. 1.6)[2].

The microporosity of zeolites along with their exceptional chemical and ther-

mal stability showed superior performance in various industrial fields such as petroleum refining, ion exchange for water softening, treatment of liquid waste and separation of gases. Consequently, the market demand for zeolites significantly increased (the zeolite contribution to the global economy was estimated around $350 billion[5]) to exceed the level supplied by natural resources, thereby posing an urgent necessity for a synthetic alternative. For this reason the scientist aimed at mimicking the natural geothermal conditions that leads to the formation of zeolites by employing hydrothermal techniques along with structure directing agents (SDAs) to achieve the desired topology[32, 33, 34, 35, 36].
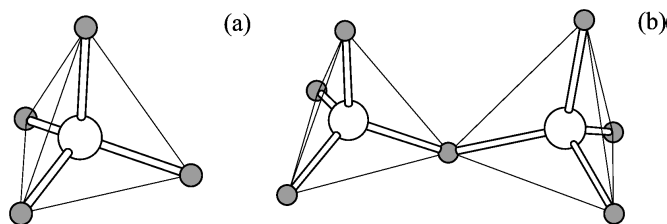
Figure 1.4: (a) TO_4 tetrahedron; (b) TO_4 tetrahedra sharing a common oxygen vertex. From [2]

However, despite the successful synthesis of several natural zeolites[37], the application field of zeolites was restricted to small molecules mainly due to the difficulty of i) designing zeolitic frameworks with extra large cavities beyond 1 nm[38] and/or ii) modifying the composition to contain a periodic array of intraframework organic functionality[39, 40]. As such, the scientific community, motivated by the mentioned challenges, developed hybrid organic-inorganic materials that share the chemical and topological properties of zeolites that are known as zeolitic imidazolate frameworks (ZIFs).
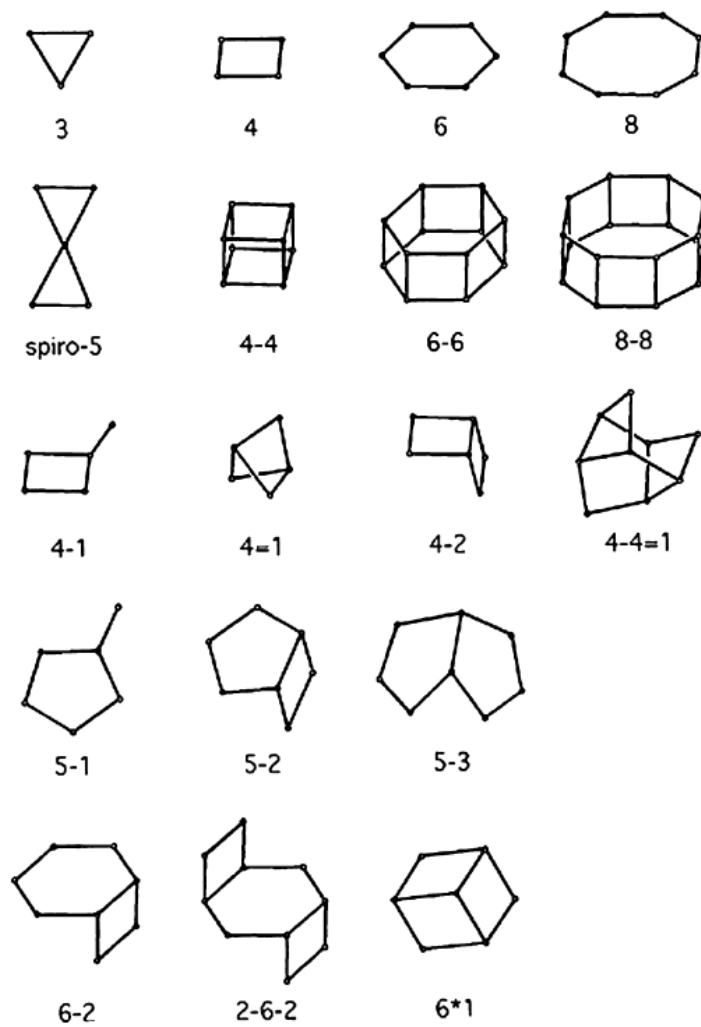
Figure 1.5: The possible structures of the secondary building units (SBUs) formed by the TO$_4$ units. From [3]. Copyright (2001) Elsevier
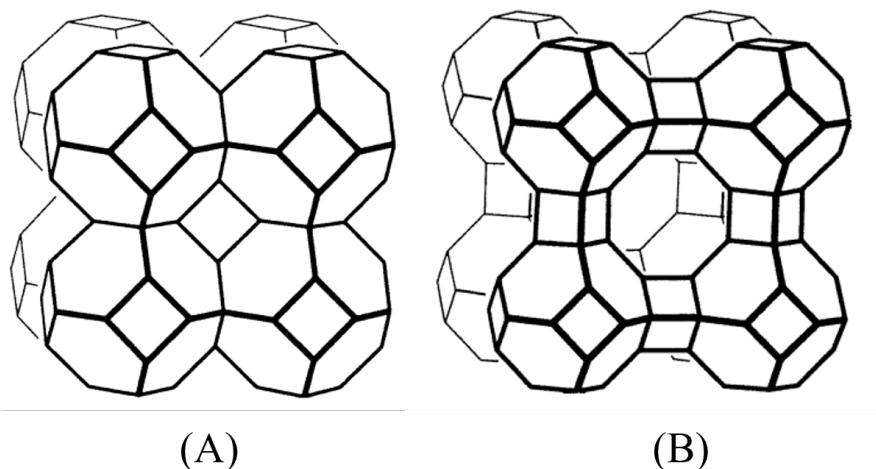
Figure 1.6: (A) SOD and (B) LTA framework types. Adapted from[4]. Copyright (2001) Elsevier

1.2.2 Zeolitic Imidazolate Frameworks (ZIFs)

ZIFs are a subclass of metal organic frameworks (MOFS) that are constructed by the corner shared tetrahedral coordination between +2 positively charged transition metals (Zn^{2+}, Cu^{2+}, Co^{2+}, Fe^{2+}) and Imidazolate linkers. The bond angle between the M^{2+} and the deprotonated ditopic nitrogen moiety of the imidazolate linker is close to 145° that is the preferred bond angle of Si-O-Si in natural zeolites (Fig. 1.7)[5]. Moreover, the topology of a certain ZIF is dictated by linker-linker interactions rather than SDAs used in synthetic zeolites, thereby, a broad range of zeolitic topologies can be achieved starting from different Imidazolate organic linkers[41] .

Furthermore, ZIFs are characterized by their permanent and tunable porosity, high surface area, and their exceptional thermal and chemical stability in various organic solvents[5, 42, 43]. Accordingly, ZIFs showed distinguished performance in various fields such as catalysis[44, 45], drug delivery[46, 47], water purification[48, 49], gas storage and separation[50, 51].
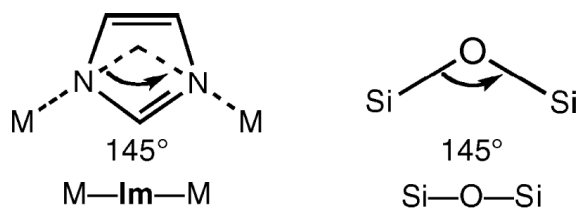
Figure 1.7: Metal- imidazolate-metal angle in ZIFs compared to the Si-O-Si bond in zeolites [5]. Copyright 2010 American Chemical Society
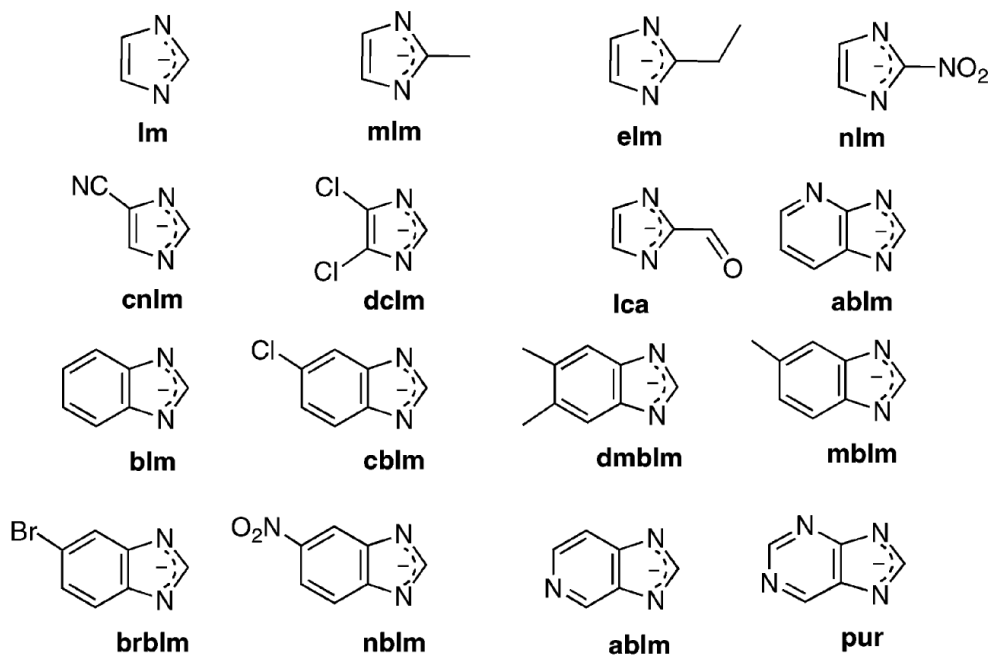
Figure 1.8: Different imidazole ligands used in ZIF synthesis [6]. Copyright 2010 American Chemical Society
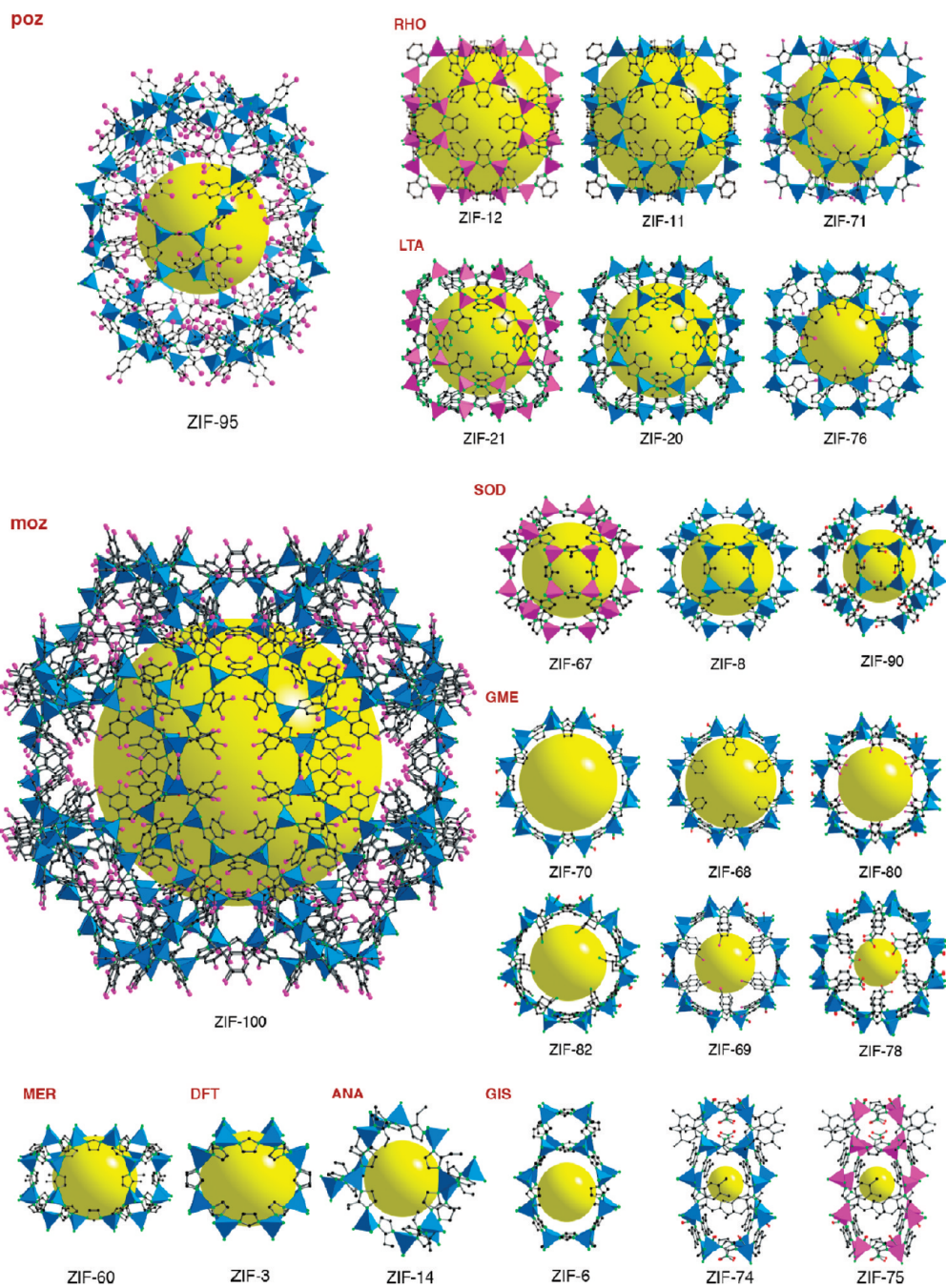
Figure 1.9: Different ZIF structures grouped by similar topologies [6]. The blue and pink tetrahedra represent the Td coordinated metal ion. The yellow spheres represent the pore in the cage. Blue is for Zn^{2+} and pink for Co^{2+}. Copyright 2010 American Chemical Society.

1.2.3   ZIF Synthesis

The promising potential of ZIF materials to act as a substitute for zeolites in various industrial applications inspired the scientific community to investigate and develop the synthetic routes in an extensive manner. The main concern was to develop environmentally friendly and cheap techniques that are able to provide high quality ZIF crystals. As such, a vast range of synthetic methods have been developed for that purpose which will be discussed briefly.

Solvothermal synthesis

This is the earliest method used for the discovery of ZIF materials by Yaghi and his co-workers[5]. It employed the use of organic solvents such as N,N-dimethylformamide (DMF), N,N-diethylformamide (DEF) at high temperatures (between 85-150 °C) for 48-96 hours. The amide solvent (DMF) dissociates into carbon monoxide and dimethylamine[52] at temperatures above 100 °C, the latter product promotes the deprotonation of the Imidazolate linker thus accelerating the formation of tetrahedral SBUs MIm_4 (M= Metal, Im= Imidazolate unit) to construct the zeolitic framework. Later on, scientists managed to modify the solvothermal method either by adding additives (such as triethylamine, sodium hydroxide, etc.) or using different solvents such as methanol (MeOH) in the purpose of enhancing the yield and modifying the morphological properties of the ZIF crystals[53, 54, 55].

Hydrothermal synthesis

Despite the success of solvothermal methods in yielding high quality ZIF crystals, the use of organic solvents posed problems for the scaled up synthesis of ZIF material due to its expensive cost and toxicity. As such, the synthesis of ZIFs using aqueous medium had been investigated. Pan et al.[56] reported the first synthesis of ZIF-8 in pure aqueous medium at room temperature. The method employed the use of high ligand (2-Methylimidazole (Hmim)) to metal (Zn^{2+}) ratio (Zn:Hmim = 1:70) with continuous stirring for 5 minutes where the ZIF crystals obtained were at the nanoscale (80 nm) and exhibited significant thermal stability (up to 300°C) and high BET surface area (1079 m^2/g). However, the excessive use of organic ligand raised the same cost and environmental concerns related to the solvothermal methods. Accordingly, several research groups exploited the potential of base additives as deprotonating agents for reducing the ligand-to-metal ratio. For instance, Gross and his co-workers reported the synthesis of pure ZIF-8 at Zn:Hmim ratio of 1:4 using triethylamine (TEA) for a reaction time of 10 minutes[57].

Ionothermal synthesis

Ionothermal synthesis is an environmentally friendly method that uses Ionic liquids (a salt in the liquid state) as solvents due to their negligible vapor pressure, non-flammability and ease of recycling[58, 59]. Morris and his co-workers were the first research group to report the synthesis of ZIF materials using 1-ethyl-3-methylimidazolium bis-[(trifluoromethyl)sulfonyl]imide as an Ionic liquid where they successfully synthesized two novel ZIF materials with unprecedented structures[60].

Sonochemical synthesis

The ultrasound waves employed by sonochemical synthesis leads to the formation and collapse of microbubbles through the reactor volume leading to the generation of high local temperature and pressure throughout the reactor, thus acting as a substitute for heating ovens and minimizing energy consumption[61]. Moreover, ZIF crystals synthesized using sonochemical methods were smaller and more uniform due to the homogeneous dispersion of the nucleation process caused by ultrasound waves[62]. The synthesis of several ZIFs (ZIF-7, ZIF-8, ZIF-11, an ZIF-20) with high percent yields over short reaction times (9 hours) had been reported using sonochemical methods[63, 64].

Reaction Diffusion Framework (RDF)

The synthesis of ZIF-8, ZIF-67 and their mixed metal derivatives using RDF had been recently reported in our lab. First, the metal salts (Zn^{2+}, Co^{2+}) and agar gel are dissolved with DMF and heated up to 100 °C. The solution is then transferred into a pyrex test tube left to cool down at room temperature for gelation to take place. Then, the organic linker (Hmim) is dissolved in water and in an equal volume of DMF solution to be added at the top of the gel and left for few days. The slow diffusion provided by RDF allows for the controlled particle size synthesis where the crystal growth is time-dependent. Moreover, the supersaturated conditions at the interface between the linker solution and the gel induces high rates of nucleation, and as function of time, the saturation gradient decreases along the tube thus favoring crystal growth over nucleation.[?, 7].

Mechanochemical synthesis

This method is a solvent-free technique for ZIF synthesis using mechanochemical setups such as mortars and ball milling machines[65]. Fernandez-Bertran et al.[66] were the first to report the synthesis of ZIF materials by manually grinding a mixture of metal oxides (zinc oxide (ZnO) Cadmium oxide (CdO), etc.) and organic linker (Imidazole) in an agate mortar. The obtained ZIFs exhibited poor porosity and excess amounts of organic linker were used. Later on, Friscic and his

co-workers reported that adding a few amount of solvent (methanol, acetone, etc.) would allow for the stochiometric synthesis of ZIFs by enhancing the mobility of the reactants[67, 68].

1.2.4 ZIF Applications

The intrinsic properties of ZIF materials such as their exceptional chemical stability in various organic solvents, permanent and tunable porosity motivated the scientists to exploit the application of ZIFs in diverse fields such as gas storage and separation, catalysis, water treatment, and drug delivery. Accordingly, some of the ZIF applications are briefly described below.

Gas storage and separation

Gas storage and separation is one of the most challenging and promising research fields due to its multidisciplinary aspect that is related to environmental, industrial and energy storage applications. Solid porous materials such as zeolites, are used as adsorbents to selectively separate the desired molecule from a mixture via the molecular sieving effect[69, 70]. Through this process, certain molecules are restricted from entering the pores of an adsorbent, thereby preventing further adsorption on the inner surface while other molecules are allowed to enter the pores and adsorb on the surface. Accordingly, the storage and selectivity of a certain adsorbent is proportional to the pore volume or surface areas of the adsorbent[50]. However, it was mentioned earlier in the introduction that one of the main limitations of zeolites is that their applications have been restricted to small molecules due to difficulties in designing extra large cavities. From this limitation rises the supremacy of ZIF materials in the field of gas storage and separation due to the vast array of organic linkers that can be employed to tune the pore size of zeolitic framework depending on the target gas molecule.

CO_2 and H_2 gases are the main concern in environmental and energy applications respectively, thus the application of ZIF materials for gas storage and separation was mainly focused on these two molecules. Li and his co-workers [71, 72] reported that ZIF-7 showed a high H_2/CO_2 selectivity (6.48) due to the fact that ZIF-7 has a pore size of 0.3 nm which is between the kinetic diameters of CO_2 and H_2 (0.33 and 0.29 nm respectively) which favored the capture of H_2.

Moreover, ZIF-8 that is characterized by a 0.34 nm pore size aperture showed superior performance in separating H_2 from large gas molecules. For instance, Bux et al.[73] showed that ZIF-8 had a high H_2/CH_4 separation factor (11.2) due to the large size of CH_4 (0.38 nm) compared to the pore size of ZIF-8.

Furthermore, Yaghi and his co-workers[42] reported the synthesis of two colossal ZIFs: ZIF-95 and ZIF-100 with pore sizes of 0.365 and 0.335 nm respectively that

showed superior performance as selective carbon dioxide reservoirs out of various mixtures (CO_2/CH_4, CO_2/CO, CO_2/N_2) compared to BPL carbon that is widely used in gas storage and separation industry.

Water treatment

The use of ZIF materials as adsorbents for water treatment from heavy metals and organic dyes had been investigated by several research groups. ZIFs in general possess hydrophobic cages due to organic linkers which reduces the chances for water adsorption on the microporous surface. However, computational studies (such as DFT (density functional theory) calculations and GCMC (grand canonical Monte Carlo method) simulations) showed that the process of adsorption takes place at the external surface area due to lewis acid- basic sites that result from crystal defects and the dissociative adsorption of water[74, 75].

For example, Li et al.[76] reported that applying ZIF-8 for trace arsenate (As) removal from water outperformed other adsorbents with an unprecedented adsorption capacity of 76.5 mg/g at low equilibrium concentration of 9.8 μ/L. Moreover, Huang[77] and his co-workers applied both ZIF-8 and ZIF-67 for removing Pb^{2+} and Cu^{2+} from wastewater. The saturated adsorption capacities using both ZIFs was 1348.42 mg/g for Pb^{2+} and 617.51 mg/g for Cu^{2+} which is higher than the adsorption capacity of other porous materials.

The potential of ZIF materials for organic dye removal from water was investigated through the most typical organic dyes such as congo red, and methyl orange. For instance, Zhang et al.[78] reported that the adsorption capacities of ZIF-67 on congo red and methyl orange are 3900 and 1340 mg/g respectively with a constant removal efficiency of both dyes for five cycles.

Drug delivery

The chemical stability, pH sensitivity, and drug loading capacities are the main parameters considered in the design of drug delivery vehicles. Accordingly, the intrinsic properties of ZIF materials such as their exceptional chemical stability in aqueous solvents, their tunable microporosity that allows for increased drug loading capacity, and the sensitivity to low pH values qualifies them to be promising candidates as drug delivery vehicles.

Sun et al.[46] reported the first use of ZIF-8 as an efficient pH-sensitive drug vehicle for the delivery of anticancer agents. Their study shows that ZIF-8 possess a pH-sensitive dissolution property at mild acidic conditions (pH = 5) that provides an excellent control on drug release, and remarkable loading capacity of Fluorouracil (around 660 mg/g).

Moreover, the significant high thermal stability of ZIF materials may act as a pro-

tection shield for the encapsulated drug at high processing temperatures. For instance, Liedana et al.[79] reported the encapsulation of Caffeine - an amphiphilic drug with significant lipolytic activity and cosmetic applications - in ZIF-8 that allows for the controlled release of the dug along with the thermal protection in case of high temperature process.

Catalysis

Catalysis is the process of accelerating the rates of chemical reactions through utilizing small amounts of inert materials called catalysts that can be regenerated and reused at the end of the reaction. In general, a catalyst lowers the activation energy needed for a reaction to proceed, thus providing an alternative low energy pathway that can be achieved at mild conditions and faster rates compared to the non-catalyzed mechanisms.

Heterogeneous catalysis is a type of catalysis where each of the catalyst and the reactants or products exist in a different phase, therefore adsorption is a critical property of a heterogeneous catalyst. Accordingly, the tunable and permanent porosity, high surface area, chemical and thermal robustness are the main parameters to be considered in the design of heterogeneous catalysts, as they ensure high adsorption capacities and long life times.

Owing to their intrinsic properties, ZIF materials showed superior performance in diverse catalytic applications such as transesterification[75], Friedel-Crafts acylation[80], synthesis of carbonates[81], etc. For instance, Kalidindi et al.[82] reported the use of ZIF-8 for the dehydrogenation of dimethylamine borane (DMAB) that is considered to be a high-capacity hydrogen-storage material. The main challenge in the use of DMAB in fuel cells is the sluggish kinetics of dehydrogenation at temperatures below 130 °C[83] which is significantly higher than the standard fuel-cell operating temperatures (<85°C)[84]. However, the strong caging effects combined with the polar and Lewis acid/base properties of ZIF-8 porous matrix allowed the dehydrogenation process to be achieved at room temperature and to re-activate the ZIF-8 cavities at 70°C which is much lower than the operating temperature limit of fuel cells.

Furthermore, Xue and his co-workers[85] reported the use of ZIF-8 as a robust catalyst for oxygen reduction reaction (ORR) in microbial fuel cells (MFC). The ZIF-8-MFC showed an outstanding ORR performance in a neutral pH solution with a maximum power density that is 1.62 times higher than regular Pt/C-MFC over a 110 hour operation time.

1.3   ZIF-L and ZIF-(8, 67)

1.3.1   Transition from ZIF-L to ZIF-(8, 67)

Among the ZIF family, ZIF-8 is the most studied due to its exceptional thermal stability (up to 600 °C), large surface area (up to 1800 m^2/g), and chemical stability in various organic solvents[5]. ZIF-8 adopts a sodalite topology (SOD) and a cubic crystal structure formed by the tetrahedral coordination between Zn^{2+} ions and 2-Methylimidazole (Hmim) with the molecular formula (Zn(mim)$_2$)(Fig. 1.10).
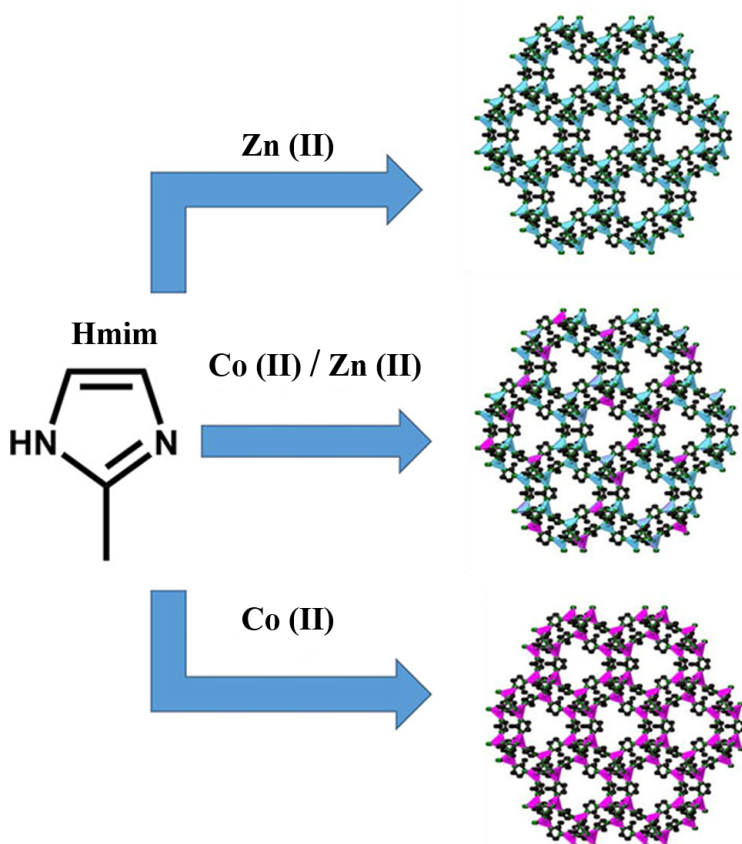
Figure 1.10: Reaction scheme between 2-Methylimidazole (Hmim) and Zn(II) and/or Co(II) to give the ZIF crystals. Adapted from [7]

Usually, ZIF-8 is synthesized via solvothermal techniques using organic solvents such as N,N-dimethylform-amide, and methanol[86][5]. Such techniques, when considered for the scaled-up synthesis of ZIF-8 would pose economic and environmental challenges due to expensive and toxic organic solvents, and energy consumption associated with further procedures to purify and activate the products. Accordingly, the scientific community investigated alternative green synthetic

routes. Yichang[56] and his coworkers reported the synthesis of ZIF-8 nanoparticles in pure aqueous medium at room temperature. However, the used Zn:Hmim ratio was significantly high (1:70). Later on, researchers investigated the synthesis of ZIF-8 at lower ratios. Gross[57] and his co-workers used triethylamine (TEA) with low Zn:Hmim (1:16) for the aqueous synthesis of ZIF-8. Although the obtained nanoparticles displayed a polyhedral morphology, the products exhibited low surface area when compared to literature values.

Kida et al.[87] investigated the synthesis of ZIF-8 in pure aqueous medium by varying the Zn:Hmim ratio from 1:20 to 1:100. All products below 1:40 exhibited poor crystallinity and mixed crystal structure probably due to impurities while products above 1:40 were confirmed to be ZIF-8. Moreover, crystal size decreased from micrometer to nanometer with the increase of the Zn:Hmim ratio, thus reflecting the importance of ligand saturation on the rate of formation and crystal growth. In 2013, Chen et al. [88] reported the synthesis of a new two-dimensional zeolitic imidazolate framework ZIF-L at 1:8 Zn:Hmim ratio in an aqueous medium. ZIF-L crystallizes in an orthorhombic system with the formula $(Zn(mim)_2(Hmim)_{1/2}(H_2O)_{3/2})$. Like ZIF-8 $(Zn(mim)_2)$, all Zn atoms are tetrahedrally coordinated in the form ZnN_4; however, in ZIF-L there exist two crystallographic types of Zn atoms. Zn_1 is bridged to neighboring metals through four imidazolate units, while Zn_2 is bridged through three units and coordinated to a single imidazolate molecule(fig. 1.11). The two-dimensional layers stack up to form the ZIF-L framework which is stabilized by hydrogen bonding between the singly coordinated imidazole and the free Hmim molecule that exists between the layers. Despite its low surface area (160 m^2/g), ZIF-L showed superior selectivity for CO_2 adsorption (up to 0.94 mmol/g) when compared to other ZIFs with higher surface area (ZIF-8, ZIF-95, ZIF-100). Since both ZIF-L and ZIF-8 share the same precursors, it is well accepted that the orthorhombic topology of ZIF-L is a part of the SOD topology of ZIF-8 (see Fig. 3 in[88]). This topological resemblance along with the importance of Zn:Hmim ratios and the choice of solvent inspired the scientific community to investigate the possibility of a topotactic phase transition from ZIF-L to ZIF-8.

Low et al.[89] reported the first study of ZIF-L to ZIF-8 transition upon heating previously prepared ZIF-L in various organic solvents (DMF, EtOH, MeOH, acetone, etc.) at 60 °C for 72 hours. The detailed characterization of ZIF samples as a function of time was limited to the transition in EtOH. A mixture of ZIF-L and ZIF-8 was obtained between 4 hours and 48 hours where the PXRD patterns show the increase in the intensity of the three main characteristic peaks of ZIF-8 at $2\theta = 7.3°$, 12.7°, and 18.0° as a function of time. Pure ZIF-8 was obtained after 72 hours and exhibited a BET specific surface area of 1333 m^2/g; however, the morphology was not polyhedral (nanoflakes). Low suggested that the transformation should be accompanied by the increase of [Hmim] in the solution since ZIF-L contains an additional Hmim per two Zn centers while ZIF-8 does not; as
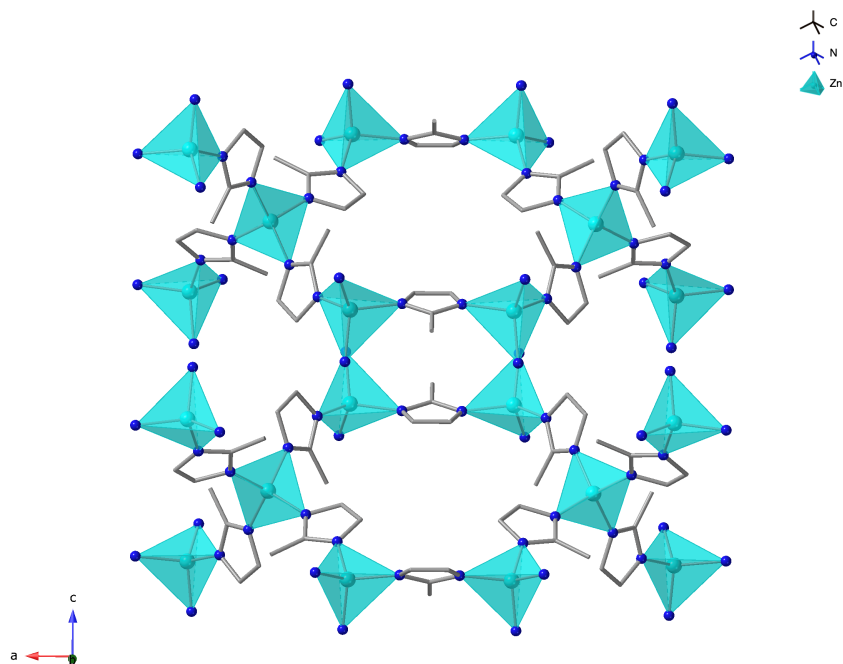
Figure 1.11: The two-dimensional layer structure of ZIF-L.

such the increase of [Hmim] in the solution would provide indirect evidence concerning the transformation mechanism. For this reason, the phase transition was monitored by in situ ^{1}H NMR. It was observed that the intensity of resonance peaks at 2.4 ppm and 7 ppm (correspond to CH_3- and $CH-$ of Hmim) increased as a function of time, thus ensuring that the transformation does not proceed via dissolution-recrystallization since there was no consumption of released Hmim. The Sharp-Hancock plot[90] of this transformation supports a phase transition that follows a geometric contraction model.

Later on, Zhang and his coworkers[91] substituted Co^{2+} for Zn^{2+} such that the Co:Hmim was 1:8. The PXRD pattern for the synthesized product was identical to that of ZIF-L, as such the new product was considered to be ZIF-L-Co. Like ZIF-8, ZIF-67[92] possesses a sodalite topology and cubic crystal structure formed by the tetrahedral coordination between Co^{2+} and [Hmim]. Based on this analogy and the fact that ZIF-L-Co and ZIF-67 share the same precursors, Zhang and his co-workers investigated the possibility of ZIF-L-Co to ZIF-67 phase transition as a function of Co:Hmim ratio at room temperature in an aqueous medium. ZIF-L-Co was the dominant phase for ratios below 1:32, while ZIF-67 was the dominant phase for greater ratios (1:40 and 1:48). To understand the formation mechanism of ZIF-67 and its relation to ZIF-L-Co, the ratio was fixed at 1:48 and samples were taken at different time intervals to be analyzed by powder x-

ray diffraction (PXRD) and scanning electron microscopy (SEM). For the first 10 min, the dominant phase was ZIF-L-Co with nanoflake morphology, as a function of time, the intensity of ZIF-67 peaks increases along with the gradual growth of the nanoflakes into polyhedral-shaped crystals. After 120 min, pure ZIF-67 is obtained with well-defined polyhedral crystals without any intermediates. This ensures that initially ZIF-L-Co is formed then it undergoes a phase transition to yield ZIF-67.

Fu et al.[93] reported the phase transition from ZIF-L to ZIF-8 controlled by the presence of polyvinylpyrrolidone (PVP) as a function of reaction time. In their study the Zn:Hmim was fixed at 1:8 with the addition of PVP. After a reaction time of two hours, rhombic dodecahedral was obtained upon washing the products with EtOH, while irregular shaped ZIF-L was obtained upon washing with pure water. For the case where pure water is used as a washing solvent, further reaction times influenced the morphology of ZIF-L where rod-like crystals were obtained after 10 hours. However, when EtOH was the washing solvent, after a reaction time of 10 hours, both ZIF-L (rod-like) and ZIF-8 (rhombic dodecahedral) were obtained, and for reaction times greater than 10 hours (15 h and 24 h) only rod-like crystals were obtained. To confirm the role of PVP in the phase transition, the same reaction conditions were performed in the absence of PVP and using EtOH as a washing solvent yielded leaf-like ZIF-L. Thus phase transition was controlled by PVP and EtOH.

The most recent study on the phase transition from ZIF-L to ZIF-8 was reported by Khan et al.[94] using triethylamine (TEA) as a deprotonating agent in an aqueous medium. The Zn:Hmim was fixed at 1:8 and the TEA/Total mole fraction was varied between 0.0002 and 0.002, the reaction time was 60 min for all samples. ZIF-L crystals with the leaf-like structure were obtained for mole fractions up to 0.0005 (with 0.0001 increments). As the TEA:Total mole ratio increased (0.00006 and 0.0009), the leaf-like structure broke down into flower-like clusters denoting the transition phase. When the mole fraction was increased to 0.002, pure ZIF-8 crystals were obtained that exhibited cubic hexagonal morphology, a thermal stability up to 600 °C, and a high specific BET surface area 1472 m^2/g.

1.3.2 Controlled Particle Size Synthesis of ZIF-8

Importance of particle size

Several studies have been reported to investigate the effect of crystal size on the performance of ZIF-8 in various applications. For instance, Linder-Patton et al.[95] studied the influence of crystal size on the catalytic activity of ZIF-8 for transesterification and Knoevenegal condensation reactions. In their study, they observed that ZIF-8 nano-crystals had a better performance than the micron-sized crystals due to high amounts of Zn^{2+} leaching from the nanoparticles.

Therefore, they concluded that ZIF-8 nano-crystals are more susceptible to mechanical degradation due to surface etching throughout the reaction course than larger crystals that enhanced the overall catalytic activity. Moreover, other studies reported that ZIF-8 nano-crystals have higher surface areas and decreased diffusion resistance that enhances the adsorption properties in gas storage and separation[96, 97].

Factors that influence the particle size

The main synthetic factors that control the particle size distribution of ZIF-8 are the choice of solvent, nature of metal source, temperature and the Zn:Hmim ratio. The effect of these factors on the resultant particle size of ZIF-8 material had been extensively investigated by several research groups that will be discussed briefly.

The Nature of Metal Source: To understand the metal source effect on the particle size of ZIF-8, Schejn and his co-workers[98] fixed the Zn:Hmim at 1:8 and a reaction time of 1 hour at room temperature. The zinc salts used were as follows: zinc acetylacetonate hydrate ($Zn(acac)_2$), zinc nitrate ($Zn(NO_3)_2$), zinc sulfate ($ZnSO_4$), zinc aceteate ($Zn(OAc)_2$), zinc chloride ($ZnClO_4$), zinc iodide (ZnI_2), and zinc bromide ($ZnBr_2$). The particle size of the crystals obtained was: 85, 192, 247, 312, 480, 388, 589 and 1160 nm respectively.

The Choice of Solvent: Bustamante et al.[99] investigated the influence of several solvents on the particle size of ZIF-8. In their study, $Zn(NO_3)_2$ was used as a metal source and the Metal:Hmim ratio was fixed at 1:8 and all the reaction took place at room temperature. The solvents investigated were: Methanol, Ethanol, n-Propanol, 2-Propanol, n-Butanol, 2-Butanol, and n-Octanol. The resultant particle size of the ZIF-8 crystals obtained was: 134, 342, 212, 421, 324, 372, and 413 nm respectively. Moreover, in their study they reported that ZIF-8 phase was not obtained upon using water as a solvent at the mentioned conditions.

The Zn:Hmim ratio: For ZIF-8 synthesis, the Zn:Hmim is the most critical parameter that controls the nature and size of the resultant ZIF material. Jian and his co-workers[100] reported that for the aqueous synthesis of ZIF-8 using $Zn(NO_3)_2$ as a metal source at room temperature, ZIF-8 micron-sized crystals is not obtained only until the Zn:Hmim reached 1:35. Moreover, upon increasing the Zn:Hmim ratio up to 1:70, the crystal size dropped from the micron scale to the nano scale, thus reflecting the importance of ligand supersaturation on the size of ZIF-8 particles.

The Temperature Effect: The reaction temperature effects the crystals size indirectly through its influence on the Hmim levels of supersaturation. Accordingly, the low solubility of Hmim at lower temperatures would result in high levels of supersaturation that favors the formation of nano sized ZIF-8 crystals[101, 102].

Micromixers for the Controlled Particle Size Synthesis of ZIF-8

Although the synthesis of ZIF-8 nanoparticles had been successfully reported using conventional batch reactors[56, 103, 104, 105], the main challenge was in the reproducibility of these results. It is well known that the rate of chemical reactions that yield only one product is directly related to the quality of mixing. Considering the case of ideal mixing, reactants would be uniformly mixed in the reactor's space in a time scale shorter than that of the reaction, thus the rate is limited by the molecular diffusion between the reactants. However, in the case of poor mixing, the reaction's time scale would be longer than that of mixing, therefore the reaction's rate would be limited by the rate of mixing. Moreover, the absence of automation and human errors leads to significant batch-to-batch variations thus failing to ensure reproducibility of the synthesized products. Moreover, the use of batch reactors for the scaled up synthesis of ZIF-8 would demand high levels of energy consumption thus increasing the overall cost of the synthesis process.

To overcome these limitations, scientists exploited the potential of micro mixing synthetic routes for the fast and continuous synthesis of ZIFs. Such techniques follow a two-step process through which the precursor solutions are fed into syringes that are pumped into a micromixer. The main advantage of micromixers is the high surface-to-volume ratio they provide due to miniaturized mixing volumes (diameter of the mixing cavity in the ranges of mm to μm), thus increasing the contact area between the reactants and enhancing the reaction's kinetics.

Moreover, flow regimes in the mixer can be easily controlled and quantified using the Re formula (equation 1.1). For $Re < 2000$ viscous forces dominate and the flow regime is considered laminar, consequently the reactants mixture would have an elevated scale of segregation (poor mixing) that minimizes the interfacial area for molecular diffusion. However, for $Re > 4000$, the inertial forces dominate and the flow regime is turbulent and characterized by a reduced scale of segregation (ideal mixing) for the reactants mixture and increased interfacial area for molecular diffusion[1]. When using micromixing for synthesis all variables in the Re equation are constant except for the flow rate which can be set to different values by the operator. This allows for minimal energy consumption by the pumps where the flow rate can be optimized to a minimal value that ensures turbulent flow.

Yamamoto and his co-workers[101] were the first research group to report the synthesis of ZIF-8 in an aqueous medium using micromixing technology. In their study, they studied the particle size of ZIF-8 as function of Re using a T-shaped micromixer (inner diameter (ID) of 330 μm). ZIF-8 particle size decreased from around 500 nm to reach 200 nm as the Re increased from 100 to 2000, where the flow regime is laminar. Interestingly, for $2000 < Re < 4000$ where the flow regime is in a transition state between laminar and turbulent, the particle size reached

a constant value of 188 nm $\pm$ 33 nm. In addition, Polyzoidis et al.[106] reported that using a T-shaped micromixer (ID = 550 μM), the synthesis of ZIF-8 was scaled up to around 640 g/day using a mixture of methanol and ammonia as a solvent.

Later on, Watanabe et al.[102] investigated the potential of a central collision-type micromixer (also known as K-mixer[107]) for the synthesis of mono disperse ZIF-8 nanoparticles. The K-mixer design features an inlet plate that branches each of the two inlet streams into seven channels (channel width of 100 μm) radially arranged around the mixing plate where the fluids collide. After collision, the reaction solution flows out the micromixer through an outlet plate channel with a size of 360 μm. The synthesis of ZIF-8 was achieved in an aqueous medium at Zn:Hmim ratios ranging from 1:40 to 1:200. The maximum size obtained using the K-mixer was 1.8 μm $\pm$ 0.2 μm at R = 40 and $[Zn^{2+}]$ = 0.025 M, while the minimum size obtained was 51 nm $\pm$ 20 nm at Zn:Hmim 1:200 and $[Zn^{2+}]$ = 0.025 M.

The most recent study on using micromixers for the controlled particle size synthesis of ZIF-8 was reported by Parulkar and Brunelli[108]. In their study, they used a Jet micromixer that is composed of a main line that has an inlet and outlet port along the axis with diameter of 0.5 mm, and two jet-mixing inlets directed radially inward (diameter of 0.25 mm) to combine with the flow through the mainline. ZIF-8 synthesis was done using methanol as a solvent; triethylamine base (TEA) was used to accelerate deprotonation of the organic ligand in the aim of achieving a stoichiometric synthesis of ZIF-8 (i.e Hmim/Zn = 2) instead of the supersaturated use of Hmim reported in previous studies (Zn:Hmim 1:70). The minimum size they reached was 57 nm $\pm$ 8 nm at which the Hmim:Zn:TEA molar ratio was 2:1:2.

1.3.3 ZIF-(8, 67) Mixed Metal Derivatives

ZIF-8 and ZIF-67 share the same sodalite topology which allows the synthesis of bimetallic (Zn, Co) ZIF-8 without altering the framework's topology (Fig. 1) leading to significant enhancement of the ZIF material's catalytic properties. For instance, Saliba[7] and his co-workers reported that doping ZIF-8 with cobalt extended the photocatalytic activity of ZIF-8 from the ultraviolet to the visible region through reducing the large optical band for ZIF-8. Furthermore, it had been reported that cobalt doped ZIF-8 showed higher uptake capacity of CO_2 and H_2[109], in addition to an enhanced catalytic performance for the chemical fixation of CO_2[110].

1.4 Aim of the Present Work

The main challenges in the field of ZIF research are the development of environmentally friendly and cost effective synthetic routes, and the controlled particle size synthesis of the ZIF crystals. Although the synthesis of ZIF-8 nano crystals in aqueous medium had been successfully reported, excessive amounts of organic linker had been employed, since at stochiometric Zn:Hmim ratios, ZIF-L is obtained. Moreover, the poor mixing performance at the macroscale of conventional batch reactors and the absence of automation, result in severe fluctuations of ZIF-8 particle size between different trials under the same conditions.

To overcome these challenges, in the present work, we report the potential of a multi-inlet vortex mixer (MIVM) for the synthesis of pure ZIF-8 at relatively low Zn:Hmim ratios, and for the reproducible particle size synthesis. In the first part of our study, we varied the Zn:Hmim ratio in order to identify the minimum value necessary for yielding ZIF-8. The Zn:Hmim ratio is then fixed at a value that normally gives ZIF-L, then we vary the Zn-Hmim flow rates thereby increasing the local Zn:Hmim ratio in the mixing chamber up to a value that yields ZIF-8 with reduced organic ligand consumption. The same procedure is followed to study the transition from ZIF-L-Co to ZIF-67.

In the second part of the study, we report the controlled particle size synthesis of ZIF-8, ZIF-67 and their mixed metal derivatives as function of Reynolds number (Re). The mean particle size and the standard deviation from the mean of all ZIF samples significantly decrease as the Re increases. Moreover, the performance of the MIVM for the reproducible synthesis of ZIF-8 nanoparticles is shown to be better than that of a conventional batch reactor. Finally, we report the controlled cobalt doping of ZIF-8 as function of initial Zn:Co ratios of the metal precursor solution, and as a function of varying the flow rates of metal precursor solutions that have the same concentration.

Chapter 2

Materials and Methods

2.1 Synthesis of ZIF Crystals

2.1.1 Materials

Zinc nitrate hexahydrate ($Zn(NO_3)_2 \cdot 6H_2O$, 99% purity) was purchased from Fisher scientific, Cobalt nitrate hexahydrate ($Co(NO_3)_2 \cdot 6H_2O$, 99% purity) from Strem chemicals and 2-Methylimidazole (Hmim, 99% purity) was bought from ACROS. All materials were used without any further purification.

2.1.2 Mixing Apparatus

The multi-inlet vortex mixer (MIVM) is characterized by four inlet ports with a diameter of 0.11 cm, a circular main mixing cavity with a 0.6 cm diameter and depth of 0.15 cm, and an outlet port of 0.13 cm diameter and 1.35 cm length. The precursor solutions were pumped into the mixer using two digitally controlled pumps (Harvard Apparatus, PHD 2000 programmable, Holliston, MA).

2.1.3 Transition From ZIF-L-(Zn, Co) to ZIF-(8, 67)

The concentration of metal ions was kept constant through all the experiments $[Zn^{2+}] = [Co^{2+}] = 0.05$ M. For the transition as function of Zn:Hmim ratio, solutions with [Hmim] = 0.5 M, 0.75 M, 1, 1.25 M, 1.5 M, 1.75 M were prepared. As such the Zn:Hmim ratios were as follow: 1:10, 1:15, 1:20, 1:25, 1:30, and 1:35, respectively. The precursor solutions where fed to four syringes (two for metal ions, and two for Hmim) to be pumped into MIVM. The flow rate of all syringes was fixed at 10 mL/min.

As for the transition as function of Zn:Hmim flow rate, the organic linker concentration was fixed at [Hmim] = 0.15 M. Two syringes were filled with Zn^{2+} and
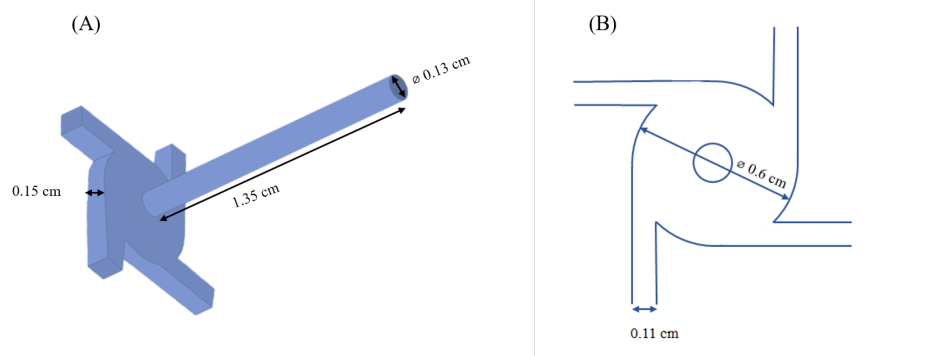
Figure 2.1: Three dimensional (A), and schematic representation (B) of the MIVM showing the dimensions of the four inlets, the outlet, and the main mixing chamber.

the other two with Hmim. The flow rate for the Zn ions was fixed at 10 mL/min while that for Hmim was varied as follows: 10 mL/min, 15 mL/min, 20 mL/min, 25 mL/min and 30 mL/min. The same procedure was followed for ZIF-L-Co to ZIF-67 transition. All solutions were prepared using double distilled water. The collected ZIF samples were aged for 1 2 hours followed by centrifugation at 5700 rpm for 15 min. The samples were washed four times with ethanol (EtOH) and freeze dried overnight for characterization.
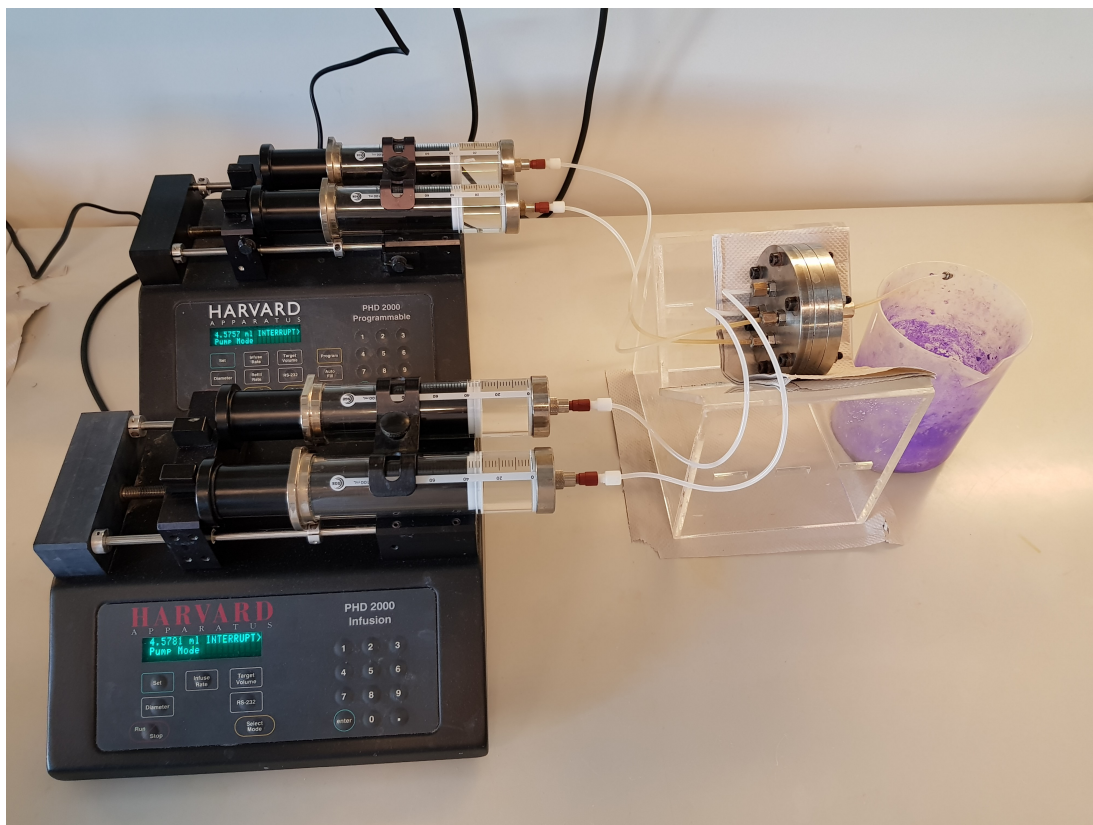
Figure 2.2: An image showing the mixing apparatus composed of two pumps, four syringes, and the multi-inlet vortex mixer (MIVM).

2.1.4 Particle Size of ZIFs as Function of Reynolds Number (Re)

Two-Syringe System

An aqueous solution of 2-Methylimidazole [Hmim = 3.5 M] is prepared in double distilled water. The aqueous metal precursor solutions were prepared in double distilled water where the total metal concentration was [M^{2+} = 0.05 M](for ZIF-8 M = Zn^{2+}, for ZIF-67 M = Co^{2+}, for bimetallic ZnCo-ZIF-8 three atomic Zn:Co ratios are used as follows : 75:25, 50:50, and 25:75). Each precursor solution is fed into two separate syringes. The synthesis of all ZIFs is done at three flow rates : 6 mL/min, 20 mL/min, and 59 mL/min. The samples are then centrifuged at 5700 rpm for 20 minutes to remove excess solvent, then washed four times in ethanol, and dried overnight for further characterization.

Four-Syringe System

The four syringes system study is done only for ZIF-8. The same concentrations of the precursor solutions were used ($[Zn^{2+}]$ = 0.05 M and [Hmim] = 3.5 M). However, the total number of used syringes is four where each of the metal and organic linker solutions are fed into two syringes. The synthesis of ZIF-8 is done at the following flow rates: 0.625 mL/min, 10 mL/min, 20 mL/min, 30 mL/min, 40 mL/min, 50 mL/min, and 60 mL/min.

Batch Synthesis of ZIF-8

The synthesis of ZIF-8 is done by adding 6 mL of Hmim solution ([Hmim] = 3.5 M) to a 50 mL beaker containing 6 mL of Zn^{2+} solution ($[Zn^{2+}$ = 0.05 M]). The reaction is left to proceed for 30 min at a stirring rate of 500 rpm at room temperature.

Viscosity Measurement

The viscosity of the Hmim solution was measure using a Discovery Series Hybrid Rheometer—DHR (TA-Instruments, NewCastle, DE, USA), at 25 °C.

Controlled Cobalt Doping of ZIF-8 as Function of Flow Rate

For this study the total number of syringes used is three. The three syringes were fed with the following aqueous solutions: $[Zn^{2+}]$ = 0.05 M, $[Co^{2+}]$ = 0.05 M, and [Hmim] = 3.5 M respectively. The flow rate for the pump that holds the [Hmim] and one of the metal solutions (Zn^{2+} or Co^{2+}) syringes was fixed at 60 mL/min. The flow rate of the second pump holding the other metal solution (Zn^{2+} or Co^{2+}) is varied as follows: 15 mL/min, 30 mL/min, 45 mL/min, 60 mL/min.

2.2 Characterization of ZIF Crystals

All ZIF samples synthesized were centrifuged at 5700 rpm for 20 minutes, then washed four times in ethanol and freeze-dried overnight for characterization.

2.2.1 Powder X-ray Diffraction (PXRD)

The powder X-ray diffraction (PXRD) patterns were recorded on a Bruker D8 Advance XRD diffractometer using $CuK(\alpha)$ radiation (λ = 1.5406 Å) at 40 kV and 40 mA in the 2θ range of 5°-40°. The scanning rate is set at 0.0200 °/second

2.2.2 Scanning Electron Microscopy Analysis (SEM)

Scanning electron microscopy images (SEM) were taken using a Tescan Mira operating at 20 kV. Prior to analysis, samples are coated with a 25 nm layer of platinum using a sputtering machine. The mean particle size of the ZIF samples was calculated using the Mira software from around 100 particles assuming that the crystals are spheres. The errors on the measurements are reported as the sample standard deviation from the mean, calculated using:

$$S = \sqrt{\frac{\sum_{i=1}^{N} (x_i - \bar{x})^2}{N-1}}$$

where S is the sample standard deviation, N is the number of particles, $x_1, x_2, ..., x_N$ is the size of each particle, and $\bar{x}$ is the mean particle size.

2.2.3 Thermogravimetric analysis (TGA)

Thermogravimetric analysis (TGA) of the ZIF samples was performed under nitrogen atmosphere with a heating rate of 5 °C/minute and a temperature ranging from 30 °C to 1000 °C using a TG 209 F1 Iris (Netzsch, Germany).

2.2.4 Nitrogen Adsorption and BET calculation

The specific Brunauer–Emmett–Teller (BET) surface area of the ZIF samples and nitrogen adsorption-desorption isotherms were obtained using a Micromeritics 3Flex analyzer, Micromeritics ASAP 2420 analyzer, and Gemini VII 2390 analyzer. Prior to the N_2 adsorption/desorption measurements, all samples were degassed at 200 °C for 3 hours under nitrogen atmosphere.

2.2.5 Atomic Absorption Analysis (AA)

The ratio of cobalt to zinc incorporated into the ZIF framework of doped samples is determined using THERMO LABSYSTEMS, SOLAAR atomic absorption spectrophotometer with ASX-510 auto sampler, and SOLAAR acquisition data. Prior to the analysis, all ZIF samples were soaked in ethanol for 3 days to clean any trace of unreacted meatl species (Zn^{2+} and Co^{2+}). Then the samples were dissolved using 1 M hydrochloric acid (HCl) solution and diluted with double distilled water.

Chapter 3

Transition from ZIF-L to ZIF-(8, 67)

3.1 Transition as Function of Metal:Hmim Ratio

3.1.1 Microscopic Characterization

The PXRD pattern of the synthesized ZIF samples at different Metal:Hmim ratios compared to the simulated ZIF-(8,67) and ZIF-L are shown in Fig. 3.1. For Zn:Hmim ratios up to 1:20, orthorhombic ($Cmce$ space group with cell parameters $a = 24.1191(5)$, $b = 17.0604(3)$, and $c = 19.7398(4)$) ZIF-L is the dominant phase where the peaks are in good agreement with the simulated pattern of ZIF-L. The SEM images (Fig. 3.2) show a two dimensional leaf-like crystals arranged into hierarchical flower-like morphology. Moreover, since ZIF-L is characterized by major weight loss signal at around 250 °C attributed to the removal of the weakly linked 1/2 Hmim linker and guest water molecules, whereas ZIF-8 withstands temperatures up to 650 °C, therefore, the TGA analysis would give us an insight regarding the phase composition. Moreover, the first derivative of the weight loss (%) as function of temperature (°C) is plotted to clearly visualize the weight loss signals at different temperatures. As such, the TGA curves for those ZIF samples (Figs. 3.5A and 3.6A) show a major weight loss peak at 250 °C thus affirming that only ZIF-L is formed.

When the ratio reaches 1:25, the intensity of the three main characteristic peaks of the SOD cubic ZIF-8 ($I43m$ space group with cell parameters a= 16.9910(12) , b= 6.9910(12) , and c= 16.9910(12)) at 2θ= 7.3°, 12.7°, and 18.0° significantly increases along with the decrease of the ZIF-L peaks. The leaf-like morphology gradually develops into concave octahedral crystals marking the transition from a 2D to 3D structure. Furthermore, the TGA curve shows two major weight loss breakdowns at 250 °C and 650 °C that correspond to ZIF-L and ZIF-8
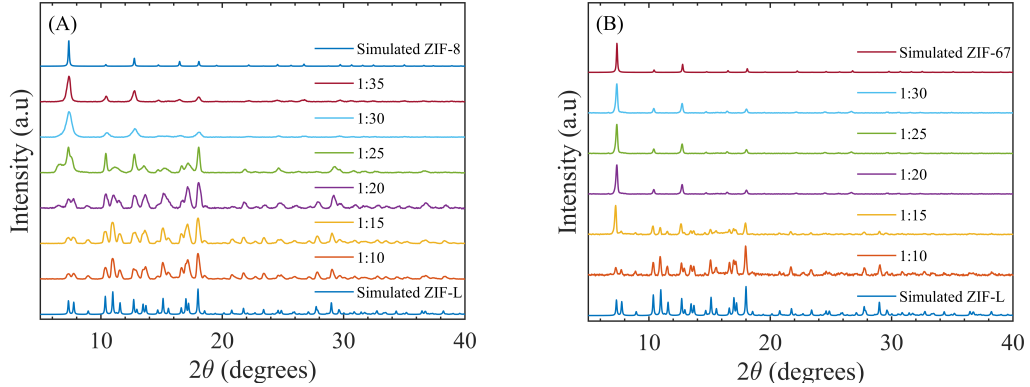
Figure 3.1: PXRD comparison between as synthesized ZIF samples at: (A) different Zn:Hmim ratios and the simulated ZIF-8 and ZIF-L, (B) at different Co:Hmim ratios and the simulated ZIF-67 and ZIF-L.

respectively. Therefore, at 1:25 a hybrid and homogeneous mixture of ZIF-L and ZIF-8 crystals is obtained.

For ratios 1:30 and 1:35 the PXRD is in exact match with that for simulated SOD cubic ZIF-8 with no sign of any peak pertaining to ZIF-L. However, the full transition to pure ZIF-8 is only achieved at a ratio of 1:35 since the TGA curve of 1:30 shows a minor weight loss at 250 °C while that of 1:35 possess a weight loss signal only at 650 °C. Moreover, the SEM images show that for 1:30 the crystals are intermediate between the octahedral and spherical morphology with rigid surfaces remarking that full crystal growth is not accomplished, while for 1:35 the crystals exhibit a smooth spherical morphology ensuring that pure ZIF-8 is formed.

The transition from orthorhombic ZIF-L-Co ($Cmce$ space group with cell parameters $a = 24.1191(5)$, $b = 17.0604(3)$, and $c = 19.7398(4)$) to SOD cubic ZIF-67 ($I43m$ space group with cell parameters $a = 16.9910(12)$, $b = 6.9910(12)$, and $c = 16.9910(12)$) follows the same trend as that of ZIF-L to ZIF-8 with minor differences. For Co:Hmim 1:10, the crystals exhibit a two dimensional leaf-like morphology (Fig. 3.3) and the PXRD pattern (Fig. 3.1) is in exact match with simulated ZIF-L thereby confirming that the major phase is ZIF-L. Although the TGA curve (Figs. 3.5 and 3.6) shows a major weight loss at 240 °C, there is another significant weight loss at around 450 °C which suggests that the transition is already taking place but the proportion of ZIF-67 phase is not enough to be detected by the PXRD. Interestingly, the PXRD pattern for the 1:15 ratio show the signals of both ZIF-L and ZIF-67, and the morphology changes from rod-like to flower-like. The TGA curve is similar to 1:10 ratio, however, the weight loss decreases at 240 °C and increases at 450 °C thereby confirming that the ZIF-67 phase proportion has increased. For ratios beyond 1:15, only ZIF-67 is obtained

as observed by PXRD. The flower-like morphology develops into protruded polyhedron at 1:20 to become smooth and regular at ratios 1:25 and 1:30. Moreover, the TGA curve for the 1:20 ratio shows a major weight loss at 450 °C and a minor weight loss at 240 °C, thereby ensuring that transition is not complete. As for 1:25 and 1:30 ratios, there is only one major weight loss signal at 450 °C which assures that the full transition to ZIF-67 has been achieved.

To further investigate the effect of the initial Metal:Hmim ratio on the size and morphology of the ZIF crystals, the ratio is increased to 1:50 for both ZIF-8 and ZIF-67. Accordingly, a smooth regular polyhedral morphology (Fig. 3.4) is achieved for both ZIF-8 and ZIF-67 crystals rather than irregular protruded polyhedras. As for particle size, both ZIF-8 and ZIF-67 crystals decrease in size; however, the particle size decrease is more significant in ZIF-8 as it reaches the nano scale unlike ZIF-67 where it remains at the micron level.
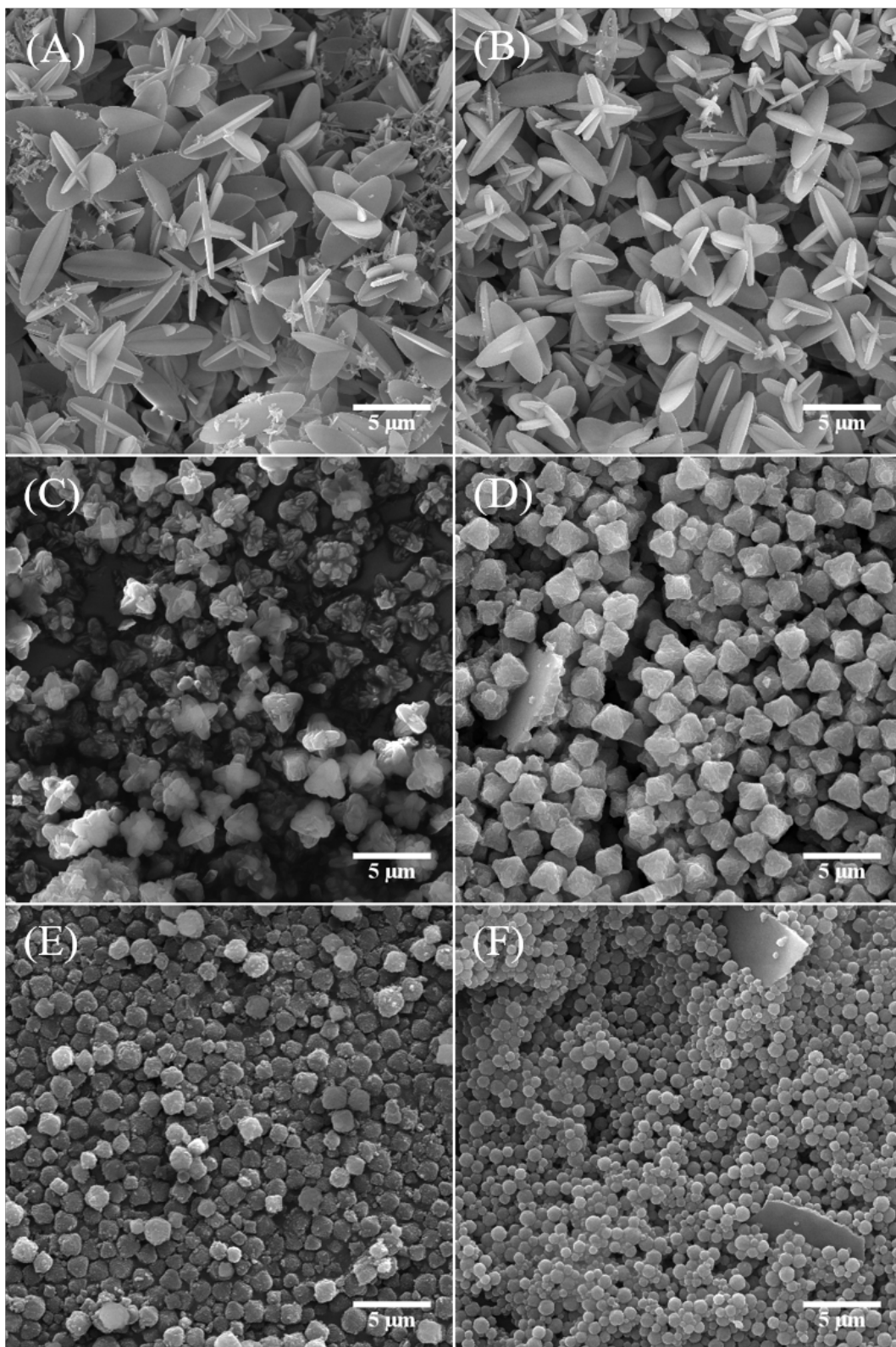
Figure 3.2: SEM images of ZIF samples at different Zn:Hmim ratios: (A) 1:10, (B) 1:15, (C) 1:20, (D) 1:25, (E) 1:30, and (F) 1:35.
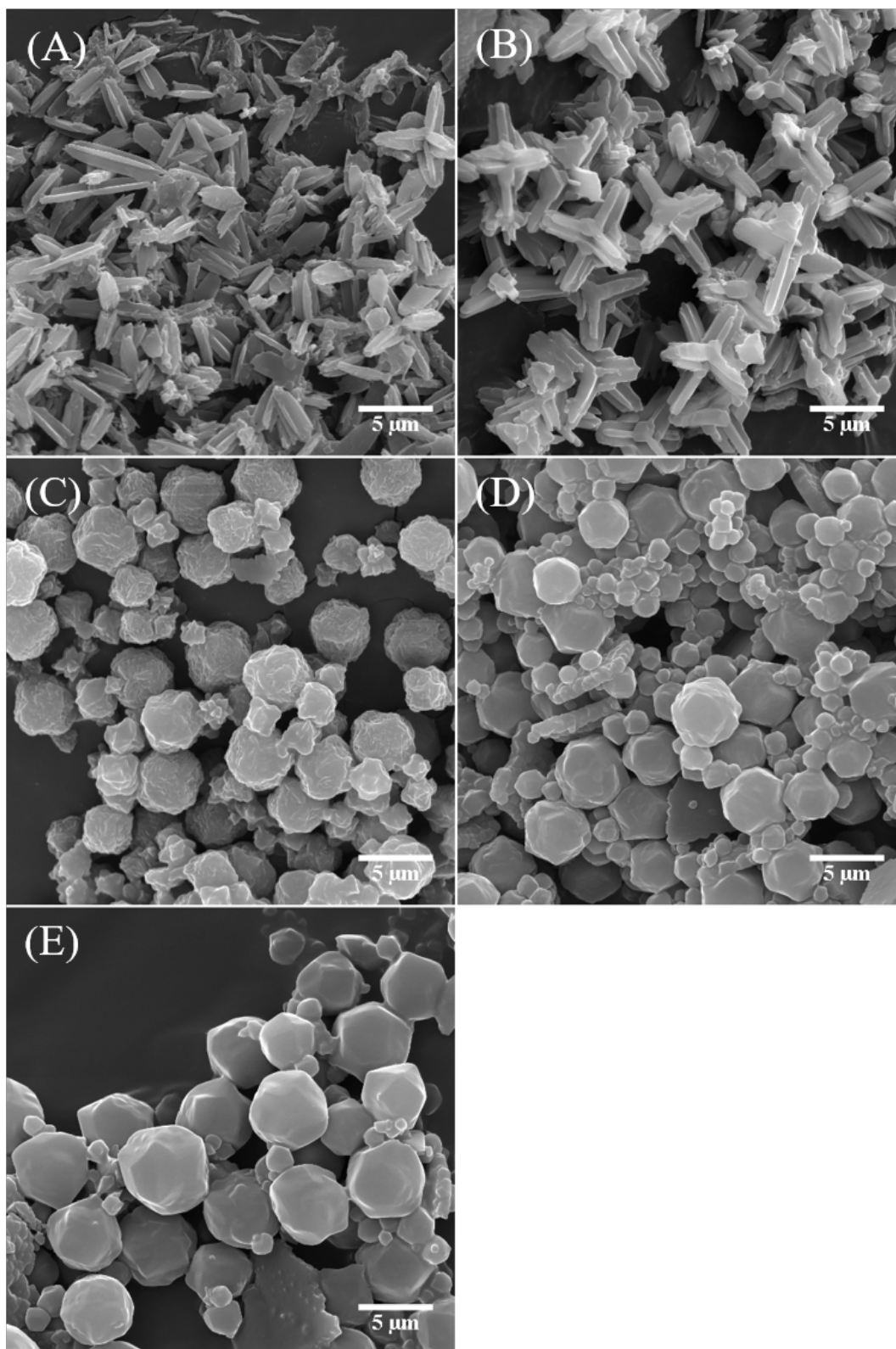
Figure 3.3: SEM images of ZIF samples at different Co:Hmim ratios: (A) 1:10, (B) 1:15, (C) 1:20, (D) 1:25, and (E) 1:30.
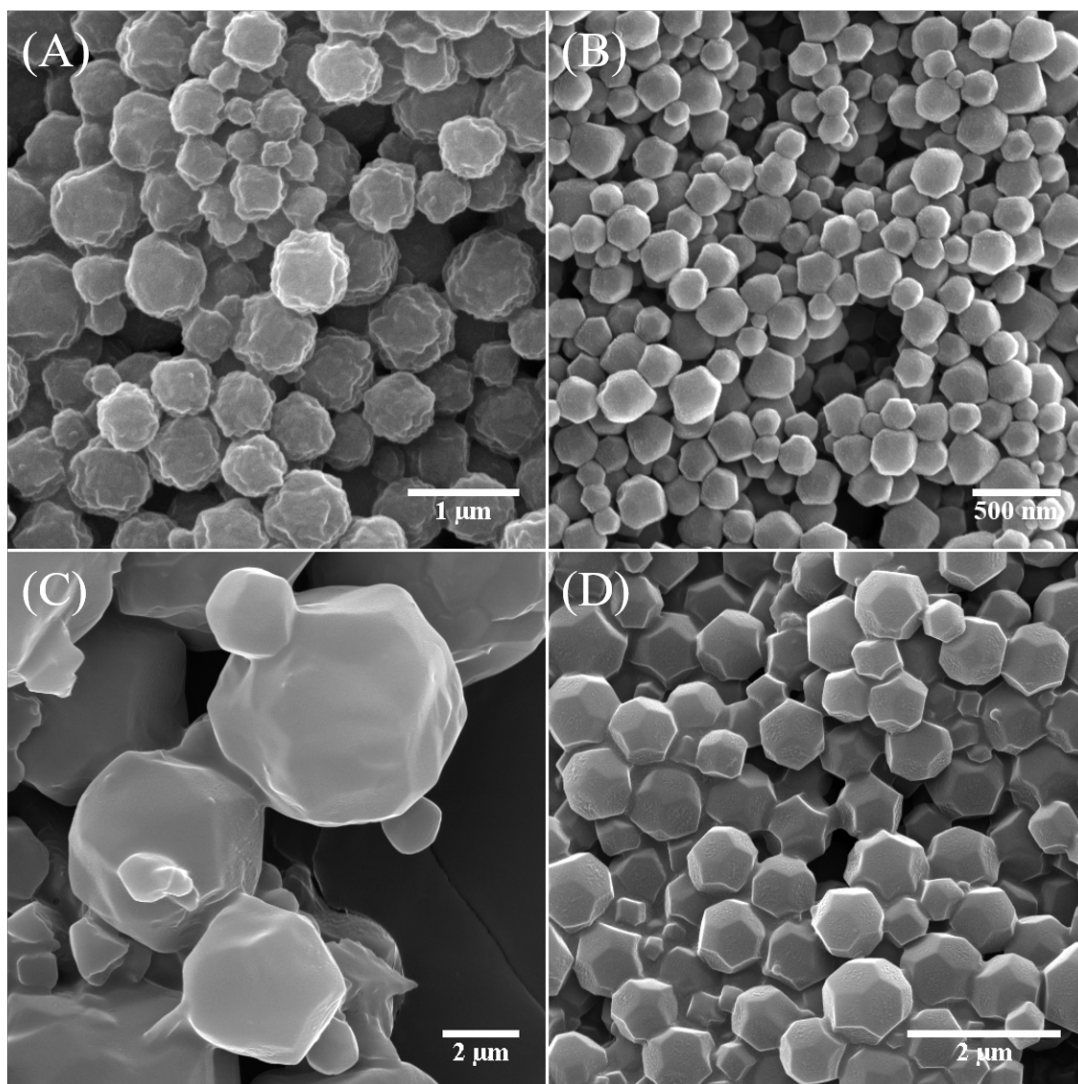
Figure 3.4: SEM images of ZIF samples at: (A) Zn:Hmim 1:35, (B) Zn:Hmim 1:50, (C) Co:Hmim 1:30, and (D) Co:Hmim 1:50 showing the effect of the initial Metal:Hmim ratio on the morphology and size of ZIF particles.
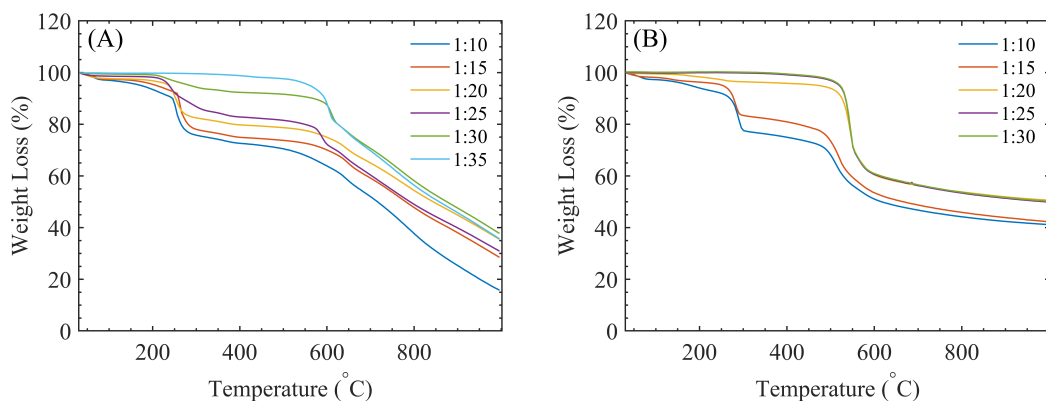
Figure 3.5: Thermogravimetric curves of ZIF samples at: (A) different Zn:Hmim ratios, and (B) different Co:Hmim ratios.

Figure 3.6: First derivative of the weight loss as a function of temperature for the thermogravimetric curves of ZIF samples at: (A) different Zn:Hmim ratios, and (B) different Co:Hmim ratios.

3.2 Transition as Function of Metal-Hmim Flow Rate

3.2.1 Microscopic characterization

After identifying the critical Metal:Hmim ratios to ensure the full transition from two dimensional ZIF-L to three-dimensional ZIF-8/67 at the ratio 1:35 for ZIF-8 and 1:25 for ZIF-67, we managed to achieve the transition for both ZIFs by controlling the flow rate of Hmim. The main goal is to start at a fixed Metal:Hmim ratio of 1:15 where the Metal-Hmim flow rates are varied as follows: 10-10 mL/min, 10-15 mL/min, 10-20 mL/min, 10-25 mL/min and 10-30 mL/min. As such, the local Metal:Hmim ratios in the mixing chamber are expected to increase as follows: 1:15, 1:22.5, 1:30, 1:37.5 and 1:45. Accordingly, the full transition from ZIF-L to ZIF-8/67 is expected at the flow rates 10-25 mL/min and 10-15 mL/min respectively, since these flow rates correspond to Metal:Hmim ratios that lie beyond the critical values necessary for the synthesis of pure ZIF-8/67 identified in the previous section.
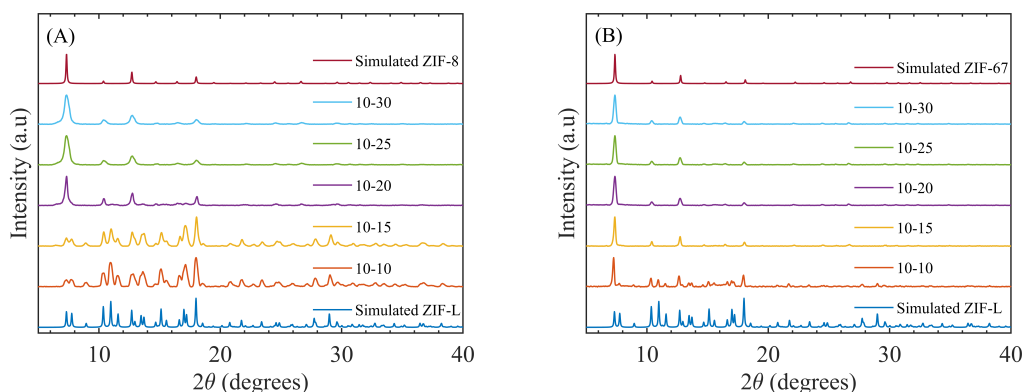
Figure 3.7: PXRD comparison between as synthesized ZIF samples at: (A) different Zn-Hmim flow rates (mL/min) and the simulated ZIF-8 and ZIF-L, (B) at different Co-Hmim flow rates (mL/min) and the simulated ZIF-67 and ZIF-L.

For Metal-Hmim at 10-10 mL/min for both Zn and Co, the results are identical to Metal:Hmim 1:15 as discussed earlier. For Zn-Hmim at 10-15 mL/min, flower shaped ZIF-L (Fig. 3.8) is the dominant phase where the PXRD pattern (Fig. 3.7) is in good agreement with the simulated ZIF-L, and there is only one major weight loss at 250 °C (Figs. 3.10 and 3.11). However, when reaching 10-20 mL/min, an intermediate octahedral shaped ZIF-L/ZIF-8 phase is obtained with a mixed PXRD pattern and two major weight loss signals at 250 °C and 640 °C. As for 10-25 mL/min and 10-30 mL/min, although the PXRD spectrum is in exact agreement with ZIF-8, ZIF crystals at 10-25 mL/min exhibit an intermediate morphology between concave octahedral and polyhedral while at 10-30 mL/min

crystals exhibit well developed polyhedral morphology. Moreover, the TGA curve at 10-25 mL/min shows a minor weight loss at 240 °C while that of 10-30 mL/min shows only one weight loss at 650 °C, thereby confirming that the full phase transition to ZIF-8 is achieved at 10-30 mL/min.

For the Co-Hmim system, the PXRD pattern for all ZIF samples synthesized after 10-10 mL/min is in exact match with simulated ZIF-67 (Fig. 3.7) and the crystals exhibit a smooth polyhedral morphology (Fig. 3.9) except for the ZIF sample at 10-15 mL/min. When referring to the TGA curves (Fig. 3.10 and 3.11), we can see the 10-15 mL/min sample show a minor weight loss at 240 °C while the other ZIF samples showed only one weight loss signal at 450 °C, thus the full transition to ZIF-67 is achieved at 10-20 mL/min.

Furthermore, the broadening in the basal peak at $2\theta = 7.3$ °, for both ZIF-8 and ZIF-67 corresponds to the decrease in the particle size as a function of increasing the local Metal:Hmim due to increasing the Metal-Hmim flow rate. This decrease in particle size can be observed in the SEM images of ZIF-8 and ZIF-67 in Figures 3.8 and 3.9.
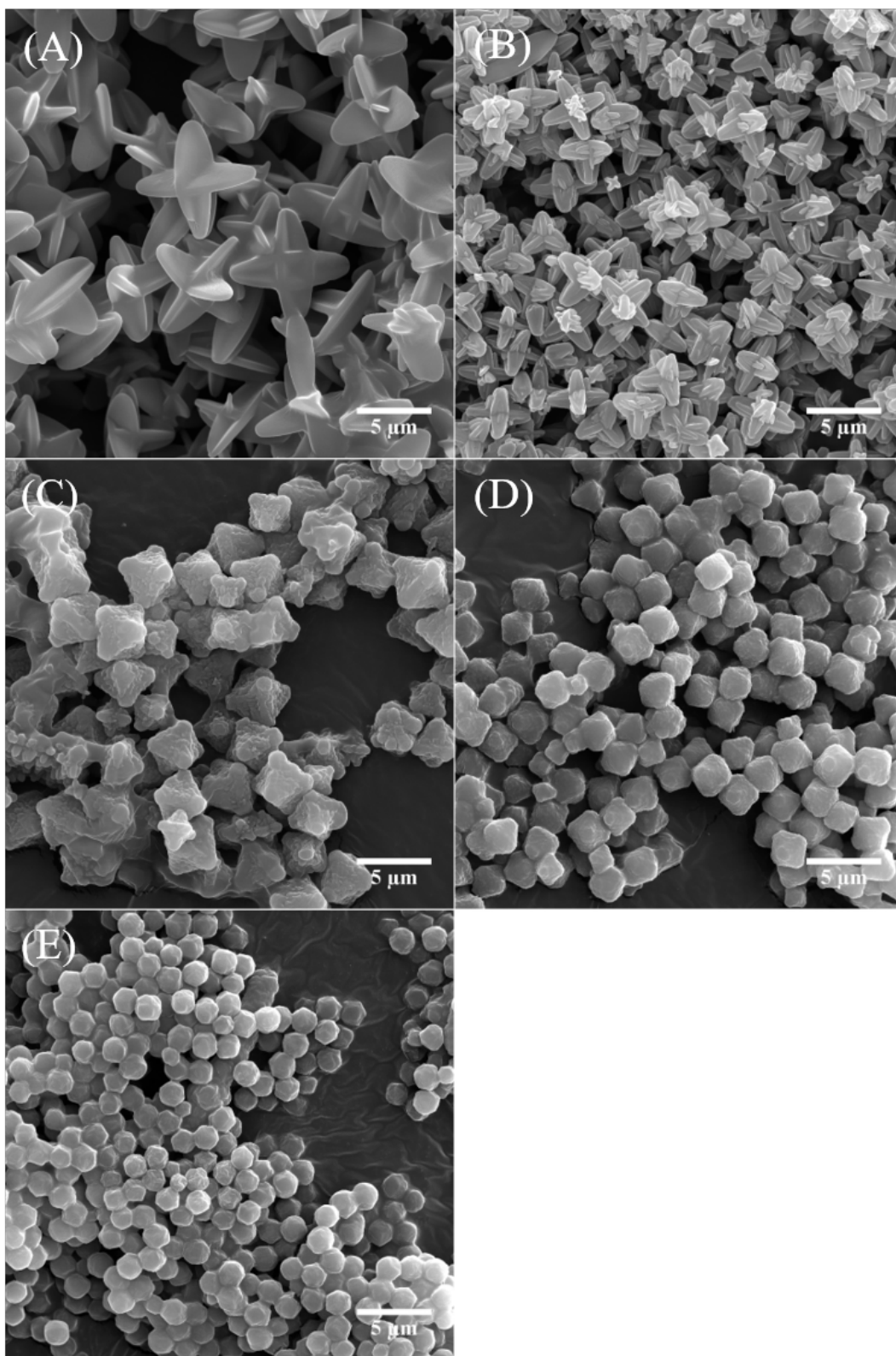
Figure 3.8: SEM images of ZIF samples at different Zn-Hmim flow rates: (A) 10-10 mL/min, (B) 10-15 mL/min, (C) 10-20 mL/min, (D) 10-25 mL/min, and (E) 10-30 mL/min.

40
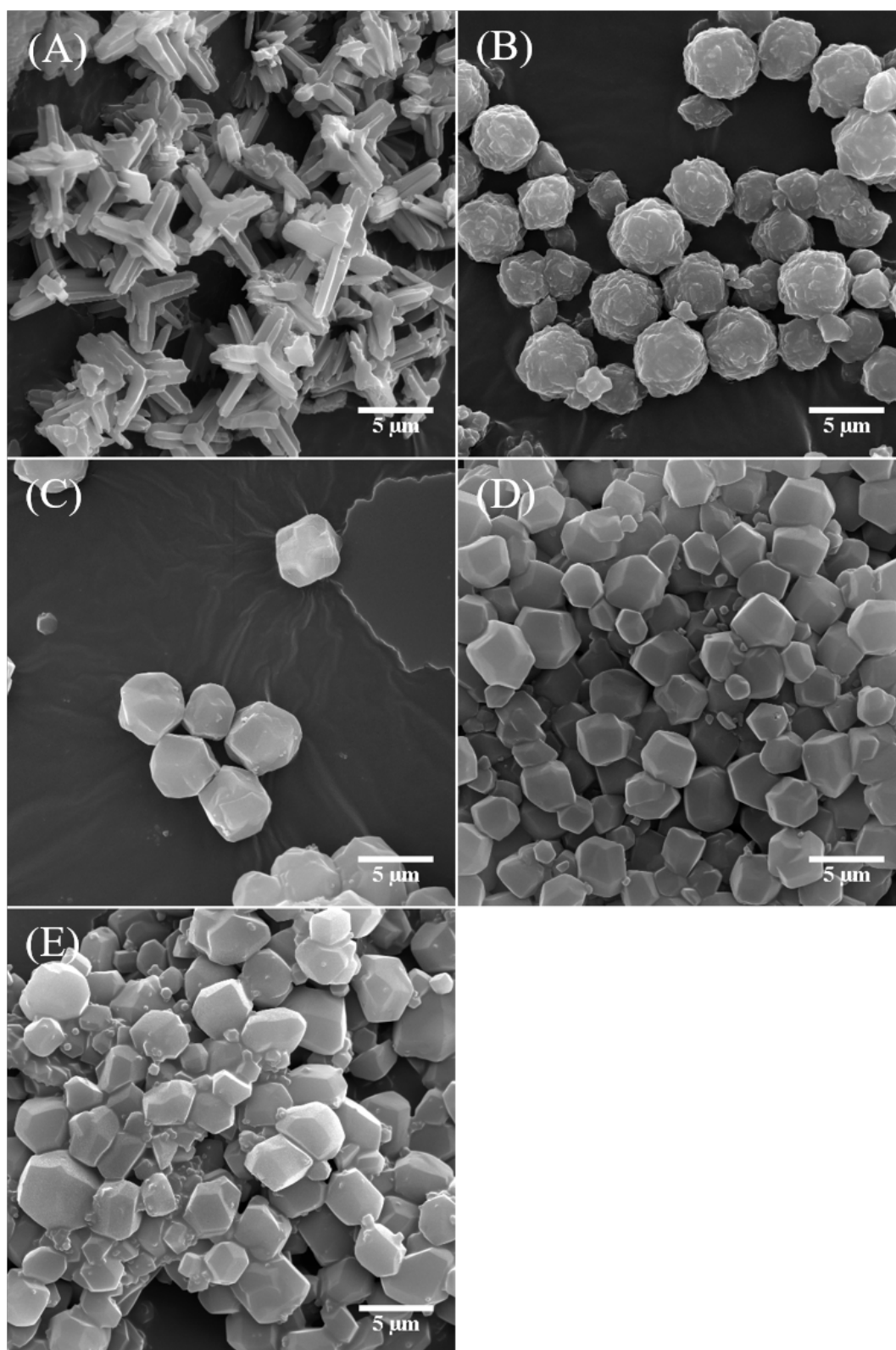
Figure 3.9: SEM images of ZIF samples at different Co-Hmim flow rates: (A) 10-10 mL/min, (B) 10-15 mL/min, (C) 10-20 mL/min, (D) 10-25 mL/min, and (E) 10-30 mL/min.
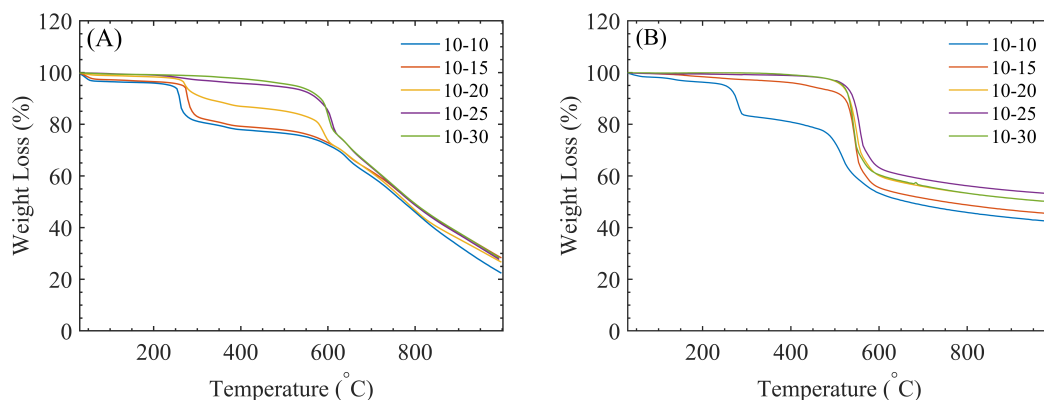
Figure 3.10: Thermogravimetric curves of ZIF samples at: (A) different Zn-Hmim flow rates (mL/min), and (B) at different Co-Hmim flow rates (mL/min).
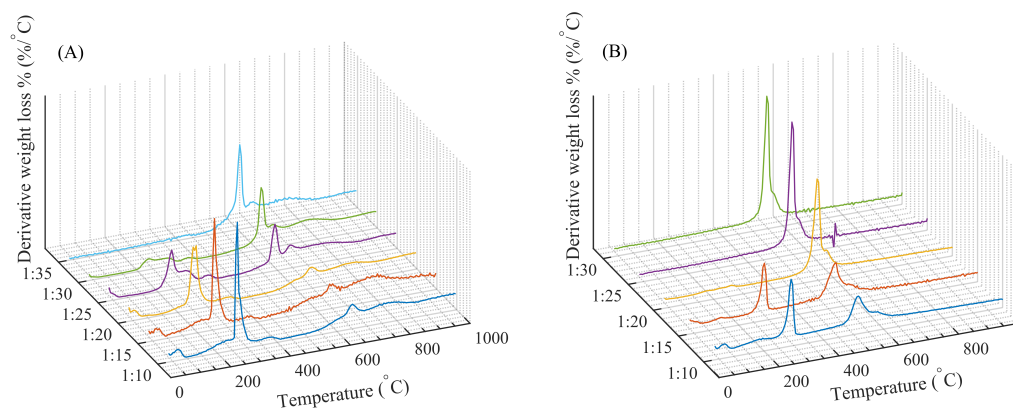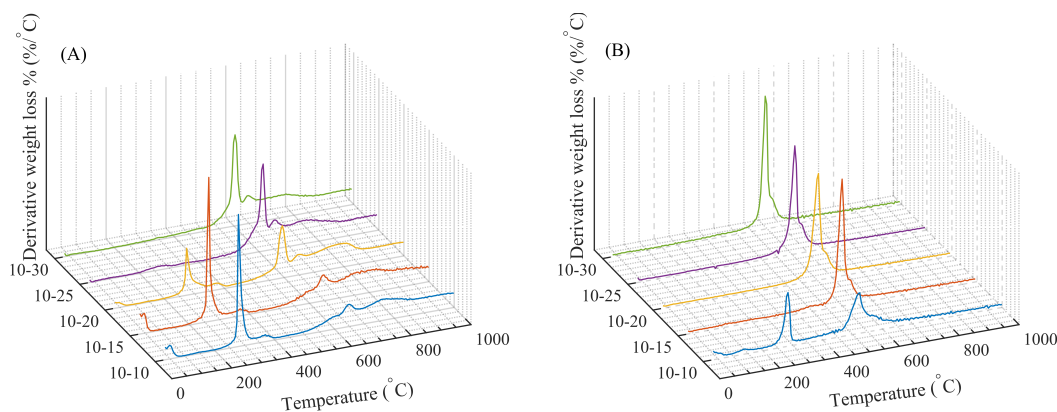

Figure 3.11: First derivative of the weight loss as a function of temperature for the thermogravimetric curves of ZIF samples at: (A) different Zn-Hmim flow rates, and (B) different Co-Hmim flow rates.

3.2.2 Textural Properties of the ZIF samples at Different Metal-Hmim Flow Rates

It is well known that ZIFs and MOFs are characterized by high surface areas due to their permanent and tunable porosity that can be understood via nitrogen adsorption isotherms analysis. ZIF-L has a lower BET surface area (160 m^2/g) compared to ZIF-8 (up to 1800 m^2/g) due to smaller micropore volume and higher density of metal atoms per unit volume. As such the transition from two dimensional orthorhombic ZIF-L to three dimensional cubic ZIF-8 is confirmed by the increase in the specific BET surface area, micropore volume and micropore area that are summarized in table 3.1.

All the adsorption isotherms for the Zn system are of type I which confirms the microporous nature of the ZIF material (Fig. 3.12). For Zn-Hmim at 10-10 mL/min and 10-15 mL/min low BET surface areas are obtained (103 m^2/g and 218 m^2/g respectively) along with low micropore volumes since ZIF-L is the dominant phase. However, when the Zn-Hmim flow rate increases to 10-15 mL/min and 10-20 mL/min the BET surface area increases to reach 825 m^2/g and 1100 m^2/g respectively. Moreover, the micropore volume significantly increases to reach 0.2953 cm^3/g and 0.5669 cm^3/g for 10-20 mL/min and 10-25 mL/min respectively, thereby confirming that the obtained ZIF samples are in a transition phase between ZIF-L and ZIF-8 where the latter flow rate is closer to complete transition more than the former flow rate. The highest BET surface area (1710 m^2/g) and micropore volume (0.6146 cm^3/g) is obtained for Zn-Hmim at 10-30 mL/min marking the complete phase transition to SOD cubic ZIF-8.

Similarly for the Co system, the microporous property of the synthesized ZIF samples is confirmed by the type (I) nitrogen adsorption isotherms obtained (Fig. 3.13). The ZIF sample at Co-Hmim 10-10 mL/min shows a BET surface area of 270 m^2/g and a micropore volume of 0.0972 cm^3/g that are higher than the literature values reported for ZIF-L[88], thus ensuring that the ZIF sample at this flow rate acts as a transition phase between ZIF-L-Co and ZIF-67. All other ZIF samples at different Co-Hmim flow rates reach a constant specific BET surface area (around 1300 m^2/g) and micropore volume (around 0.6 cm^3/g) which is consistent with reported literature values for ZIF-67[111][7] and confirms that the transition is complete.

Zn-Hmim flow rate (mL/min)	Specific BET surface area (m^2/g)	Micropore volume (cm^3/g)
10-10	115	0.0329
10-15	223	0.0979
10-20	824	0.2953
10-25	1110	0.5669
10-30	1710	0.6146

Co-Hmim flow rate (mL/min)	Specific BET surface area (m^2/g)	Micropore volume (cm^3/g)
10-10	279	0.0972
10-15	1335	0.6296
10-20	1242	0.5970
10-25	1300	0.6221

Table 3.1: Specific BET surface area, micropore volume and micropore area for the as synthesized ZIF samples at different Metal-Hmim flow rates.
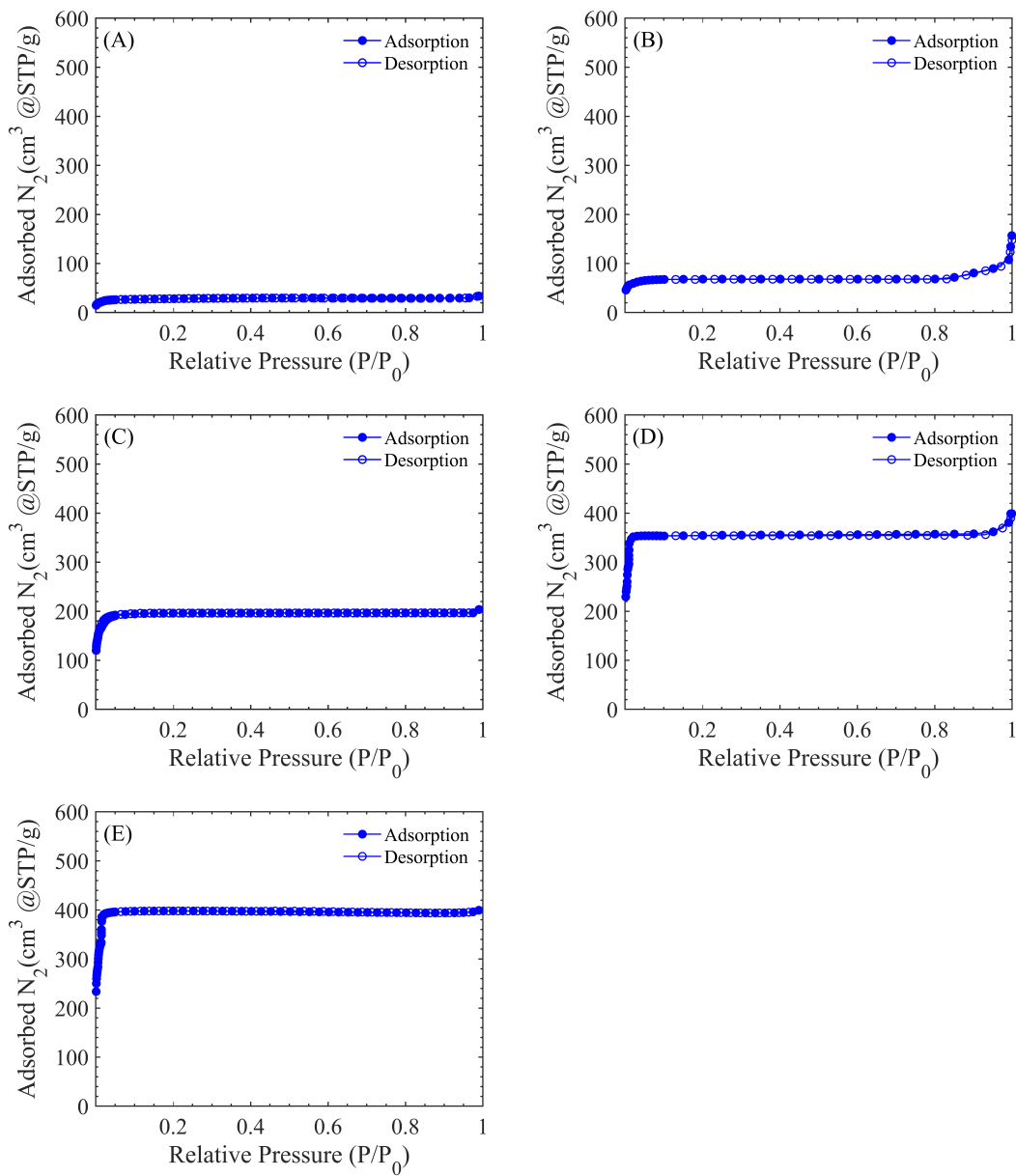
Figure 3.12: Nitrogen adsorption and desorption isotherms at 77 K for ZIF samples at different Zn-Hmim flow rates: (A) 10-10 mL/min, (B) 10-15 mL/min, (C) 10-25 mL/min, and (D) 10-30 mL/min.
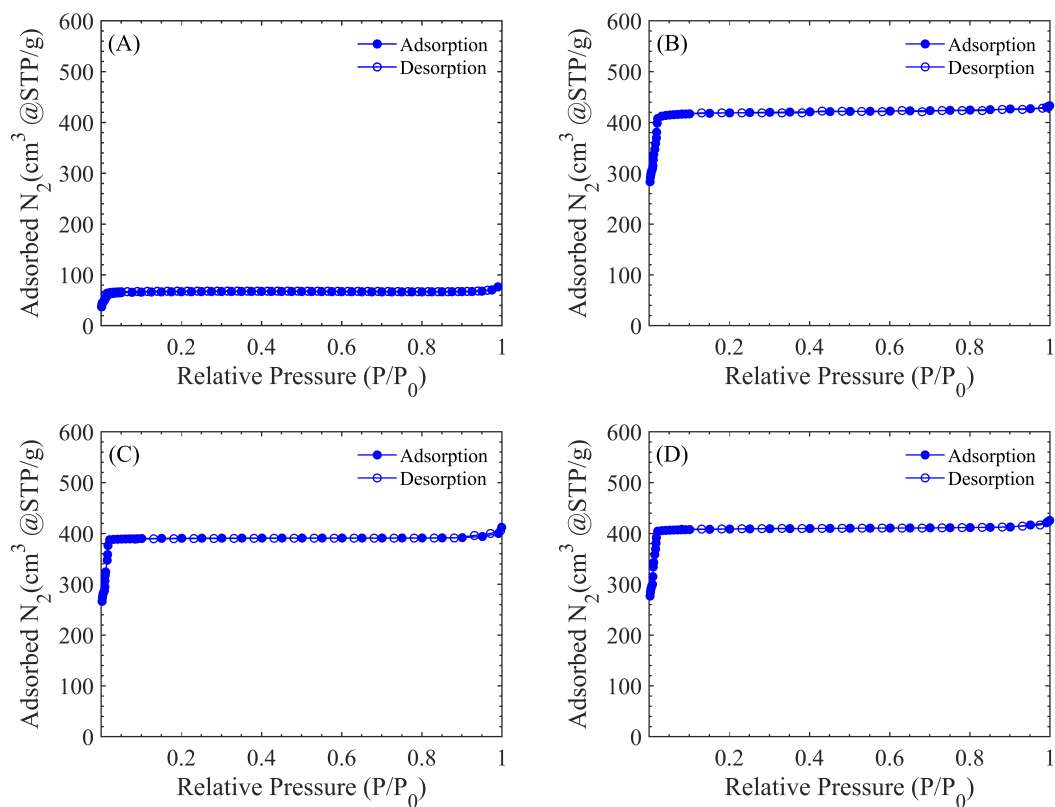
Figure 3.13: Nitrogen adsorption and desorption isotherms at 77 K for ZIF samples at different Co-Hmim flow rates: (A) 10-10 mL/min, (B) 10-15 mL/min, (C) 10-25 mL/min, and (D) 10-30 mL/min.

Chapter 4

# Controlled Particle Size Synthesis of ZIF-8, ZIF-67 and their Mixed Metal Derivatives

4.1 Particle Size Control

4.1.1 Calculation of Reynolds Number

As discussed in the introduction and observed earlier in the previous chapter, a high Metal:Hmim ratio is necessary for the formation of ZIF nanoparticles. For this reason, the Metal:Hmim ratio used in this chapter is 1:70 to ensure the rapid nucleation resulting from the supersaturation condition of Hmim solution. The Reynolds numbers corresponding to the flow rates used during the synthesis are calculated using equation 1.1 where the dynamic viscosity of Hmim at a concentration of 3.5 M and 25 °C is measured and found to be equal to 2.6 centipoise (cP), that is higher than that of water (0.86 cP). In addition, the measured density of the Hmim solution is 1003 kg/m^3 that is slightly higher than that of water (997 Kg/m^3). The velocity of the streams is calculated at the inlets; the mixing chamber diameter is $L = 0.6$ cm.

4.1.2 Two-Syringe System

Since most micromixers possess only two inlets that limit the total number of fluid streams into two, we manage to study the controlled particle size of the ZIF samples using only two of the four inlets. Figure **??** shows that the PXRD patterns of the as synthesized ZIF samples which is in good agreement with the simulated patterns of ZIF-8 and ZIF-67, confirming the successful synthesis of the ZIF samples without impurities.
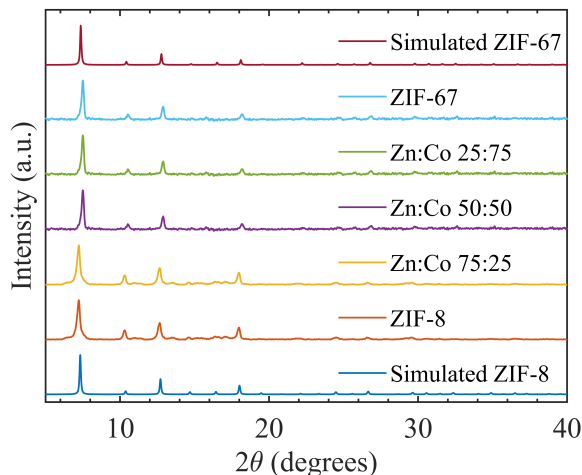
Figure 4.1: PXRD comparison of the synthesized ZIF samples and the simulated ZIF-8 and ZIF-67, and their mixed metal derivatives at initial Zn:Co ratios of 75:25, 50:50, and 25:75.

The effect of the Reynolds number number on the particle size of the ZIF samples is summarized in Figure 4.2. The ZIF samples are ZIF-8, ZIF-67, and their mixed metal derivatives at initial Zn:Co ratios of 75:25, 50:50, and 25:75.

For ZIF-8, as Re number increases from 950 (corresponding to 6 mL/min) to 3170 (20 mL/min), the particle size decreases from 187 nm ± 21 nm to 126 nm ± 21 nm. With a further increase in Re to 9345 (59 mL/min), the particle size decreases to reach a minimal value of 104 nm ± 12 nm. Figure 4.3 shows the SEM images of the as synthesized ZIF-8 at different Re numbers, where it can be clearly observed that the particle size decreases with the increase of Re numbers. Moreover, the particle size distribution tends to be more uniform as the standard deviation from the mean decreases as Re increases, as shown in Figure 4.5.

Furthermore, the effect of Re number on the particle size of ZIF-67 is more noticeable than ZIF-8. The size of ZIF-67 particles significantly decreases from 1090 nm at $Re = 951$, to 402 nm at $Re = 3170$, along with a remarkable decrease in the standard deviation from 406 nm to 53 nm as shown in Figure 4.6. Furthermore, when Re increases from 3170 to reach 9345, the decrease in the particle size is relatively slight as it decreases from 402 nm to 325 nm, with comparable values of standard deviation of 53 nm and 66 nm, respectively. The SEM images shown in Figure 4.4 clearly illustrate the decrease in particle size, and the normal distributions in Figure 4.6 show the variation in the standard deviation from the mean particle size. This trend in standard deviation may be due to the large particle size of ZIF-67 crystals that grows beyond the nanoscale reaching a few microns.

Similarly, the mixed metal derivatives of the ZIF samples showed the same trend as ZIF-8 and ZIF-67 with a decrease of the mean particle size and the standard deviation while increasing Re. The SEM images and the normal distributions are shown in Figures 4.7 to 4.12. On the other hand, the mean particle size increases as the initial Zn:Co ratio is varied from 75:25 to 25:75 for all Re.
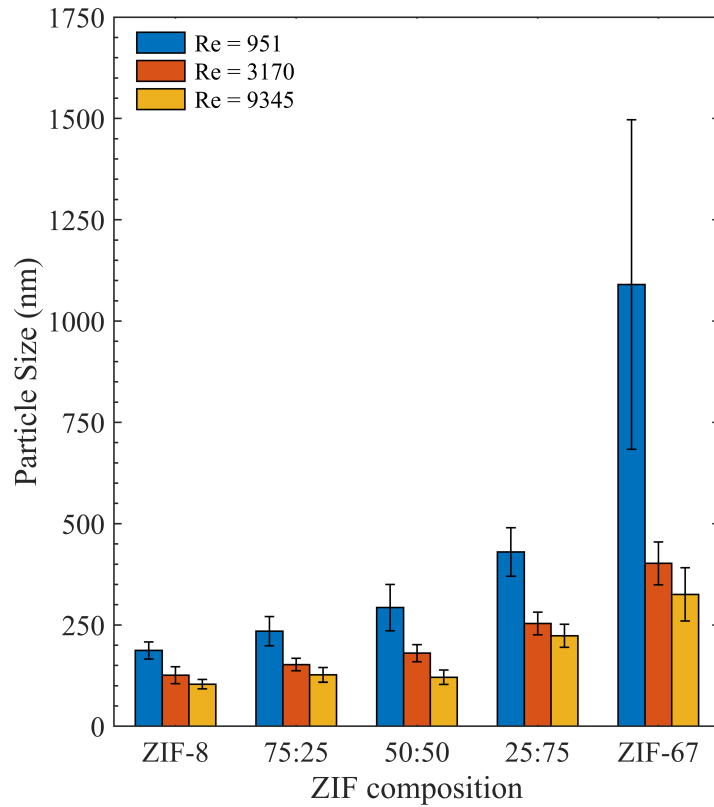
Figure 4.2: Particle size (nm) of ZIF-8, ZIF-67, and their mixed metal derivatives with different initial Zn:Co ratios as a function of Reynolds number (Re).
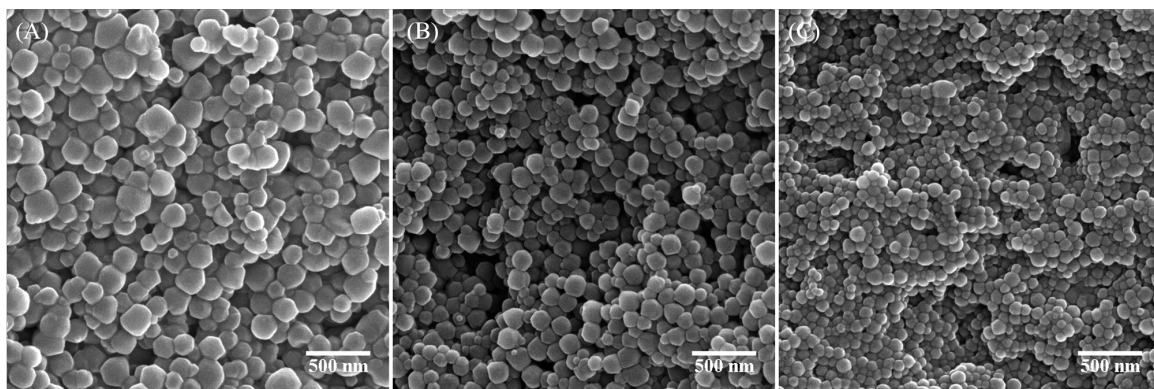
Figure 4.3: SEM images of as synthesized ZIF-8 at (A) $Re = 951$, (B) $Re = 3170$, and (C) $Re = 9345$ showing the decrease in particle size.
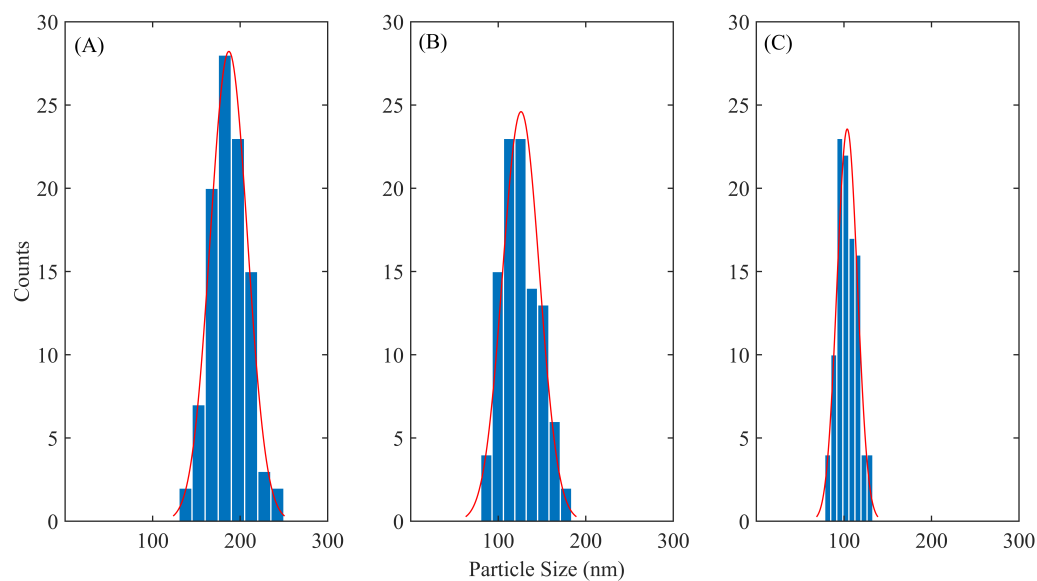
Figure 4.4: The normal distribution of particle size of ZIF-8 sample showing a standard deviation of (A) 21 nm at $Re = 951$, (B) 20 nm at $Re = 3170$, and (C) 12 nm at $Re = 9345$.
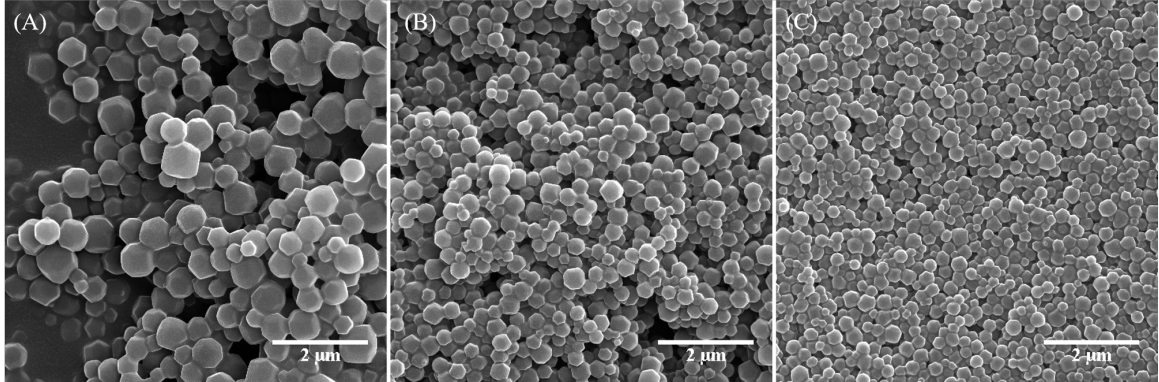
Figure 4.5: SEM images of as synthesized ZIF-67 at (A) $Re = 951$, (B) $Re = 3170$, and (C) $Re = 9345$ showing the decrease in particle size.
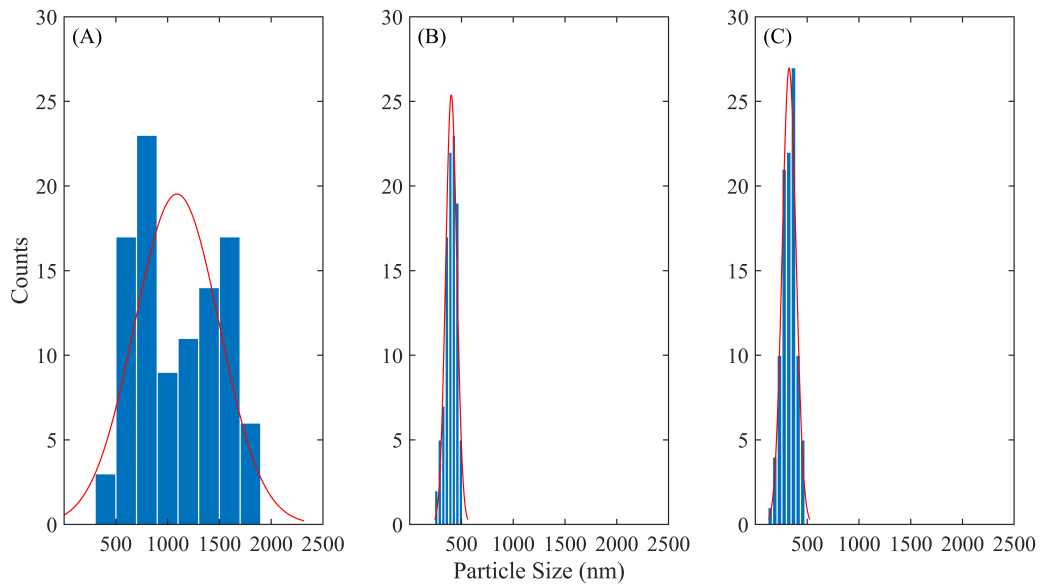
Figure 4.6: The normal distribution of particle size of ZIF-67 sample showing a standard deviation of (A) 406 nm at $Re = 951$, (B) 53 nm at $Re = 3170$, and (C) 65 nm at $Re = 9345$.
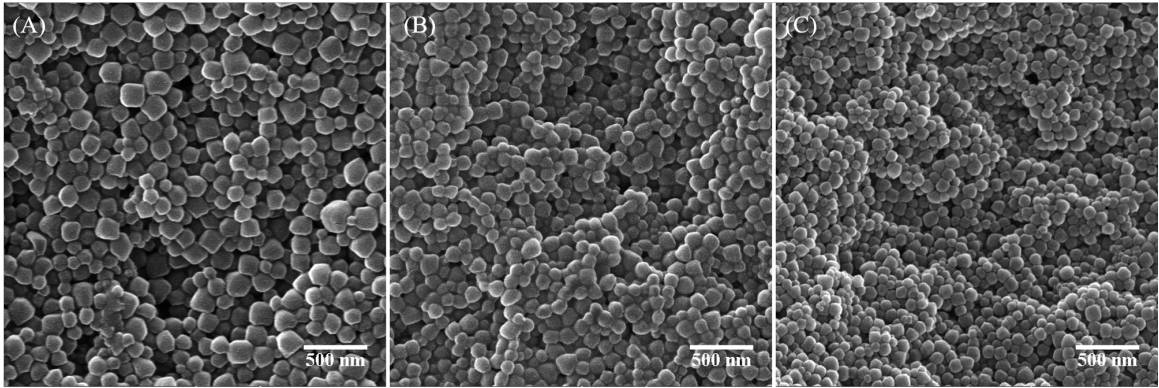
Figure 4.7: SEM images of as synthesized Zn:Co 75:25 ZIF samples at (A) $Re = 951$, (B) $Re = 3170$, and (C) $Re = 9345$.
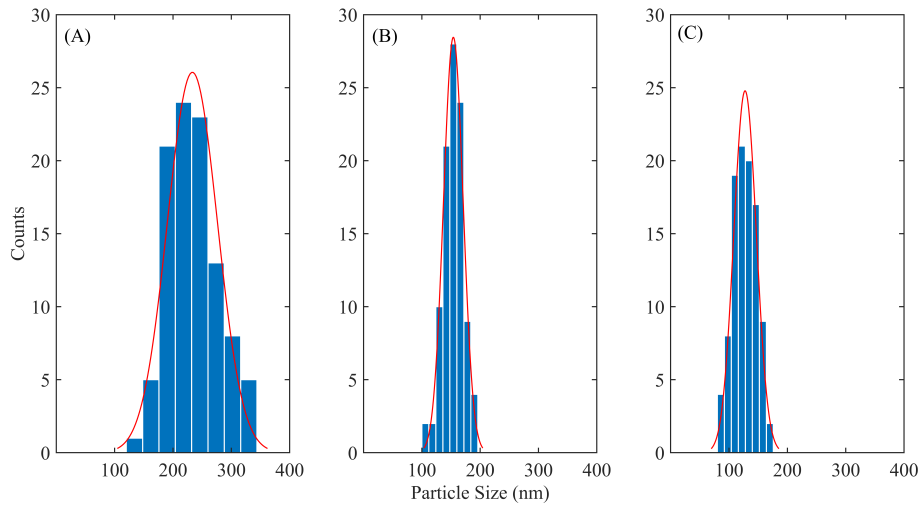
Figure 4.8: The normal distribution of particle size of Zn:Co 75:25 sample showing a standard deviation of (A) 36 nm at $Re = 951$, (B) 16 nm at $Re = 3170$, and (C) 18 nm at $Re = 9345$.
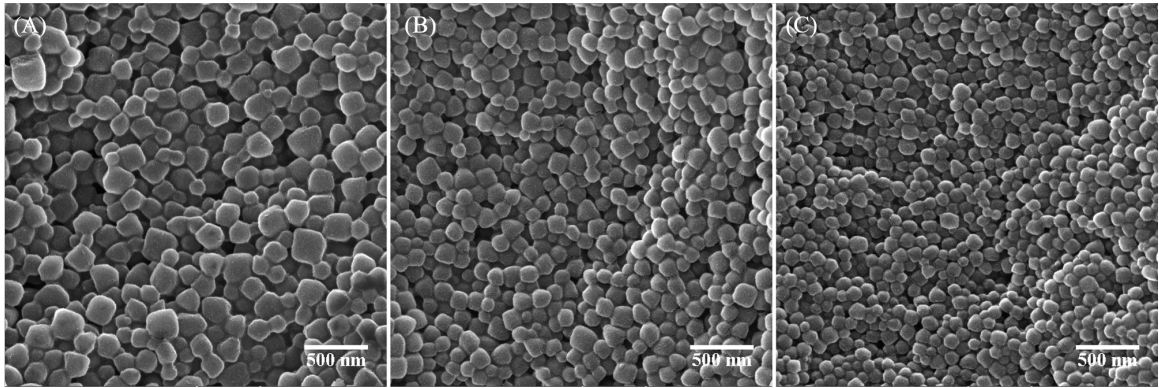
Figure 4.9: SEM images of as synthesized Zn:Co 50:50 ZIF samples at (A) $Re = 951$, (B) $Re = 3170$, and (C) $Re = 9345$.
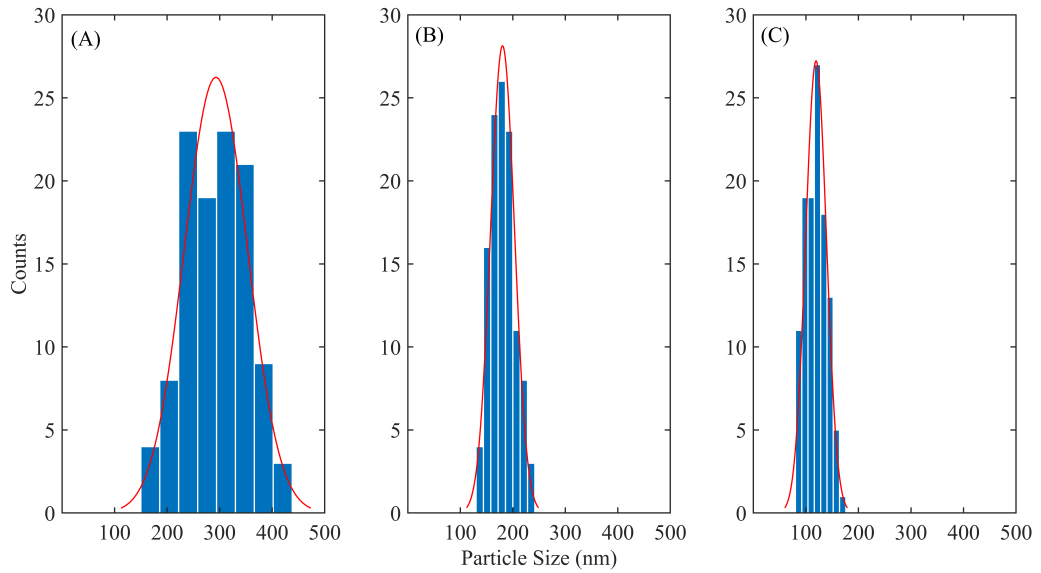
Figure 4.10: The normal distribution of particle size of initial Zn:Co ratio 75:25 sample showing a standard deviation of (A) 57 nm at $Re = 951$, (B) 21 nm at $Re = 3170$, and (C) 18 nm at $Re = 9345$.
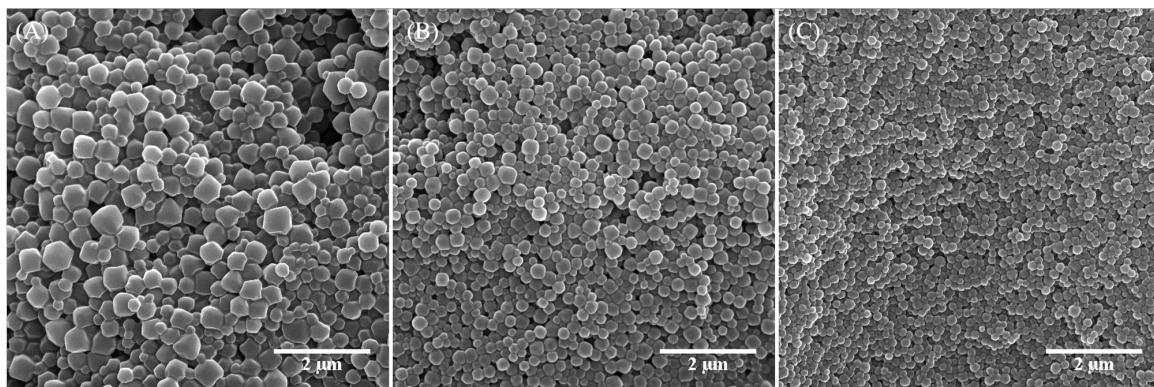
Figure 4.11: SEM images of as synthesized Zn:Co 25:75 ZIF samples at (A) Re = 951, (B) $Re = 3170$, and (C) $Re = 9345$.
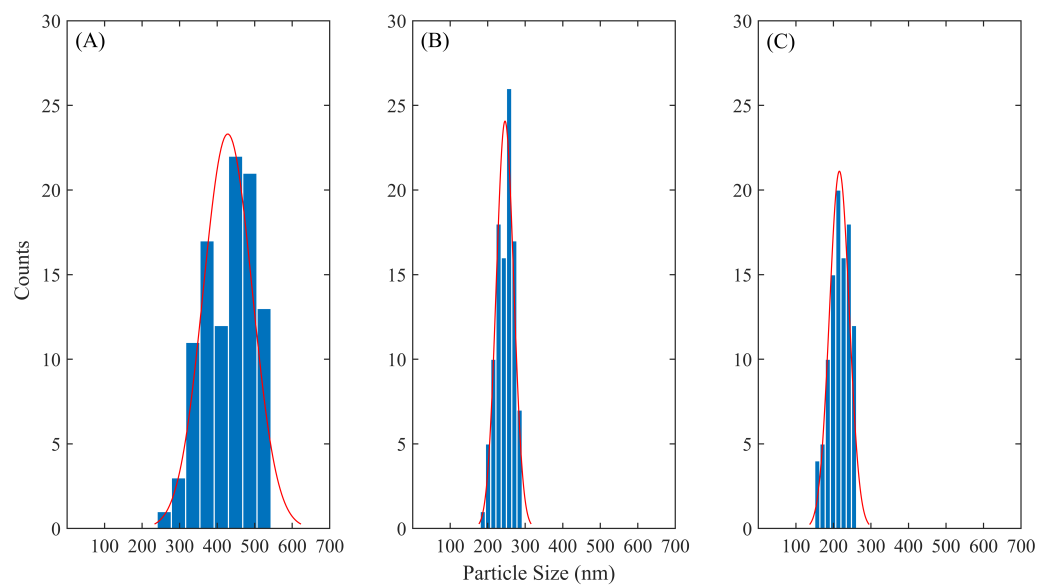
Figure 4.12: The normal distribution of particle size of initial Zn:Co ratio 25:75 sample showing a standard deviation of (A) 60 nm at $Re = 951$, (B) 28 nm at $Re = 3170$, and (C) 28 nm at $Re = 9345$.

The BET surface area and thermal stability of all ZIF samples are enlisted in table 4.1. The microporosity of all the ZIF samples is confirmed to be of type (I) adsorption isotherms as shown in Figure 4.15 in the appendix. The calculated BET surface areas are relatively high and are in good agreement with the literature values[5, 111].

Moreover, the TGA curves (Figs. 4.13 and 4.14) show that all ZIF samples have a significant thermal stability up to a temperature that ranges between ~ 540 °C and ~ 600 °C.

ZIF Sample	Specific BET surface area (m^2/g)	Thermal Stability (°C)
ZIF-8	1500	600
Zn:Co 75:25	1182	584
Zn:Co 50:50	1224	543
Zn:Co 25:75	1339	534
ZIF-67	1256	545

Table 4.1: Specific BET surface area, and thermal stability for the as synthesized ZIF samples.

For all the samples, no weight loss signal is observed before the decomposition temperature of the framework showing the absence of any guest molecules (Slovent, or unreacted material). The major weight loss for the ZIF samples corresponds to the degradation of the framework as a result of the carbonization of the imidazolate units4.13. Furthermore, the first derivative of the TGA curves is plotted in Fig. 4.14 where the peaks correspond to the degradation temperatures of ZIF-8 at 600 °C, Zn:Co 75:25 at 584 °C, Zn:Co 50:50 at 543 °C, Zn:Co 25:75 at 534 °C, and ZIF-67 at 545 °C.
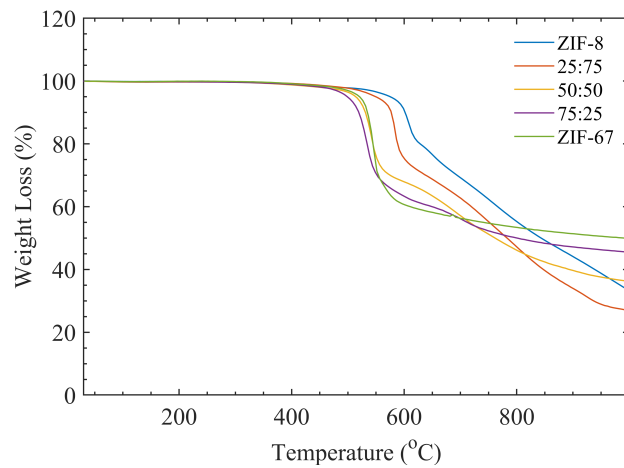
Figure 4.13: Thermogravimetric curves of the as synthesized ZIF samples.
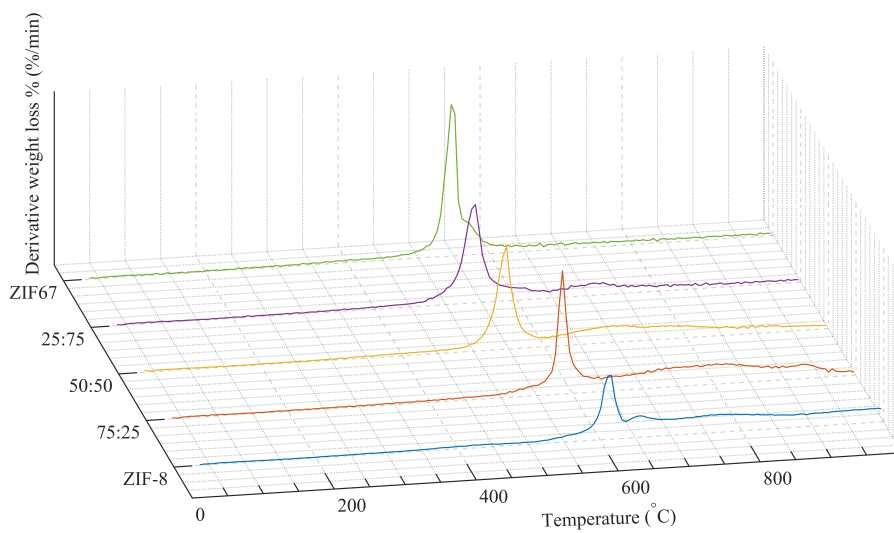
Figure 4.14: First derivative of the weight loss as a function of temperature for the thermogravimetric curves of the as synthesized ZIF samples.
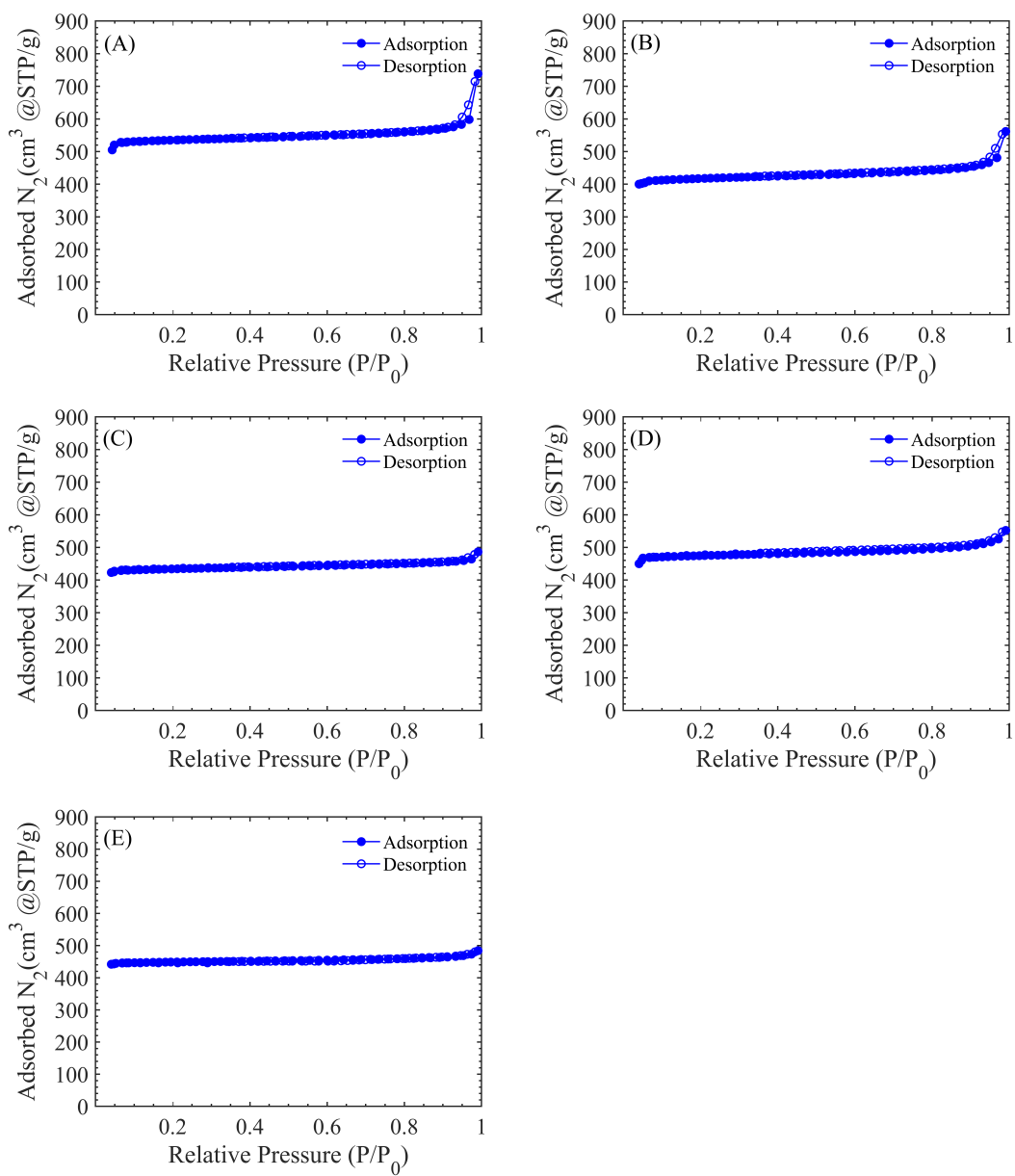
Figure 4.15: Nitrogen adsorption and desorption isotherms at 77 K for the as synthesized ZIF samples: (A) ZIF-8, (B) Zn:Co 75:25, (C) Zn:Co 50:50, (D) Zn:Co 25:75, and (E) ZIF-67.

4.1.3 Four-Syringe System

Since the maximum Re that can be reached using the two-syringe system is 9500 due to limitations imposed by the flow rate limit of the used pumps, we manage to study the effect of higher Re numbers by using a four-syringe system where we can reach values up to 19000.

The particle size controlled synthesis using four syringes is conducted for ZIF-8 only. Fig. 4.16 shows the particle size from the two-syringe system and the four-syringe system at different Re numbers.

At $Re = 200$ where the flow regime is laminar, the particle size is 380 nm $\pm$ 101 nm, and 353 nm $\pm$ 67 nm for the two-syringe and four syringe systems, respectively.This large deviation from the mean particle size for both systems is due to the poor mixing quality of the laminar regime where the rate of the reaction is limited by the rate of mixing. Therefore, the reaction proceeds before the complete homogenization of the reaction mixture leading to large deviation in the particle size. The normal distribution for the particle size at $Re = 200$ for both systems is represented in Figure 4.17.

As Re regime increases to 3100 where the flow regime is considered to be in a transition between laminar and turbulent, a significant decrease in the particle size and in the standard deviation for both systems is observed. The particle size decreased to reach 126 nm $\pm$ 21 nm for the two-syringe system, and 97 nm $\pm$ 17 nm for the four-syringe system. Figure 4.18 shows the normal distribution of the particle size at $Re = 3100$ for both systems.

For Re numbers beyond 4000 where the flow regime is turbulent, the particle size for both systems reached a constant value. This steady state behavior of the particle size occurs because the reaction kinetics are no longer limited by the rate of mixing, since at the turbulent regime, the rate of the chemical reaction is limited by molecular diffusion between the species. Accordingly, the minimal particle size achieved by the two-syringe system is 101 nm $\pm$ 11 nm, and 77 nm $\pm$ 10 nm for the four-syringe system. The normal distribution for the particle size at $Re = 6300$ for both systems is represented in Figure 4.19.

When using the four-syringe system, the particle size remains constant for Re number values greater than 9500, therefore the maximal mixing performance of the MIVM is achieved starting from $Re = 6000$ which corresponds to a total flow rate of 80 mL/min.

When observing the mean particle sizes and standard deviations obtained using the two-syringe system and the four-syringe system at the same Reynolds number, we conclude that there is no significant difference between the two systems as shown in the normal distributions in Figures 4.17, 4.18, and 4.19.
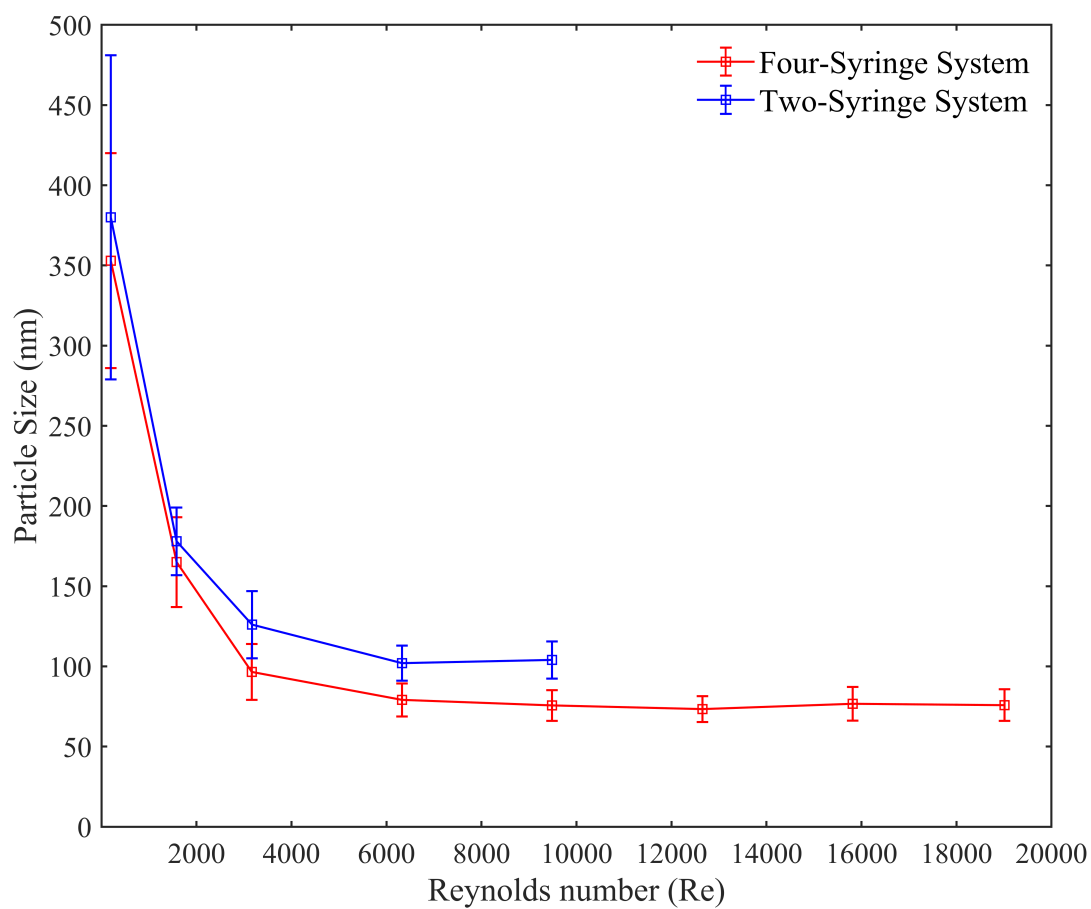
Figure 4.16: Particle size (nm) of ZIF-8 synthesized using the four-syringe system and the two-syringe as function of the Reynolds number (Re).
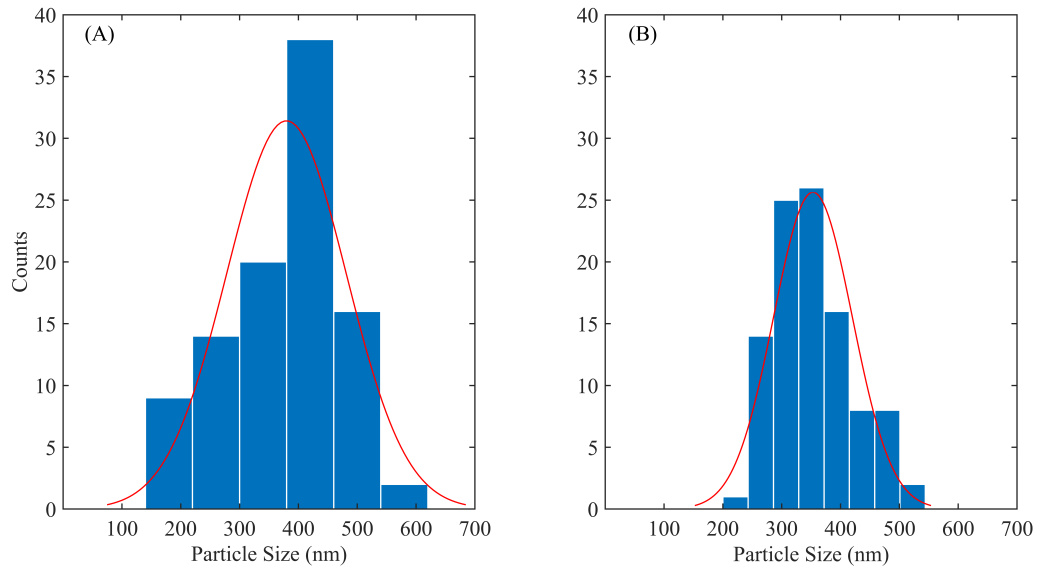
Figure 4.17: The normal distribution of particle size of ZIF-8 sample at $Re = 200$ showing a standard deviation of (A) 101 nm for the two-syringe system, and (B) 67 nm for the four-syringe system.
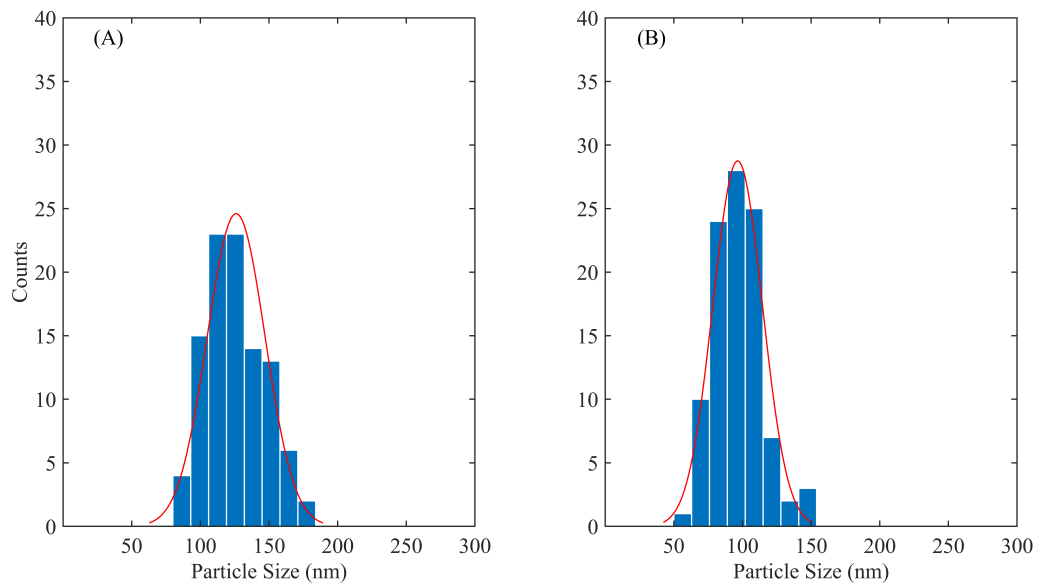
Figure 4.18: The normal distribution of particle size of ZIF-8 sample at $Re = 3100$ showing a standard deviation of (A) 21 nm for the two-syringe system, and (B) 17 nm for the four-syringe system.
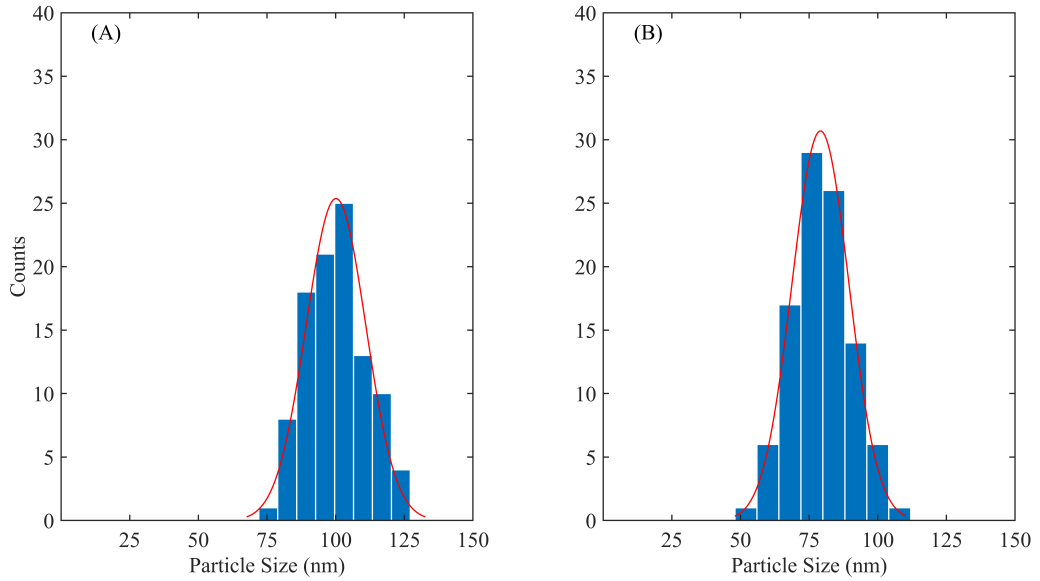
Figure 4.19: The normal distribution of particle size of ZIF-8 sample at $Re = 6300$ showing a standard deviation of (A) 11 nm for the two-syringe system, and (B) 10 nm for the four-syringe system.

4.1.4 Particle Size Control in Batch Reactor vs MIVM

To highlight the MIVM importance for the controlled and reproducible particle size synthesis of ZIF-8, we compare the five results obtained from the MIVM using the four-syringe system for $Re > 6000$ to those obtained from five trials using a batch reactor.

Using the MIVM, the mean particle size obtained is 77 nm with a standard deviation of 2 nm, while using a batch reactor, the mean particle size obtained is 98 nm with a reproducibility standard deviation of 20 nm that is ten times greater than that of the MIVM. This confirms that although batch reactors can yield ZIF-8 nanoparticles, they fail to achieve reproducible results.

Setup	Mean particle size (nm)	Standard deviation ($\pm$ nm)
MIVM (Four-syringe system)	77	2
Batch	98	20

Table 4.2: The mean particle size (nm) of ZIF-8 and the standard deviation ($\pm$ nm) for five trials using MIVM (Four-syringe system) and a typical batch reactor.

4.2 Mixed Metal Derivatives of ZIF-(8, 67

4.2.1 Doping as a Function of Initial Zn:Co Ratio

Atomic absorption spectroscopy (AA) is a technique that determines the elemental concentration of Zn^{2+} and Co^{2+} metal ions in the sample, the experimental Zn:Co ratio is then calculated. As such, the three ZIF samples prepared using different initial Zn:Co ratios at the three flow rates are analyzed using AA spectroscopy. The results are summarized in table 4.3.

	Flow rate (mL/min)		
ZIF Sample	6	20	59
Zn:Co 75:25	78:22	74:46	77:23
Zn:Co 50:50	54:46	51:49	50:50
Zn:Co 25:75	24:76	26:74	30:70

Table 4.3: Experimental Zn:Co ratios as measured using (AA) starting from fixed initial Zn:Co ratios of 75:25, 50:50, and 25:75 at different flow rates.

The results show that the experimental Zn:Co ratios are very close to the initial ones, thereby confirming the MIVMs potential for the controlled synthesis of cobalt doped ZIF-8.

4.2.2 Doping as a Function of Flow Rate

In general, the cobalt doping of ZIF-8 is controlled by varying the initial Zn:Co ratio before mixing with Hmim. However, the unique design of the MIVM that features four inlets allows the controlled doping of ZIF-8 by varying the flow rate.

Accordingly, the doping of ZIF-8 is possible starting from precursor metal solutions that have the same concentration and separated in two different syringes. This can be done by fixing the flow rate of a pump that holds the Hmim ([Hmim] = 3.5 M) solution and one of the metal precursor solution ($[Zn^{2+}]$ = 0.05 M or $[Co^{2+}]$ = 0.05 M), and varying the flow rate of the second pump that holds the other metal solution.

Figure 4.20 shows the mean Incorporated Metal (%) and the standard deviation obtained for three trials. Upon fixing the flow rate of the Zn^{2+} solution on the first pump at 60 mL/min and varying the flow rate of Co^{2+} on the second pump from 15 mL/min to 60 mL/min, the incorporated Co (%) increases from 16% $\pm$ 1.7 2% to reach 48% $\pm$ 8% respectively. On the other hand, when fixing the flow rate of Co^{2+} at 60 mL/min and varying the flow rate of Zn^{2+} from 15 mL/min to 60 mL/min, the incorporated Zn (%) increases from 40% $\pm$ 13% to reach 52% $\pm$ 10%

respectively (Fig. 4.20). In both systems, the incorporated Metal (%) increases gradually as a function of increasing the flow rate, however, the incorporated Zn^{2+} (%) is greater than the incorporated Co^{2+} (%) for all the flow rates. This suggests that the Zn^{2+} incorporation in the framework is kinetically favored over the incorporation of Co^{2+}. Therefore, the unique design of the MIVM allows for the controlled cobalt doping of ZIF-8 through varying the flow rates of two metal solutions that have the same concentration.
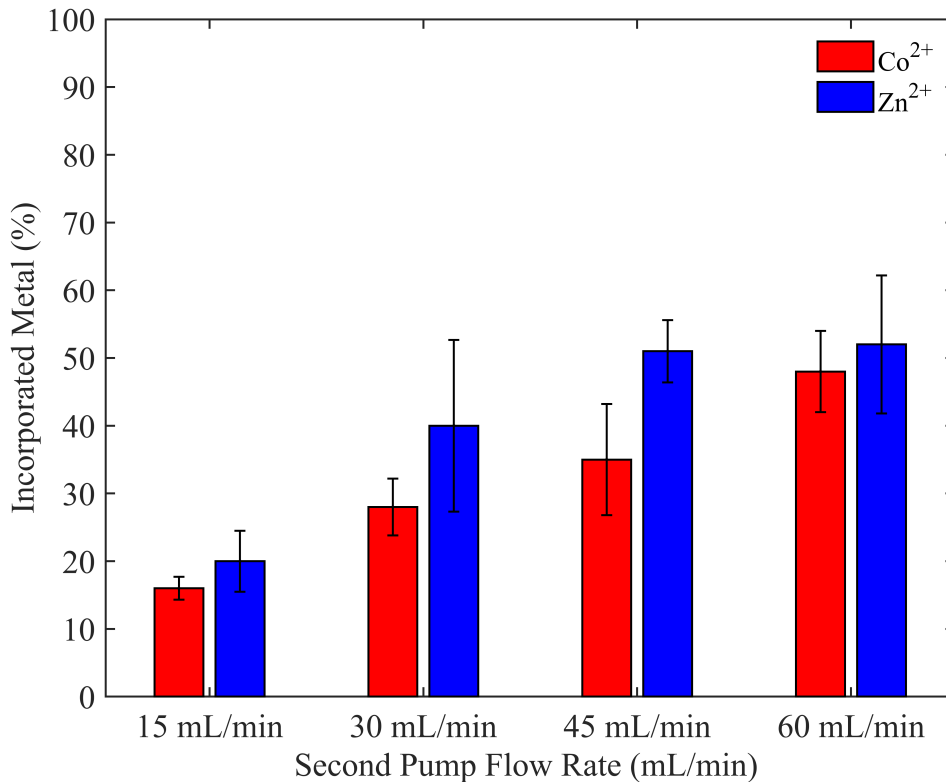
Figure 4.20: The mean value and standard deviation of incorporated (Co%) (Red), and incorporated (Zn%) (Blue) as function of the second pump flow rate (mL/min) containing Co^{2+} and Zn^{2+}, respectively. The flow rate of the first pump containing the Zn^{2+} or Co^{2+} solution and the Hmim solution is fixed at 60 mL/min. The initial concentrations are: [Co] = [Zn] = 0.05, [Hmim] = 3.5 M.

Moreover, to confirm that Co^{2+} is tetrahedrally coordinated in the ZIF-8 framework without altering its topology, visible diffuse reflectance is performed for all the ZIF samples synthesized using the three-syringe system. Figures 4.21 and 4.22 show that for all ZIF samples, there exists one characteristic band at 585 nm, and a shoulder at 540 nm that correspond to the tetrahedral coordination of Co^{2+}[112], therefore cobalt is successfully incorporated in the ZIF-8 framework without altering its topology.
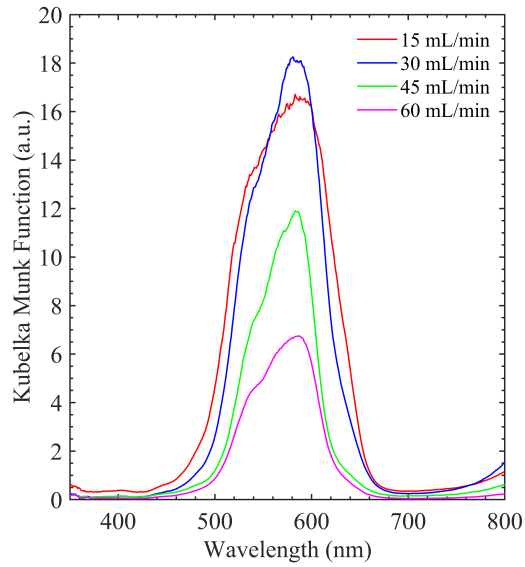
Figure 4.21: Visible diffuse reflectance of the ZIF samples as function of the second pump flow rate (mL/min) that contains the (Co^{2+}) solution.
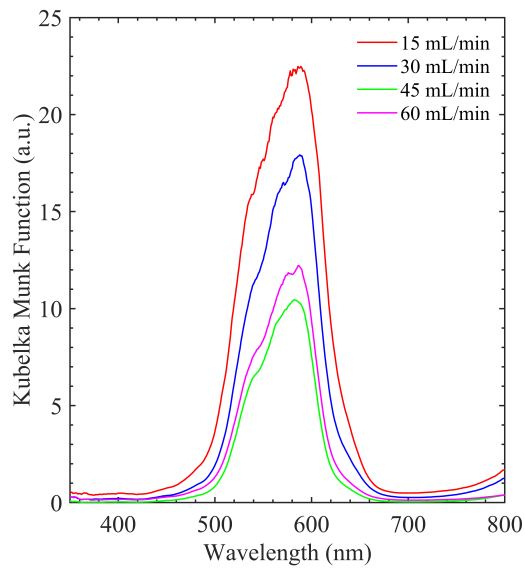
Figure 4.22: Visible diffuse reflectance of the ZIF samples as function of the second pump flow rate (mL/min) that contains the (Zn^{2+}) solution.

Chapter 5

Conclusion and Future Work

5.1 Conclusion

In this work, we successfully reported the controlled transition from ZIF-L-(Zn, Co) to ZIF-(8, 67) in an aqueous medium using MIVM. The critical Metal:Hmim ratio necessary for the formation of pure ZIF-8 and ZIF-67 was determined to be 1:35 and 1:25, respectively. Then, the Metal:Hmim is fixed at 1:15 that favors the formation of ZIF-L(Zn, Co), where through varying the flow rates, the local Metal:Hmim in the mixing chamber increased beyond 1:35 and 1:25 for ZIF-8 and ZIF-67 respectively. The transition from two-dimensional ZIF-L-(Zn, Co) to three-dimensional ZIF-(8, 67) is monitored through the PXRD, TGA, and surface area analysis.

In addition, we reported the controlled particle size synthesis of ZIF-8, ZIF-67, and their mixed metal derivatives as a function of the Reynolds number (Re). The particle size and standard deviation from the mean for all ZIF samples decreases as Re increases from 951 to 9345. This control over the particle size is related to the improved mixing as the fluid regime shifts from laminar at $Re < 2000$ to turbulent for $Re > 4000$. Moreover, the maximal mixing performance of the MIVM for controlled particle size synthesis of ZIF samples is reached starting from $Re = 6000$. The MIVM offers higher reproducibility than typical batch reactors where the particle size of ZIF-8 obtained after 5 trials is 77 ± 2nm when using the MIVM, while using a typical batch reactor the particle size obtained is 98 ± 20 nm. Finally, the MIVM geometric design featuring four inlets allows the cobalt doping of ZIF-8 starting from separated metal precursor solutions that have the same concentration. The incorporation of Cobalt in the ZIF-8 framework can be controlled starting from fixed concentrations by varying the flow rate of the metal solutions.

5.2 Future Work

5.2.1 Mixed-Linker ZIFs

The main advantage of ZIFs over natural zeolites is the vast array of tunable topologies that can be achieved by using different functionaliztion of the imidazolate linker[5]. Moreover, several studies have been reported on controlling the framework porosity and functionality through the synthesis of mixed-linker ZIFs. The main parameter considered for the successful synthesis of mixed linker ZIFs is that the used linkers should have the same geometric and chemical similarities such as solubility, the length of the carbon chain, and the functional groups[113].

For instance, Ding et al.[114] reported the synthesis of Amino-functional ZIF-8 nanocrystals by microemulsion based mixer linker strategy. The linker of ZIF-8 (2-methylimidazole) and the amino linker (2-aminobenzimidazole) were dissolved in an organic phase in the presence of a surfactant and oscillated to form a microemulsion that reacts with an aqueous phase of Zn^{2+}. The resultant NH_2-ZIF-8 material showed the same pore structure, crystal structure and thermal stability of pure ZIF-8. In addition, the presence of the amino-groups improved the CO_2 affinity to ZIF-8, thus increasing the CO_2/N_2 selectivity of ZIF-8. Moreover, Yang and his co-workers[115] reported the synthesis of three new ZIFs: ZIF-486, ZIF-376 and ZIF-414 with extra large cage sizes of 22.6, 27.5 and 45.8 Å through the combination of three different imidazolate linkers introduced in various ratios.

One of the main challenges in the field of mixed linker ZIF synthesis is the incorporation of more than two linkers in the ZIF framework, where the obtained products might be a heterogeneous phase of different ZIF materials[116]. As such, we intend to investigate the potential of the MIVM for the synthesis of mixed-linker ZIF-7-8-9 material using three different imidazolate linkers (2-Methylimidazole, Benzimidazole, and 2-Imidazolecarboxaldehyde). The four inlets of the MIVM would allow the synthesis to be achieved starting from four (three linker solutions and one zinc solution) of different or same concentrations, where through varying the flow rates we can control the ratio of the linkers during synthesis.

5.2.2 Drug Encapsulation

The intrinsic properties of ZIF materials such as chemical stability in aqueous and organic solvents, high surface areas, and sensitivity to lower pH values qualifies these materials to act as promising candidates for drug delivery applications.

Several studies have been reported on the use of ZIF materials for drug delivery. Adhikari and his co-workers[117] reported the use of ZIF-8 and ZIF-7for the encapsulation and controlled release of an anticancer drug Doxorubicin under different external stimuli. First, ZIF-8 and ZIF-7 were synthesized via conventional

synthetic routes using methanol and DMF as a solvent respectively at room temperature. Then, both ZIFs were soaked in a Doxorubicin solution for 48 hours under continuous stirring. The drug release kinetics were examined under the effect of pH and biomimetic membranes (liposomes). Interestingly, ZIF-8 drug release was more sensitive to lower pH unlike ZIF-7 that is more stable under acidic conditions, however, both ZIFs showed an excellent drug release control upon contact with biomimetic membrane. Furthermore, Li et al.[118] investigated the use of ZIF-8 for the drug delivery of an anti-tumor drug Fluorouracil (5-FU). In their study, The drug loading was achieved through soaking ZIF-8 in a 5-FU solution for 3.5 days under continuous stirring at room temperature. They reported that Fluorouracil@ZIF-8 significantly improved the therapeutic outcome in a nude mouse model with tumor lung metastasis compared to other drug delivery techniques.

Despite the superior performance of ZIF materials as drug delivery vehicles for different drugs, the main challenges lie in the long time periods necessary to load the drugs into the ZIF framework and in ensuring the reproducible synthesis of controlled particle size ZIF materials. Accordingly, we intend to investigate the MIVMs potential for the encapsulation of different drugs (5-FU, Doxorubicin, etc.) during the formation of ZIF-8 nanoparticles inside the mixing chamber. The unique geometric design of the MIVM featuring four inlets would allow the synthesis to be achieved starting from precursor solutions that are in separate syringes. Moreover, through controlling the flow rate of the syringe containing the drug solution, we can optimize the amounts of drug needed to achieve the maximum loading capacity of ZIF-8, thereby reducing the over all cost of the process. The high mixing performance of the MIVM at high Re discussed earlier is expected to reduce the drug loading time from few days to few seconds along with the reproducible synthesis of high quality ZIF-8 nanoparticles.

Bibliography

[1] E. L. Paul, V. A. Atiemo-Obeng, and S. M. Kresta, *Handbook of industrial mixing: science and practice*. John Wiley & Sons, 2004.

[2] R. Xu, W. Pang, J. Yu, Q. Huo, and J. Chen, *Chemistry of zeolites and related porous materials: synthesis and structure*. John Wiley & Sons, 2009.

[3] C. Baerlocher, D. Olson, and W. Meier, *Atlas of Zeolite framework types (formerly: Atlas of Zeolite structure types)*. Elsevier, 2001.

[4] P. Jacobs, E. M. Flanigen, J. Jansen, and H. van Bekkum, *Introduction to zeolite science and practice*, vol. 137. Elsevier, 2001.

[5] K. S. Park, Z. Ni, A. P. Côté, J. Y. Choi, R. Huang, F. J. Uribe-Romo, H. K. Chae, M. O'Keeffe, and O. M. Yaghi, "Exceptional chemical and thermal stability of zeolitic imidazolate frameworks," *Proceedings of the National Academy of Sciences*, vol. 103, no. 27, pp. 10186–10191, 2006.

[6] A. Phan, C. J. Doonan, F. J. Uribe-Romo, C. B. Knobler, M. O'keeffe, and O. M. Yaghi, "Synthesis, structure, and carbon dioxide capture properties of zeolitic imidazolate frameworks," 2009.

[7] D. Saliba, M. Ammar, M. Rammal, M. Al-Ghoul, and M. Hmadeh, "Crystal growth of zif-8, zif-67, and their mixed-metal derivatives," *Journal of the American Chemical Society*, vol. 140, no. 5, pp. 1812–1823, 2018.

[8] K. Boodhoo and A. Harvey, "Process intensification: an overview of principles and practice," *Process Intensification for Green Chemistry: Engineering Solutions for Sustainable Chemical Processing, John Wiley, Sons*, pp. 1–31, 2013.

[9] V. Hessel, H. Löwe, and S. Hardt, *Chemical micro process engineering: fundamentals, modelling and reactions*, vol. 1. John Wiley & Sons, 2004.

[10] K. Jähnisch, V. Hessel, H. Löwe, and M. Baerns, "Chemistry in microstructured reactors," *Angewandte Chemie International Edition*, vol. 43, no. 4, pp. 406–446, 2004.

[11] V. Hessel and H. Löwe, "Microchemical engineering: components, plant concepts user acceptance–part i," *Chemical Engineering & Technology: Industrial Chemistry-Plant Equipment-Process Engineering-Biotechnology*, vol. 26, no. 1, pp. 13–24, 2003.

[12] O. Wörz, K. Jäckel, T. Richter, and A. Wolf, "Microreactors, a new efficient tool for optimum reactor design," *Chemical Engineering Science*, vol. 56, no. 3, pp. 1029–1033, 2001.

[13] C.-Y. Lee, C.-H. Lin, and L.-M. Fu, "Passive micromixers," *Encyclopedia of Microfluidics and Nanofluidics*, pp. 2663–2673, 2015.

[14] V. Khaydarov, E. Borovinskaya, and W. Reschetilowski, "Numerical and experimental investigations of a micromixer with chicane mixing geometry," *Applied Sciences*, vol. 8, no. 12, p. 2458, 2018.

[15] N.-T. Nguyen and Z. Wu, "Micromixers—a review," *Journal of Micromechanics and Microengineering*, vol. 15, no. 2, p. R1, 2004.

[16] V. Hessel, H. Löwe, and F. Schönfeld, "Micromixers—a review on passive and active mixing principles," *Chemical Engineering Science*, vol. 60, no. 8-9, pp. 2479–2501, 2005.

[17] M. Ståhl, B. L. Åslund, and Å. C. Rasmuson, "Reaction crystallization kinetics of benzoic acid," *AIChE Journal*, vol. 47, no. 7, pp. 1544–1560, 2001.

[18] H.-C. Schwarzer and W. Peukert, "Combined experimental/numerical study on the precipitation of nanoparticles," *AIChE Journal*, vol. 50, no. 12, pp. 3234–3247, 2004.

[19] H.-C. Schwarzer, F. Schwertfirm, M. Manhart, H.-J. Schmid, and W. Peukert, "Predictive simulation of nanoparticle precipitation based on the population balance equation," *Chemical Engineering Science*, vol. 61, no. 1, pp. 167–181, 2006.

[20] T. Iwasaki and J.-i. Yoshida, "Free radical polymerization in microreactors. significant improvement in molecular weight distribution control," *Macromolecules*, vol. 38, no. 4, pp. 1159–1163, 2005.

[21] C. Rosenfeld, C. Serra, C. Brochon, and G. Hadziioannou, "Influence of micromixer characteristics on polydispersity index of block copolymers synthesized in continuous flow microreactors," *Lab on a Chip*, vol. 8, no. 10, pp. 1682–1687, 2008.

[22] A. Nagaki, Y. Tomida, and J.-i. Yoshida, "Microflow-system-controlled anionic polymerization of styrenes," *Macromolecules*, vol. 41, no. 17, pp. 6322–6330, 2008.

[23] A. Nagaki, K. Kawamura, S. Suga, T. Ando, M. Sawamoto, and J.-i. Yoshida, "Cation pool-initiated controlled/living polymerization using microsystems," *Journal of the American Chemical Society*, vol. 126, no. 45, pp. 14702–14703, 2004.

[24] S. J. Haswell, R. J. Middleton, B. O'Sullivan, V. Skelton, P. Watts, and P. Styring, "The application of micro reactors to synthetic chemistry," *Chemical Communications*, no. 5, pp. 391–398, 2001.

[25] G. S. Reddy, N. S. Reddy, K. Manudhane, M. V. Rama Krishna, K. J. S. Ramachandra, and S. Gangula, "Application of continuous flow micromixing reactor technology for synthesis of benzimidazole drugs," *Organic Process Research & Development*, vol. 17, no. 10, pp. 1272–1276, 2013.

[26] Y. Liu, C. Cheng, R. K. Prud'homme, and R. O. Fox, "Mixing in a multi-inlet vortex mixer (mivm) for flash nano-precipitation," *Chemical Engineering Science*, vol. 63, no. 11, pp. 2829–2842, 2008.

[27] W. S. Saad and R. K. Prud'homme, "Principles of nanoparticle formation by flash nanoprecipitation," *Nano Today*, vol. 11, no. 2, pp. 212–227, 2016.

[28] B. K. Johnson and R. K. Prud'homme, "Chemical processing and micromixing in confined impinging jets," *AIChE Journal*, vol. 49, no. 9, pp. 2264–2282, 2003.

[29] B. K. Johnson and R. K. Prud'homme, "Flash nanoprecipitation of organic actives and block copolymers using a confined impinging jets mixer," *Australian Journal of Chemistry*, vol. 56, no. 10, pp. 1021–1024, 2003.

[30] W. Meier, D. Olson, and D. H. Olson, *Atlas of zeolite structure types*. Butterworth-Heinemann, 1987.

[31] J. V. Smith, "Topochemistry of zeolites and related materials. 1. topology and geometry," *Chemical Reviews*, vol. 88, no. 1, pp. 149–182, 1988.

[32] R. F. Lobo, S. I. Zones, and M. E. Davis, "Structure-direction in zeolite synthesis," *Journal of Inclusion Phenomena and Molecular Recognition in Chemistry*, vol. 21, no. 1-4, pp. 47–78, 1995.

[33] A. Corma, F. Rey, J. Rius, M. J. Sabater, and S. Valencia, "Supramolecular self-assembled molecules as organic directing agent for synthesis of zeolites," *Nature*, vol. 431, no. 7006, p. 287, 2004.

[34] S. T. Wilson, B. M. Lok, and E. M. Flanigen, "Crystalline metallophosphate compositions," Jan. 12 1982. US Patent 4,310,440.

[35] M. E. Davis, C. Saldarriaga, C. Montes, J. Garces, and C. Crowdert, "A molecular sieve with eighteen-membered rings," *Nature*, vol. 331, no. 6158, p. 698, 1988.

[36] C. Kresge, M. Leonowicz, W. J. Roth, J. Vartuli, and J. Beck, "Ordered mesoporous molecular sieves synthesized by a liquid-crystal template mechanism," *Nature*, vol. 359, no. 6397, p. 710, 1992.

[37] E. M. Flanigen, "Molecular sieve zeolite technology-the first twenty-five years," *Pure and Applied Chemistry*, vol. 52, no. 9, pp. 2191–2211, 1980.

[38] J.-L. Paillaud, B. Harbuzaru, J. Patarin, and N. Bats, "Extra-large-pore zeolites with two-dimensional channels formed by 14 and 12 rings," *Science*, vol. 304, no. 5673, pp. 990–992, 2004.

[39] K. Yamamoto, Y. Sakata, Y. Nohara, Y. Takahashi, and T. Tatsumi, "Organic-inorganic hybrid zeolites containing organic frameworks," *Science*, vol. 300, no. 5618, pp. 470–472, 2003.

[40] C. W. Jones, K. Tsuji, and M. E. Davis, "Organic-functionalized molecular sieves as shape-selective catalysts," *Nature*, vol. 393, no. 6680, p. 52, 1998.

[41] H. Hayashi, A. P. Cote, H. Furukawa, M. O'Keeffe, and O. M. Yaghi, "Zeolite a imidazolate frameworks," *Nature materials*, vol. 6, no. 7, p. 501, 2007.

[42] B. Wang, A. P. Côté, H. Furukawa, M. O'Keeffe, and O. M. Yaghi, "Colossal cages in zeolitic imidazolate frameworks as selective carbon dioxide reservoirs," *Nature*, vol. 453, no. 7192, p. 207, 2008.

[43] M. Eddaoudi, D. F. Sava, J. F. Eubank, K. Adil, and V. Guillerm, "Zeolite-like metal–organic frameworks (zmofs): design, synthesis, and properties," *Chemical Society Reviews*, vol. 44, no. 1, pp. 228–249, 2015.

[44] L. T. Nguyen, K. K. Le, H. X. Truong, and N. T. Phan, "Metal–organic frameworks for catalysis: the knoevenagel reaction using zeolite imidazolate framework zif-9 as an efficient heterogeneous catalyst," *Catalysis Science & Technology*, vol. 2, no. 3, pp. 521–528, 2012.

[45] U. P. Tran, K. K. Le, and N. T. Phan, "Expanding applications of metal-organic frameworks: zeolite imidazolate framework zif-8 as an efficient heterogeneous catalyst for the knoevenagel reaction," *ACS Catalysis*, vol. 1, no. 2, pp. 120–127, 2011.

[46] C.-Y. Sun, C. Qin, X.-L. Wang, G.-S. Yang, K.-Z. Shao, Y.-Q. Lan, Z.-M. Su, P. Huang, C.-G. Wang, and E.-B. Wang, "Zeolitic imidazolate framework-8 as efficient ph-sensitive drug delivery vehicle," *Dalton Transactions*, vol. 41, no. 23, pp. 6906–6909, 2012.

[47] J. Zhuang, C.-H. Kuo, L.-Y. Chou, D.-Y. Liu, E. Weerapana, and C.-K. Tsung, "Optimized metal–organic-framework nanospheres for drug deliv-

71

ery: evaluation of small-molecule encapsulation," *ACS Nano*, vol. 8, no. 3, pp. 2812–2819, 2014.

[48] A. Nalaparaju and J. Jiang, "Ion exchange in metal–organic framework for water purification: insight from molecular simulation," *The Journal of Physical Chemistry C*, vol. 116, no. 12, pp. 6925–6931, 2012.

[49] S. Li, Y. Chen, X. Pei, S. Zhang, X. Feng, J. Zhou, and B. Wang, "Water purification: Adsorption over metal-organic frameworks," *Chinese Journal of Chemistry*, vol. 34, no. 2, pp. 175–185, 2016.

[50] B. Li, H.-M. Wen, W. Zhou, and B. Chen, "Porous metal–organic frameworks for gas storage and separation: what, how, and why?," *The Journal of Physical Chemistry Letters*, vol. 5, no. 20, pp. 3468–3479, 2014.

[51] Q. Song, S. Nataraj, M. V. Roussenova, J. C. Tan, D. J. Hughes, W. Li, P. Bourgoin, M. A. Alam, A. K. Cheetham, S. A. Al-Muhtaseb, *et al.*, "Zeolitic imidazolate framework (zif-8) based polymer nanocomposite membranes for gas separation," *Energy & Environmental Science*, vol. 5, no. 8, pp. 8359–8369, 2012.

[52] G. Long, M. E. Meek, H. Canada, and M. J. Lewis, "Concise international chemical assessment document 31 n,n-dimethylformamide,"

[53] Y. Ban, Y. Li, X. Liu, Y. Peng, and W. Yang, "Solvothermal synthesis of mixed-ligand metal–organic framework zif-78 with controllable size and morphology," *Microporous and Mesoporous Materials*, vol. 173, pp. 29–36, 2013.

[54] D. Peralta, G. Chaplais, A. Simon-Masseron, K. Barthelet, and G. D. Pirngruber, "Synthesis and adsorption properties of zif-76 isomorphs," *Microporous and Mesoporous Materials*, vol. 153, pp. 1–7, 2012.

[55] X.-C. Huang, Y.-Y. Lin, J.-P. Zhang, and X.-M. Chen, "Ligand-directed strategy for zeolite-type metal–organic frameworks: zinc (ii) imidazolates with unusual zeolitic topologies," *Angewandte Chemie International Edition*, vol. 45, no. 10, pp. 1557–1559, 2006.

[56] Y. Pan, Y. Liu, G. Zeng, L. Zhao, and Z. Lai, "Rapid synthesis of zeolitic imidazolate framework-8 (zif-8) nanocrystals in an aqueous system," *Chemical Communications*, vol. 47, no. 7, pp. 2071–2073, 2011.

[57] A. F. Gross, E. Sherman, and J. J. Vajo, "Aqueous room temperature synthesis of cobalt and zinc sodalite zeolitic imidizolate frameworks," *Dalton transactions*, vol. 41, no. 18, pp. 5458–5460, 2012.

[58] K. Bernardo-Gusmão, L. F. T. Queiroz, R. F. de Souza, F. Leca, C. Loup, and R. Réau, "Biphasic oligomerization of ethylene with

nickel–1, 2-diiminophosphorane complexes immobilized in 1-n-butyl-3-methylimidazolium organochloroaluminate," *Journal of Catalysis*, vol. 219, no. 1, pp. 59–62, 2003.

[59] R. D. Rogers, "Ionic liquids: industrial applications to green chemistry," in *ACS symposium series*, American Chemical Society, 2002.

[60] G. A. Martins, P. J. Byrne, P. Allan, S. J. Teat, A. M. Slawin, Y. Li, and R. E. Morris, "The use of ionic liquids in the synthesis of zinc imidazolate frameworks," *Dalton Transactions*, vol. 39, no. 7, pp. 1758–1762, 2010.

[61] K. S. Suslick, D. A. Hammerton, and R. E. Cline, "Sonochemical hot spot," *Journal of the American Chemical Society*, vol. 108, no. 18, pp. 5641–5642, 1986.

[62] W.-J. Son, J. Kim, J. Kim, and W.-S. Ahn, "Sonochemical synthesis of mof-5," *Chemical Communications*, no. 47, pp. 6336–6338, 2008.

[63] B. Seoane, J. M. Zamaro, C. Tellez, and J. Coronas, "Sonocrystallization of zeolitic imidazolate frameworks (zif-7, zif-8, zif-11 and zif-20)," *CrystEngComm*, vol. 14, no. 9, pp. 3103–3107, 2012.

[64] H.-Y. Cho, J. Kim, S.-N. Kim, and W.-S. Ahn, "High yield 1-l scale synthesis of zif-8 via a sonochemical route," *Microporous and Mesoporous Materials*, vol. 169, pp. 180–184, 2013.

[65] M. Schlesinger, S. Schulze, M. Hietschold, and M. Mehring, "Evaluation of synthetic methods for microporous metal–organic frameworks exemplified by the competitive formation of [cu2 (btc) 3 (h2o) 3] and [cu2 (btc)(oh)(h2o)]," *Microporous and Mesoporous Materials*, vol. 132, no. 1-2, pp. 121–127, 2010.

[66] J. Fernández-Bertrán, M. Hernández, E. Reguera, H. Yee-Madeira, J. Rodriguez, A. Paneque, and J. Llopiz, "Characterization of mechanochemically synthesized imidazolates of ag+ 1, zn+ 2, cd+ 2, and hg+ 2: Solid state reactivity of nd10 cations," *Journal of Physics and Chemistry of Solids*, vol. 67, no. 8, pp. 1612–1617, 2006.

[67] T. Friščić, S. L. Childs, S. A. Rizvi, and W. Jones, "The role of solvent in mechanochemical and sonochemical cocrystal formation: a solubility-based approach for predicting cocrystallisation outcome," *CrystEngComm*, vol. 11, no. 3, pp. 418–426, 2009.

[68] P. J. Beldon, L. Fábián, R. S. Stein, A. Thirumurugan, A. K. Cheetham, and T. Friščić, "Rapid room-temperature synthesis of zeolitic imidazolate frameworks by using mechanochemistry," *Angewandte Chemie International Edition*, vol. 49, no. 50, pp. 9640–9643, 2010.

[69] J. Rouquerol, F. Rouquerol, P. Llewellyn, G. Maurin, and K. S. Sing, *Adsorption by powders and porous solids: principles, methodology and applications*. Academic press, 2013.

[70] R. T. Yang, *Gas separation by adsorption processes*. Butterworth-Heinemann, 2013.

[71] Y.-S. Li, F.-Y. Liang, H. Bux, A. Feldhoff, W.-S. Yang, and J. Caro, "Molecular sieve membrane: supported metal–organic framework with high hydrogen selectivity," *Angewandte Chemie International Edition*, vol. 49, no. 3, pp. 548–551, 2010.

[72] Y. Li, F. Liang, H. Bux, W. Yang, and J. Caro, "Zeolitic imidazolate framework zif-7 based molecular sieve membrane for hydrogen separation," *Journal of Membrane Science*, vol. 354, no. 1-2, pp. 48–54, 2010.

[73] H. Bux, F. Liang, Y. Li, J. Cravillon, M. Wiebcke, and J. Caro, "Zeolitic imidazolate framework membrane with molecular sieving properties by microwave-assisted solvothermal synthesis," *Journal of the American Chemical Society*, vol. 131, no. 44, pp. 16000–16001, 2009.

[74] C. Chizallet and N. Bats, "External surface of zeolite imidazolate frameworks viewed ab initio: multifunctionality at the organic- inorganic interface," *The Journal of Physical Chemistry Letters*, vol. 1, no. 1, pp. 349–353, 2009.

[75] C. Chizallet, S. Lazare, D. Bazer-Bachi, F. Bonnier, V. Lecocq, E. Soyer, A.-A. Quoineaud, and N. Bats, "Catalysis of transesterification by a nonfunctionalized metal- organic framework: acido-basicity at the external surface of zif-8 probed by ftir and ab initio calculations," *Journal of the American Chemical Society*, vol. 132, no. 35, pp. 12365–12377, 2010.

[76] J. Li, Y.-n. Wu, Z. Li, B. Zhang, M. Zhu, X. Hu, Y. Zhang, and F. Li, "Zeolitic imidazolate framework-8 with high efficiency in trace arsenate adsorption and removal from water," *The Journal of Physical Chemistry C*, vol. 118, no. 47, pp. 27382–27387, 2014.

[77] Y. Huang, X. Zeng, L. Guo, J. Lan, L. Zhang, and D. Cao, "Heavy metal ion removal of wastewater by zeolite-imidazolate frameworks," *Separation and Purification Technology*, vol. 194, pp. 462–469, 2018.

[78] Z.-h. Zhang, J.-l. Zhang, J.-m. Liu, Z.-h. Xiong, and X. Chen, "Selective and competitive adsorption of azo dyes on the metal–organic framework zif-67," *Water, Air, & Soil Pollution*, vol. 227, no. 12, p. 471, 2016.

[79] N. Liedana, A. Galve, C. Rubio, C. Tellez, and J. Coronas, "Caf@ zif-8: one-step encapsulation of caffeine in mof," *ACS Applied Materials & Interfaces*, vol. 4, no. 9, pp. 5016–5021, 2012.

[80] L. T. Nguyen, K. L. Ky, and T. Nam, "A zeolite imidazolate framework zif-8 catalyst for friedel-crafts acylation," *Chinese Journal of Catalysis*, vol. 33, no. 4-6, pp. 688–696, 2012.

[81] X. Zhou, H. P. Zhang, G. Y. Wang, Z. G. Yao, Y. R. Tang, and S. S. Zheng, "Zeolitic imidazolate framework as efficient heterogeneous catalyst for the synthesis of ethyl methyl carbonate," *Journal of Molecular Catalysis A: Chemical*, vol. 366, pp. 43–47, 2013.

[82] S. B. Kalidindi, D. Esken, and R. A. Fischer, "B-n chemistry@ zif-8: Dehydrocoupling of dimethylamine borane at room temperature by size-confinement effects," *Chemistry–A European Journal*, vol. 17, no. 24, pp. 6594–6597, 2011.

[83] A. B. Burg and C. L. Randolph, "The n-methyl derivatives of b2h7n," *Journal of the American Chemical Society*, vol. 71, no. 10, pp. 3451–3455, 1949.

[84] A. W. van den Berg and C. O. Areán, "Materials for hydrogen storage: current research trends and perspectives," *Chemical Communications*, no. 6, pp. 668–681, 2008.

[85] W. Xue, Q. Zhou, F. Li, and B. S. Ondon, "Zeolitic imidazolate framework-8 (zif-8) as robust catalyst for oxygen reduction reaction in microbial fuel cells," *Journal of Power Sources*, vol. 423, pp. 9–17, 2019.

[86] G. Lu, S. Li, Z. Guo, O. K. Farha, B. G. Hauser, X. Qi, Y. Wang, X. Wang, S. Han, X. Liu, *et al.*, "Imparting functionality to a metal–organic framework material by controlled nanoparticle encapsulation," *Nature Chemistry*, vol. 4, no. 4, p. 310, 2012.

[87] K. Kida, M. Okita, K. Fujita, S. Tanaka, and Y. Miyake, "Formation of high crystalline zif-8 in an aqueous solution," *CrystEngComm*, vol. 15, no. 9, pp. 1794–1801, 2013.

[88] R. Chen, J. Yao, Q. Gu, S. Smeets, C. Baerlocher, H. Gu, D. Zhu, W. Morris, O. M. Yaghi, and H. Wang, "A two-dimensional zeolitic imidazolate framework with a cushion-shaped cavity for co 2 adsorption," *Chemical Communications*, vol. 49, no. 82, pp. 9500–9502, 2013.

[89] Z.-X. Low, J. Yao, Q. Liu, M. He, Z. Wang, A. K. Suresh, J. Bellare, and H. Wang, "Crystal transformation in zeolitic-imidazolate framework," *Crystal Growth & Design*, vol. 14, no. 12, pp. 6589–6598, 2014.

[90] J. Hancock and J. Sharp, "Method of comparing solid-state kinetic data and its application to the decomposition of kaolinite, brucite, and baco3," *Journal of the American Ceramic Society*, vol. 55, no. 2, pp. 74–77, 1972.

[91] J. Zhang, T. Zhang, D. Yu, K. Xiao, and Y. Hong, "Transition from zif-l-co to zif-67: a new insight into the structural evolution of zeolitic imidazolate frameworks (zifs) in aqueous systems," *CrystEngComm*, vol. 17, no. 43, pp. 8212–8215, 2015.

[92] R. Banerjee, A. Phan, B. Wang, C. Knobler, H. Furukawa, M. O'Keeffe, and O. M. Yaghi, "High-throughput synthesis of zeolitic imidazolate frameworks and application to co2 capture," *Science*, vol. 319, no. 5865, pp. 939–943, 2008.

[93] H. Fu, Z. Wang, X. Wang, P. Wang, and C.-C. Wang, "Formation mechanism of rod-like zif-l and fast phase transformation from zif-l to zif-8 with morphology changes controlled by polyvinylpyrrolidone and ethanol," *CrystEngComm*, vol. 20, no. 11, pp. 1473–1477, 2018.

[94] I. U. Khan, M. H. D. Othman, A. Ismail, N. Ismail, J. Jaafar, H. Hashim, M. A. Rahman, and A. Jilani, "Structural transition from two-dimensional zif-l to three-dimensional zif-8 nanoparticles in aqueous room temperature synthesis with improved co2 adsorption," *Materials Characterization*, vol. 136, pp. 407–416, 2018.

[95] O. M. Linder-Patton, T. J. de Prinse, S. Furukawa, S. G. Bell, K. Sumida, C. J. Doonan, and C. J. Sumby, "Influence of nanoscale structuralisation on the catalytic performance of zif-8: a cautionary surface catalysis study," *CrystEngComm*, vol. 20, no. 34, pp. 4926–4934, 2018.

[96] K. Li, D. H. Olson, J. Seidel, T. J. Emge, H. Gong, H. Zeng, and J. Li, "Zeolitic imidazolate frameworks for kinetic separation of propane and propene," *Journal of the American Chemical Society*, vol. 131, no. 30, pp. 10368–10369, 2009.

[97] G. Kumari, K. Jayaramulu, T. K. Maji, and C. Narayana, "Temperature induced structural transformations and gas adsorption in the zeolitic imidazolate framework zif-8: A raman study," *The Journal of Physical Chemistry A*, vol. 117, no. 43, pp. 11006–11012, 2013.

[98] A. Schejn, L. Balan, V. Falk, L. Aranda, G. Medjahdi, and R. Schneider, "Controlling zif-8 nano-and microcrystal formation and reactivity through zinc salt variations," *CrystEngComm*, vol. 16, no. 21, pp. 4493–4500, 2014.

[99] E. L. Bustamante, J. L. Fernández, and J. M. Zamaro, "Influence of the solvent in the synthesis of zeolitic imidazolate framework-8 (zif-8) nanocrystals at room temperature," *Journal of Colloid and Interface Science*, vol. 424, pp. 37–43, 2014.

[100] M. Jian, B. Liu, R. Liu, J. Qu, H. Wang, and X. Zhang, "Water-based synthesis of zeolitic imidazolate framework-8 with high morphology level at room temperature," *RSC Advances*, vol. 5, no. 60, pp. 48433–48441, 2015.

[101] D. Yamamoto, T. Maki, S. Watanabe, H. Tanaka, M. T. Miyahara, and K. Mae, "Synthesis and adsorption properties of zif-8 nanoparticles using a micromixer," *Chemical Engineering Journal*, vol. 227, pp. 145–150, 2013.

[102] S. Watanabe, S. Ohsaki, T. Hanafusa, K. Takada, H. Tanaka, K. Mae, and M. T. Miyahara, "Synthesis of zeolitic imidazolate framework-8 particles of controlled sizes, shapes, and gate adsorption characteristics using a central collision-type microreactor," *Chemical Engineering Journal*, vol. 313, pp. 724–733, 2017.

[103] N. Nordin, A. Ismail, A. Mustafa, P. Goh, D. Rana, and T. Matsuura, "Aqueous room temperature synthesis of zeolitic imidazole framework 8 (zif-8) with various concentrations of triethylamine," *RSC Advances*, vol. 4, no. 63, pp. 33292–33300, 2014.

[104] J. A. Thompson, K. W. Chapman, W. J. Koros, C. W. Jones, and S. Nair, "Sonication-induced ostwald ripening of zif-8 nanoparticles and formation of zif-8/polymer composite membranes," *Microporous and Mesoporous Materials*, vol. 158, pp. 292–299, 2012.

[105] M. Malekmohammadi, S. Fatemi, M. Razavian, and A. Nouralishahi, "A comparative study on zif-8 synthesis in aqueous and methanolic solutions: Effect of temperature and ligand content," *Solid State Sciences*, vol. 91, pp. 108–112, 2019.

[106] A. Polyzoidis, T. Altenburg, M. Schwarzer, S. Loebbecke, and S. Kaskel, "Continuous microreactor synthesis of zif-8 with high space–time-yield and tunable particle size," *Chemical Engineering Journal*, vol. 283, pp. 971–977, 2016.

[107] H. Nagasawa, N. Aoki, and K. Mae, "Design of a new micromixer for instant mixing based on the collision of micro segments," *Chemical Engineering & Technology: Industrial Chemistry-Plant Equipment-Process Engineering-Biotechnology*, vol. 28, no. 3, pp. 324–330, 2005.

[108] A. Parulkar and N. A. Brunelli, "High-yield synthesis of zif-8 nanoparticles using stoichiometric reactants in a jet-mixing reactor," *Industrial & Engineering Chemistry Research*, vol. 56, no. 37, pp. 10384–10392, 2017.

[109] G. Kaur, R. K. Rai, D. Tyagi, X. Yao, P.-Z. Li, X.-C. Yang, Y. Zhao, Q. Xu, and S. K. Singh, "Room-temperature synthesis of bimetallic co–zn based zeolitic imidazolate frameworks in water for enhanced co 2 and h

2 uptakes," *Journal of Materials Chemistry A*, vol. 4, no. 39, pp. 14932–14938, 2016.

[110] R. R. Kuruppathparambil, R. Babu, H. M. Jeong, G.-Y. Hwang, G. S. Jeong, M.-I. Kim, D.-W. Kim, and D.-W. Park, "A solid solution zeolitic imidazolate framework as a room temperature efficient catalyst for the chemical fixation of co 2," *Green Chemistry*, vol. 18, no. 23, pp. 6349–6356, 2016.

[111] H. Yang, X.-W. He, F. Wang, Y. Kang, and J. Zhang, "Doping copper into zif-67 for enhancing gas uptake capacity and visible-light-driven photocatalytic degradation of organic dye," *Journal of Materials Chemistry*, vol. 22, no. 41, pp. 21849–21851, 2012.

[112] J. Sebastian, K. M. Jinka, and R. V. Jasra, "Effect of alkali and alkaline earth metal ions on the catalytic epoxidation of styrene with molecular oxygen using cobalt (ii)-exchanged zeolite x," *Journal of Catalysis*, vol. 244, no. 2, pp. 208–218, 2006.

[113] J.-S. Qin, S. Yuan, Q. Wang, A. Alsalme, and H.-C. Zhou, "Mixed-linker strategy for the construction of multifunctional metal–organic frameworks," *Journal of Materials Chemistry A*, vol. 5, no. 9, pp. 4280–4291, 2017.

[114] J. A. Thompson, C. R. Blad, N. A. Brunelli, M. E. Lydon, R. P. Lively, C. W. Jones, and S. Nair, "Hybrid zeolitic imidazolate frameworks: controlling framework porosity and functionality by mixed-linker synthesis," *Chemistry of Materials*, vol. 24, no. 10, pp. 1930–1936, 2012.

[115] J. Yang, Y.-B. Zhang, Q. Liu, C. A. Trickett, E. Gutierrez-Puebla, M. A. Monge, H. Cong, A. Aldossary, H. Deng, and O. M. Yaghi, "Principles of designing extra-large pore openings and cages in zeolitic imidazolate frameworks," *Journal of the American Chemical Society*, vol. 139, no. 18, pp. 6448–6455, 2017.

[116] H. Furukawa, U. Müller, and O. M. Yaghi, ""heterogeneity within order" in metal–organic frameworks," *Angewandte Chemie International Edition*, vol. 54, no. 11, pp. 3417–3430, 2015.

[117] C. Adhikari, A. Das, and A. Chakraborty, "Zeolitic imidazole framework (zif) nanospheres for easy encapsulation and controlled release of an anticancer drug doxorubicin under different external stimuli: a way toward smart drug delivery system," *Molecular Pharmaceutics*, vol. 12, no. 9, pp. 3158–3166, 2015.

[118] S. Li, K. Wang, Y. Shi, Y. Cui, B. Chen, B. He, W. Dai, H. Zhang, X. Wang, C. Zhong, *et al.*, "Novel biological functions of zif-np as a delivery vehicle: High pulmonary accumulation, favorable biocompatibility, and

improved therapeutic outcome," *Advanced Functional Materials*, vol. 26, no. 16, pp. 2715–2727, 2016.